BOSTON UNIVERSITY

GRADUATE SCHOOL OF ARTS AND SCIENCES

Dissertation

STRONG DYNAMICS AND LATTICE GAUGE THEORY

by

DAVID SCHAICH

B.A., Amherst College, 2006

Submitted in partial fulfillment of the

requirements for the degree of

Doctor of Philosophy

2012

Approved by

First Reader

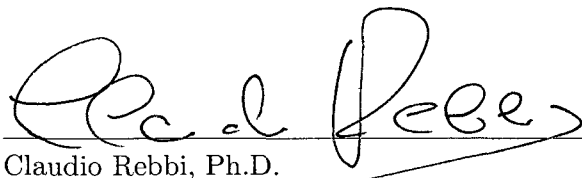

Claudio Rebbi, Ph.D.
Professor of Physics

Second Reader

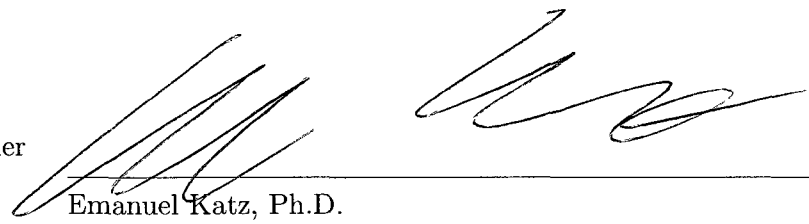

Emanuel Katz, Ph.D.
Assistant Professor of Physics

Acknowledgments

I first thank my advisors, Claudio Rebbi and Rich Brower. Over the years I have benefited tremendously from their extensive experience, knowledge and skills; wide-ranging curiosity; persistence; and passion for teaching.

I carried out the work discussed in this dissertation as a member of the Lattice Strong Dynamics (LSD) Collaboration.[1] The LSD Collaboration has introduced me to exciting work on the cutting edge of rapidly-developing and challenging field, and I am grateful to my collaborators for many informative and enjoyable exchanges on a diverse array of topics. In addition to Claudio and Rich, the LSD Collaboration includes Tom Appelquist, Adam Avakian, Ron Babich, Mike Buchoff, Michael Cheng, Mike Clark, Saul Cohen, George Fleming, Fu-Jiun Jiang, Joe Kiskis, Meifeng Lin, Ethan Neil, James Osborn, Sergey Syritsyn, Pavlos Vranas and Joe Wasem. Among this list, I especially thank Pavlos Vranas, who hosted me for a productive two-month internship at Lawrence Livermore National Laboratory (LLNL) in 2010.

Ron Babich also deserves special acknowledgement, as my predecessor on the PhD path at Boston University. I thank Ron for his guidance, and for his patient willingness to answer my stupid questions. I have also enjoyed the company of future PhDs Adam Avakian, Asher Mullokandov and Yiming Xu, whose insightful inquiries help remind me how much I still do not know, and also help me better understand the portion that I do. The high-energy theory group and Center for Computational Science at BU have both been wonderful environments in which to learn and work, for which I thank the rest of the faculty and postdocs, as well as Ilona Lappo and Cheryl Endicott of CCS.

Finally, I thank my parents, whose support has been steady and sure.

[1] http://www.yale.edu/LSD

While working on the research reported in this dissertation, I was supported first by the National Science Foundation (NSF) Integrative Graduate Education and Research Traineeship (IGERT) program[2] through grant DGE-0221680, and then by the Department of Energy (DOE) through grant DE-FG02-91ER40676. Computing support for this work came from the LLNL Institutional Computing Grand Challenge program; the DOE Scientific Discovery through Advanced Computing (SciDAC) program through the USQCD Collaboration;[3] the NSF through TeraGrid resources provided by the National Institute for Computational Sciences under grant number TG-MCA08X008;[4] and Boston University's Scientific Computing Facilities.

[2] http://www.igert.org
[3] http://www.usqcd.org
[4] http://www.teragrid.org

STRONG DYNAMICS AND LATTICE GAUGE THEORY

(Order No.)

DAVID SCHAICH

Boston University, Graduate School of Arts and Sciences, 2012

Major Professor: Claudio Rebbi, Professor of Physics

ABSTRACT

In this dissertation I use lattice gauge theory to study models of electroweak symmetry breaking that involve new strong dynamics.

Electroweak symmetry breaking (EWSB) is the process by which elementary particles acquire mass. First proposed in the 1960s, this process has been clearly established by experiments, and can now be considered a law of nature. However, the physics underlying EWSB is still unknown, and understanding it remains a central challenge in particle physics today. A natural possibility is that EWSB is driven by the dynamics of some new, strongly-interacting force. Strong interactions invalidate the standard analytical approach of perturbation theory, making these models difficult to study.

Lattice gauge theory is the premier method for obtaining quantitatively-reliable, non-perturbative predictions from strongly-interacting theories. In this approach, we replace spacetime by a regular, finite grid of discrete sites connected by links. The fields and interactions described by the theory are likewise discretized, and defined on the lattice so that we recover the original theory in continuous spacetime on an infinitely large lattice with sites infinitesimally close together. The finite number of degrees of freedom in the discretized system lets us simulate the lattice theory using high-performance computing.

Lattice gauge theory has long been applied to quantum chromodynamics, the theory of strong nuclear interactions. Using lattice gauge theory to study dynamical EWSB, as I do in this dissertation, is a new and exciting application of these methods. Of particular interest

is non-perturbative lattice calculation of the electroweak S parameter. Experimentally $S \approx -0.15(10)$, which tightly constrains dynamical EWSB. On the lattice, I extract S from the momentum-dependence of vector and axial-vector current correlators. I created and applied computer programs to calculate these correlators and analyze them to determine S. I also calculated the masses and other properties of the new particles predicted by these theories.

I find $S \gtrsim 0.1$ in the specific theories I study. Although this result still disagrees with experiment, it is much closer to the experimental value than is the conventional wisdom $S \gtrsim 0.3$. These results encourage further lattice studies to search for experimentally viable strongly-interacting theories of EWSB.

Contents

List of Tables

List of Figures

List of Abbreviations

AdS/CFT	anti-de Sitter/conformal field theory
BSM	beyond the standard model
χSB	chiral symmetry breaking
CKM	Cabibbo, Kobayashi and Maskawa
CP	charge conjugation and parity
DBW2	doubly-blocked from Wilson in two-coupling space
DOE	Department of Energy
dof	degrees of freedom
DWF	domain wall fermion
ETC	extended technicolor
eV	electron volt
EWSB	electroweak symmetry breaking
GPU	graphics processing unit
GW	Ginsparg and Wilson
HMC	hybrid Monte Carlo
IGERT	Integrative Graduate Education and Research Traineeship
IRFP	infrared fixed point
LHC	Large Hadron Collider
LSD	Lattice Strong Dynamics
LSTC	low-scale technicolor
NGB	Nambu–Goldstone boson
NSF	National Science Foundation

PCAC	partial conservation of the axial current
PNGB	pseudo-Nambu–Goldstone boson
QCD	quantum chromodynamics
SciDAC	Scientific Discovery through Advanced Computing
SM	standard model
SU	special unitary
USQCD	United States Lattice Quantum Chromodynamics
TC	technicolor
WTC	walking technicolor

Chapter 1

Introduction

In this dissertation we discuss the application of lattice gauge theory to models of electroweak symmetry breaking (EWSB) that involve new strong dynamics. After reviewing technicolor models of dynamical EWSB, and lattice gauge theory methods that are used to obtain non-perturbative predictions from strongly-interacting systems, we consider investigations of $SU(3)$ gauge theory with $N_f = 2$, 6 and 10 fermions in the fundamental representation [1, 2, 3, 4]. Our featured result is a lattice calculation of the electroweak S parameter, which we find can be significantly smaller than naïve scaling arguments would suggest, though still larger than the experimental value.

The underlying questions motivating this research concern the origins of masses for elementary particles. The explanation of elementary particles' masses has been a deep mystery since the 1960s proposal that the weak and electromagnetic interactions are combined in a unified electroweak gauge theory [5]. Although electroweak unification initially appeared incompatible with the existence of massive particles, this difficulty was overcome by the discovery that electroweak gauge invariance could be hidden through a spontaneous symmetry breaking process [6, 7, 8, 9, 10, 11]. While this generic picture of electroweak symmetry breaking has been strongly supported by experiments since the 1970s [12, 13], the dynamics underlying this process remain unknown. Understanding EWSB is a central challenge in particle physics today, and is the main goal of the CERN Large Hadron Collider (LHC).

A natural possibility is that EWSB is driven by the dynamics of some new strong force at the TeV scale [14, 15, 16]. Such dynamical EWSB results from a process much like spontaneous chiral symmetry breaking in quantum chromodynamics (QCD), the theory of

the strong nuclear force. Because perturbation theory cannot make reliable predictions for strongly-interacting theories, much of the conventional wisdom regarding dynamical EWSB relies on this superficial similarity to QCD. By making the (unjustified) assumption that new strong dynamics closely resemble the behavior of QCD, certain features of the former can be estimated from the extensive experimental information available on the strong nuclear force. Of particular interest is the electroweak S parameter [17, 18], which tightly constrains QCD-like theories of dynamical EWSB.

The value of S in a given theory is related to that theory's spectrum of vector and axial-vector states. Precision electroweak measurements provide an experimental value of S that is small or negative: for a "reference" Higgs boson mass of roughly 1 TeV, $S \approx -0.15(10)$ [13]. Taking experimental information on the spectrum of QCD and raising it to the electroweak scale produces $S = 0.32(3)$ [18]. For an $SU(N_c)$ gauge theory of new strong dynamics with N_f fermions in the fundamental representation, naïve scaling therefore suggests $S \sim 0.3\frac{N_f}{2}\frac{N_c}{3}$, in considerable disagreement with experiment even for the minimal QCD-like case with $N_f = 2$ and $N_c = 3$.

This scaling argument is "naïve" in the sense that it is not motivated by any first-principles considerations, but primarily counts degrees of freedom, assuming that they do not affect the dynamics of the theory. In fact, we know that as N_f increases for a fixed N_c, these theories behave very differently than QCD [19, 20], making QCD-based conventional wisdom unreliable. In order to determine the true theoretical status of EWSB through new strong dynamics, we need to perform non-perturbative calculations. Lattice gauge theory is the premier method for obtaining quantitatively-reliable, non-perturbative predictions from strongly-interacting theories [21, 22].

In lattice gauge theory, we discretize euclidean spacetime into a regular grid of sites connected by links. The fields and interactions described by the theory are likewise discretized, and defined on the lattice in such a way that the original theory in continuous space and time is recovered when the lattice is taken to be infinitely large, with its sites infinitesimally close together. In particular, we recover Lorentz invariance in the continuum

limit, while gauge invariance is exactly maintained even with non-zero "lattice spacing" between sites.

The finite number of degrees of freedom in the discretized system permits stochastic simulation of the lattice theory using high-performance computing. Numerical techniques for such simulations have steadily progressed for decades, primarily in application to QCD. Lattice QCD is a mature field, in the sense that the systematic effects of working in a discrete spacetime with a finite volume are understood and under control for most calculations (cf. recent reviews [23, 24, 25, 26, 27] and notable results [28, 29, 30, 31, 32, 33, 34]). The application of lattice gauge theory to strongly-interacting theories beyond QCD, especially theories relevant to dynamical EWSB, is undergoing rapid development [35, 36, 37, 38, 39], spurred by advances in both computing hardware and numerical algorithms. These calculations are still exploratory, and face severe practical challenges.

One difficulty that merits special note is our need for chiral symmetry on the lattice [40, 41, 42, 43, 44]. Common lattice discretizations of fermions explicitly break chiral symmetry, obscuring the spontaneous chiral symmetry breaking that drives EWSB in technicolor theories. We use domain wall fermions to address this issue [45, 46, 47, 48]. At the cost of adding a fifth dimension to the lattice, this fermion formulation decouples the continuum and chiral limits, making it possible (although computationally expensive) to recover chiral symmetry at non-zero lattice spacing.

Ongoing studies of $SU(3)$ lattice gauge theory with $N_f = 6$ and $N_f = 10$ fermions in the fundamental representation have produced very interesting results [1, 2, 3, 4], which this dissertation reports. More generally, non-perturbative explorations of strongly-interacting gauge theories other than QCD will help improve our understanding of quantum field theory itself, even if strong dynamics are not directly responsible for EWSB. Our featured result is the first lattice calculation of the S parameter in a theory other than scaled-up QCD. We find that S with $N_f = 6$ and $N_f = 10$ can be significantly smaller than QCD dynamics would suggest, though still larger than the experimental value.

Outline

We include considerable detail in this outline to help the reader locate information of interest. Briefly stated, Section 2 discusses the problem, Section 3 our methods and Section 4 our results.

In Section 2 we review electroweak gauge invariance and the spontaneous symmetry breaking process that hides it. We begin in Section 2.1 by considering the standard model, the simplest realization of this process. Some theoretically unsatisfying features of the standard model motivate the introduction of strongly-interacting alternatives in Section 2.2. We consider chiral symmetry breaking in QCD to illustrate the "technicolor" scenario in which a similar process at the electroweak scale drives EWSB. This framework must be extended to communicate EWSB to the fermions, which we discuss in Section 2.2.2. In Section 2.2.3 we briefly review some phenomenological challenges facing extended technicolor. These include tension between fermion masses and flavor-changing neutral currents, precision measurements of electroweak observables, and the large mass of the top quark. In Section 2.2.4 we argue that some of these challenges can be addressed by theories with approximately conformal ("walking") dynamics, as opposed to QCD-like behavior. We develop this concept in Section 2.3, and related to the "conformal windows" of gauge theories.

Moving on to the lattice gauge theory techniques we use in our investigations, Section 3.1 reviews the basic formulation of quantum field theories on the lattice, presenting the euclidean path integral (Section 3.1.1) and simple lattice actions for gauge fields (Section 3.1.2) and fermions (Section 3.1.3). Lattice fermions suffer from a "doubling problem", and we show how this is addressed both by Wilson fermions (which explicitly break chiral symmetry) and overlap fermions (which preserve a modified chiral symmetry at non-zero lattice spacing).

In Section 3.2 we present some numerical techniques we use in stochastic simulations, dividing the work into the generation (Section 3.2.1) and analysis (Section 3.2.2) of gauge configurations. For the former, we summarize the basic hybrid Monte Carlo (HMC) al-

gorithm. To illustrate simple lattice analyses, we discuss measurement of meson masses and decay constants as well as the chiral condensate $\langle\overline{\psi}\psi\rangle$. Next, in Section 3.2.3 we consider some of the challenges of working on the lattice, focusing on autocorrelations between measurements as well as systematic effects from working with massive fermions in a finite, discrete spacetime.

We discuss domain wall fermions (DWFs) in Section 3.3, first relating them to the overlap operator, then presenting their five-dimensional formulation in Section 3.3.1. Although DWF possess exact chiral symmetry at finite lattice spacing in the limit that this fifth dimension becomes infinitely long, numerical simulations must be performed on finite lattices, and in Section 3.3.2 we discuss the residual chiral symmetry breaking that results. Section 3.3.3 concludes this discussion by introducing the observables that enter our lattice calculation of the S parameter.

Section 4 brings together the preceding discussions to consider the application of lattice gauge theory to models of dynamical EWSB. We begin by presenting a brief overview of the field in Section 4.1.1, reviewing the goals and status of this work, as well as some of the unique challenges it faces. We then focus on the program and initial results of the Lattice Strong Dynamics (LSD) Collaboration in Section 4.1.2, and dedicate Section 4.2 to a detailed discussion of our lattice calculation of the S parameter. Section 4.2.1 presents the formulation of S parameter on the lattice, and Section 4.2.2 discusses our data and results. This discussion includes explicit consideration of the relevant systematic effects, controlling which is one of the topics of ongoing research we summarize in Section 4.2.3. Section 5 reviews the document and summarizes our conclusions.

Contributions

I carried out the work discussed in this dissertation as a member of the Lattice Strong Dynamics (LSD) Collaboration. Within the LSD Collaboration, I was responsible for:

- developing custom software to measure the lattice observables that go into the calculation of the S parameter, on top of the USQCD SciDAC software libraries;

- carrying out and validating these measurements on LSD Collaboration gauge configuration ensembles;
- analyzing these data to obtain results for S itself.

According to LSD Collaboration operating procedures, the final results were checked through independent analyses by other collaboration members. Similarly, I carried out such checks of other measurements, for example of m_{res}, Z_A and the light meson spectrum. My work on code development and validation was discussed and guided by regular collaboration conference calls and through direct communication with other collaboration members. The main aspect of LSD Collaboration work in which I did not play an active role was the generation of the gauge configurations themselves.

Results presented below for m_{res}, Z_A, vector and axial-vector current correlators Π, and related quantities such as the S parameter, are those produced by my own analyses. Although as mentioned above I also performed some investigations of the light meson spectrum, decay constants, $\langle\overline{\psi}\psi\rangle$ and other observables, analyses of these quantities by other members of the LSD Collaboration include refinements above and beyond what I implemented myself. For $N_f = 2$ and $N_f = 6$ I use those collaboration results in this dissertation, while for ongoing $N_f = 10$ investigations, I present my own results. I personally produced all figures in this document.

Chapter 2

Dynamical electroweak symmetry breaking

In this section we review the context of our studies: the as-yet-unknown mechanism responsible for the spontaneous symmetry breaking process that hides electroweak gauge invariance, $SU(2)_L \times U(1)_Y \to U(1)_{em}$. We proceed by considering the standard model (SM), which introduces a single elementary scalar field as the agent of electroweak symmetry breaking. This scalar field has not yet been experimentally observed, and combined with certain theoretically unsatisfying features of the standard model itself, this motivates us to consider models of physics beyond the standard model (BSM) in which a new strongly-interacting interaction is responsible for EWSB. Of course, these models have also have not yet been experimentally confirmed, and face theoretical challenges of their own. We conclude this section by considering ways in which at least some of these difficulties may be overcome if the strongly-interacting theory exhibits approximately conformal (walking) dynamics.

2.1 Electroweak symmetry breaking in the standard model

2.1.1 Electroweak interaction

The standard model joins the $SU(2)_L \times U(1)_Y$ electroweak theory with quantum chromodynamics [49, 50, 51], to form an $SU(3)_C \times SU(2)_L \times U(1)_Y$ gauge theory with fermions and gauge fields transforming as illustrated in Table 2.1. Our notation most closely resembles that used in [52, 53]; other useful reviews include [54, 55, 56, 57]. We omit discussion of well-known complications such as the three generations of fermions, quark mixing described by the Cabibbo–Kobayashi–Maskawa (CKM) matrix [58, 59], and massive neutrinos.

Table 2.1: Transformation properties of fermion and gauge fields in the standard model.

Field	$SU(3)_C$	$SU(2)_L$	$U(1)_Y$	Lorentz
$Q_L = \begin{pmatrix} u_L \\ d_L \end{pmatrix}$	3	2	1/6	$(\frac{1}{2}, 0)$
u_R	3	1	2/3	$(0, \frac{1}{2})$
d_R	3	1	-1/3	$(0, \frac{1}{2})$
$L_L = \begin{pmatrix} \nu_L \\ e_L \end{pmatrix}$	1	2	-1/2	$(\frac{1}{2}, 0)$
e_R	1	1	-1	$(0, \frac{1}{2})$
G_μ^A	8	1	0	$(\frac{1}{2}, \frac{1}{2})$
W_μ^a	1	3	0	$(\frac{1}{2}, \frac{1}{2})$
B_μ	1	1	0	$(\frac{1}{2}, \frac{1}{2})$

We organize the standard model lagrangian as

$$\mathcal{L}_{SM} = \mathcal{L}_g + \mathcal{L}_f + \mathcal{L}_H \tag{2.1}$$

$$\mathcal{L}_g = -\frac{1}{4} G^A_{\mu\nu} G^{A\mu\nu} - \frac{1}{4} W^a_{\mu\nu} W^{a\mu\nu} - \frac{1}{4} B_{\mu\nu} B^{\mu\nu} \tag{2.2}$$

$$\mathcal{L}_f = \sum_\psi \overline{\psi} i \not{D} \psi. \tag{2.3}$$

Here $a = 1, 2, 3$; $A = 1, \ldots, 8$; the explicit sum runs over the fermions $\psi = Q_L$, u_R, d_R, L_L, e_R; and the two-index objects are the usual field strength tensors, generically

$$F^k_{\mu\nu} = \partial_\mu F^k_\nu - \partial_\nu F^k_\mu + g f^{ijk} F^i_\mu F^j_\nu \tag{2.4}$$

with structure coefficients f^{ijk} determined by

$$[T^i, T^j] = i f^{ijk} T^k. \tag{2.5}$$

The generators $T^a = \frac{1}{2}\sigma^a$ and $T^A = \frac{1}{2}\lambda^A$, where σ^a are the Pauli matrices and λ^A are the Gell-Mann matrices. Finally, the sum over ψ in Eqn. 2.3 involves gauge-covariant

derivatives D_μ that we can read off from Table 2.1:

$$iD_\mu Q_L = \left(i\partial_\mu + g_3 T^A G_\mu^A + g_2 T^a W_\mu^a + \frac{g_1}{6} B_\mu\right) Q_L \tag{2.6}$$

$$iD_\mu u_R = \left(i\partial_\mu + g_3 T^A G_\mu^A + \frac{2g_1}{6} B_\mu\right) u_R \tag{2.7}$$

$$iD_\mu d_R = \left(i\partial_\mu + g_3 T^A G_\mu^A - \frac{g_1}{3} B_\mu\right) u_R \tag{2.8}$$

$$iD_\mu L_L = \left(i\partial_\mu + g_2 T^a W_\mu^a - \frac{g_1}{2} B_\mu\right) L_L \tag{2.9}$$

$$iD_\mu e_R = \left(i\partial_\mu - g_1 B_\mu\right) e_R. \tag{2.10}$$

Before specifying $\mathcal{L}_H$, we note some features of the theory as it currently stands. First, the gauge bosons G_μ^A, W_μ^a and B_μ all appear massless, since any mass term such as $\frac{1}{2} m_B^2 B_\mu B^\mu$ is not invariant under a gauge transformation $B_\mu \to B_\mu - \frac{1}{g_1}\partial_\mu \chi$.

Similarly, all fermions appear to be massless as well, due to the transformation properties in Table 2.1. Fermion mass terms have the form

$$m_\psi \overline{\psi}\psi = m_\psi \left(\overline{\psi}_L \psi_R + \overline{\psi}_R \psi_L\right), \tag{2.11}$$

where $\psi_R = \frac{1}{2}(1+\gamma_5)\psi \equiv P_R \psi$ and $\psi_L = \frac{1}{2}(1-\gamma_5)\psi \equiv P_L \psi$ are right- and left-handed fermion fields, respectively. Because the standard model is a chiral gauge theory in which right- and left-handed fermions are in different representations, we cannot construct gauge-invariant fermion mass terms using only the fields listed in Table 2.1.

Based on these considerations, it appears that chiral gauge theories such as the electroweak theory are unable to describe massive fermion and gauge boson fields. Ref. [5], which introduced the $SU(2)_L \times U(1)_Y$ electroweak theory, noted this feature as its "principal stumbling block", and this is the content of our statement in Section 1 that "electroweak unification initially appeared incompatible with the existence of massive particles".

2.1.2 Electroweak symmetry breaking

Clearly, the purpose of $\mathcal{L}_H$ in the standard model lagrangian Eqn. 2.1 is to overcome this stumbling block and allow the theory to describe the massive fields observed in nature.

We accomplish this by introducing a (complex) elementary scalar doublet $\Phi = \begin{pmatrix} \phi^+ \\ \phi^0 \end{pmatrix}$ transforming in the $(1, 2, 1/2)$ representation of $SU(3)_C \times SU(2)_L \times U(1)_Y$, with a gauge-invariant potential engineered to produce spontaneous (global) symmetry breaking,

$$\mathcal{L}_H = (D_\mu \Phi)^\dagger (D^\mu \Phi) + \mu^2 \Phi^\dagger \Phi - |\lambda| (\Phi^\dagger \Phi)^2 + \mathcal{L}_Y. \tag{2.12}$$

(We will return to the Yukawa interactions represented by $\mathcal{L}_Y$.) We have written the $\Phi^\dagger \Phi$ term with a positive sign to emphasize that the true vacuum state of the theory is not $\Phi = 0$, but can be chosen by a gauge transformation to be

$$\langle \Phi \rangle = \frac{1}{\sqrt{2}} \begin{pmatrix} 0 \\ v \end{pmatrix}, \tag{2.13}$$

where $v = \sqrt{\mu^2/|\lambda|}$. Numerically, $v = (G_F \sqrt{2})^{-1/2} \approx 246$ GeV, where $G_F = 1.16637(1) \times 10^{-5}$ GeV^{-2} is the Fermi constant. In essence, we are generalizing the Ginzburg–Landau model of superconductivity [60] to a relativistic theory with gauge group $SU(2)_L \times U(1)_Y$.

A generic $SU(2)_L \times U(1)_Y$ gauge transformation

$$\frac{e^{i\chi^a(x) T^a + i\beta(x)/2}}{\sqrt{2}} \begin{pmatrix} 0 \\ v \end{pmatrix} \tag{2.14}$$

would leave the vacuum $\langle \Phi \rangle$ invariant if $\chi^1 = \chi^2 = 0$ while $\chi^3 = \beta$, which shows that the spontaneous symmetry breaking preserves a $U(1)$ subgroup of $SU(2)_L \times U(1)_Y$, which we identify with electromagnetism. The other three independent gauge transformations correspond to the Nambu–Goldstone bosons (NGBs) expected from the three broken generators of $SU(2)_L \times U(1)_Y \to U(1)_{em}$ [61, 62, 63].

We now parameterize

$$\Phi(x) = \frac{U(x)}{\sqrt{2}} \begin{pmatrix} 0 \\ v + h(x) \end{pmatrix} \to \frac{1}{\sqrt{2}} \begin{pmatrix} 0 \\ v + h(x) \end{pmatrix}, \tag{2.15}$$

where $h(x)$ is a real scalar field (the Higgs boson) with mass $m_h = \sqrt{2}\mu = v\sqrt{2\lambda}$, and $U(x)$ is a gauge transformation that we choose to be $U(x) = 1$ (the "unitary gauge"). This choice of gauge appears to have removed the NGBs from the theory, but the remarkable fact noted by Refs. [6, 7, 8, 9, 10, 11], building on earlier work in the context of superconductivity [64, 65, 66, 67], is that the would-be-NGBs reappear as the longitudinal degrees of freedom of massive gauge bosons. The gauge boson masses come from the kinetic term $(D_\mu\Phi)^\dagger(D^\mu\Phi)$, which involves the gauge-covariant derivative

$$iD_\mu\Phi = \left(i\partial_\mu + g_2 T^a W_\mu^a + \frac{g_1}{2}B_\mu\right)\Phi. \tag{2.16}$$

The relevant terms (since here we are not interested in exploring the couplings of the Higgs boson to the gauge bosons) are

$$\begin{aligned}
\Delta\mathcal{L}_{mass} &= \frac{1}{8}\begin{pmatrix} 0 & v \end{pmatrix}\begin{pmatrix} g_2 W_\mu^3 + g_1 B_\mu & g_2(W_\mu^1 - iW_\mu^2) \\ g_2(W_\mu^1 + iW_\mu^2) & -g_2 W_\mu^3 + g_1 B_\mu \end{pmatrix}^2 \begin{pmatrix} 0 \\ v \end{pmatrix} \\
&\equiv \frac{g_2^2 v^2}{8}\begin{pmatrix} 0 & 1 \end{pmatrix}\begin{pmatrix} \sqrt{g_2^2+g_1^2}A_\mu/g_2 & \sqrt{2}W_\mu^+ \\ \sqrt{2}W_\mu^- & -\sqrt{g_2^2+g_1^2}Z_\mu/g_2 \end{pmatrix}^2 \begin{pmatrix} 0 \\ 1 \end{pmatrix} \\
&\equiv m_W^2 W_\mu^+ W^{-\mu} + \tfrac{1}{2}m_Z^2 Z_\mu Z^\mu.
\end{aligned} \tag{2.17}$$

In the second line, we define

$$W_\mu^\pm \equiv \frac{W_\mu^1 \mp iW_\mu^2}{\sqrt{2}} \qquad Z_\mu \equiv \frac{g_2 W_\mu^3 - g_1 B_\mu}{\sqrt{g_2^2+g_1^2}} \qquad A_\mu \equiv \frac{g_2 W_\mu^3 + g_1 B_\mu}{\sqrt{g_2^2+g_1^2}} \tag{2.18}$$

corresponding to the physical $W^\pm$, Z and photon, respectively. The photon is massless, and the masses of the $W^\pm$ and Z are

$$m_W = \frac{1}{2}g_2 v \qquad\qquad m_Z = \frac{\sqrt{g_2^2+g_1^2}}{2}v \equiv \frac{m_W}{\cos\theta_w}, \tag{2.19}$$

where we define the weak mixing angle

$$\cos\theta_w = \frac{g_2}{\sqrt{g_2^2+g_1^2}} \qquad\qquad \sin\theta_w = \frac{g_1}{\sqrt{g_2^2+g_1^2}} \tag{2.20}$$

Finally, in the standard model fermion masses are also obtained by introducing just this single field Φ with the spontaneous symmetry breaking potential of Eqn. 2.12. All we need are the gauge-invariant Yukawa interactions stored in $\mathcal{L}_Y$,

$$\mathcal{L}_Y = -\sum_{\psi} \lambda_\psi \left\{ \left(\overline{\psi}_L \cdot \Phi\right) \psi_R + \overline{\psi}_R \left(\Phi^\dagger \cdot \psi_L\right) \right\}, \tag{2.21}$$

where λ_ψ is an arbitrary dimensionless coupling for each fermion field ψ. The fermion mass is now obtained by expanding around the vacuum of Eqn. 2.13,

$$\mathcal{L}_Y = -\sum_{\psi} \frac{\lambda_\psi v}{\sqrt{2}} \left\{ \overline{\psi}_L \cdot \begin{pmatrix} 0 \\ 1 \end{pmatrix} \psi_R + \overline{\psi}_R \begin{pmatrix} 0 & 1 \end{pmatrix} \cdot \psi_L \right\} \tag{2.22}$$

$$\Rightarrow m_\psi = \frac{1}{\sqrt{2}} \lambda_\psi v. \tag{2.23}$$

While electroweak symmetry breaking is necessary for fermion masses generation, it is not a sufficient condition, and there is no requirement that the agent of EWSB also provide masses to the fermions. The fact that Φ plays both roles in the standard model makes this theory pleasantly simple and efficient.

2.1.3 Theoretically unsatisfying features of the standard model

Of course, theoretical simplicity is not the reason the model discussed above became the standard model of particle physics. The $SU(2)_L \times U(1)_Y \rightarrow U(1)_{em}$ EWSB framework in general predicted the existence of the weak neutral current discovered in 1973 [68, 69], and explained charged and neutral weak currents in terms of massive $W^\pm$ and Z gauge bosons experimentally observed roughly a decade later [70, 71, 72, 73, 74]. More pertinent to the standard model itself was the excellent agreement that gradually developed between precise measurements of a wide variety of observables and the predictions of the theory [12].

(The demonstration that the standard model is renormalizable also contributed to its appeal [75], but this fact holds less significance in the context of present-day attitudes concerning effective field theories.) At present, the standard model is consistent with all experimental data [76, 13]. Although global electroweak fits prefer a Higgs boson mass ($m_h \approx 95$ GeV) that has been experimentally excluded by direct searches, a range of possibilities 120 GeV $\lesssim m_h \lesssim$ 150 GeV remains viable [77].

Despite the continued phenomenological success of the standard model, there is broad consensus that this theory is likely to break down around the TeV-scale energies that are now being probed at the CERN Large Hadron Collider (LHC). (Of course the standard model does not provide a quantum theory of gravity, but the most natural scale for such physics is the Planck scale $M_{Pl} \sim 10^{19}$ GeV, well above the TeV scale.) In part, this is due to the discovery of phenomena such as dark matter that cannot be explained by the standard model [78]. In addition, there are several aspects of the standard model that are widely considered theoretically unsatisfying.

To motivate considering theories beyond the standard model, we will qualitatively review some of these arguments. The first is that although the standard model provides a description of EWSB, it does not provide any dynamical explanation of the process. Instead, the scalar field Φ and its potential in Eqn. 2.12 are introduced by hand in order to produce spontaneous symmetry breaking. All fermion masses and mixings are likewise arbitrary free parameters, and the Yukawa couplings in Eqn. 2.22 range over many orders of magnitude from $y_t \simeq 1$ for the top quark to $y_e \simeq 10^{-6}$ for the electron (and even smaller if the same framework is extended to accommodate non-zero neutrino masses). The simple fact that Φ is even an elementary scalar field may cause concern, since all known elementary particles are either fermions or gauge bosons.

The triviality of scalar field theory in four dimensions may explain why no elementary scalar fields have yet been observed. Triviality is the statement that the β function describing the scale dependence of the coupling $\lambda(\mu)$ in Eqn. 2.12 is positive [79, 80]. In

perturbation theory, the leading-order term is

$$\beta(\lambda) = \mu\frac{\partial\lambda}{\partial\mu} = \frac{3\lambda^2}{2\pi^2} + \mathcal{O}(\lambda^3) > 0. \tag{2.24}$$

(Comparable results hold non-perturbatively, established by both analytical considerations [81, 82, 83], and numerical lattice simulations [84, 85, 86, 87, 88, 89].) This requires that the standard model be considered an effective field theory valid only up to some scale Λ_{new} at which new physics become important. Solving Eqn. 2.24 then gives

$$\lambda(\mu) \approx \left[\frac{1}{\lambda(\Lambda_{new})} + \frac{3}{2\pi^2}\log\left(\frac{\Lambda_{new}}{\mu}\right)\right]^{-1} < \frac{2\pi^2}{3\log\left(\Lambda_{new}/\mu\right)}, \tag{2.25}$$

showing how the coupling flows to the trivial fixed point $\lambda \to 0$ as $\frac{\mu}{\Lambda_{new}} \to 0$. The connection between the coupling and the Higgs boson mass $m_h = v\sqrt{2\lambda}$ requires that $m_h \lesssim 700$ GeV in order for the theory to have any range of validity. If we want the standard model to be valid up to the Plank scale around which quantum gravitational effects should become important, we need $m_h \lesssim 200$ GeV [89].

There is another problem with trying to push the cutoff Λ_{new} up to very high scales, namely that quantum corrections make m_h^2 quadratically sensitive to Λ_{new}^2. In the absence of some new physics to stabilize the electroweak scale, extreme fine-tuning is necessary to maintain a large hierarchy between m_h and Λ_{new}. Supersymmetry is a popular way to stabilize the electroweak scale, but supersymmetric models accomplish this by introducing a large number of elementary scalar fields, along with $\mathcal{O}(100)$ new free parameters [90].

These considerations lead to the general expectation that some new physics will be found around the TeV scale. To motivate the form of new physics we consider, let us conclude this section by recalling our comment above that the standard model is a generalization of Ginzburg–Landau phenomenology. In the microscopic theory of superconductivity due to Bardeen, Cooper and Schrieffer (BCS) [91, 92], the scalar order-parameter field of Ginzburg and Landau is supplanted by the dynamics of the fundamental fermionic degrees of freedom. In the next section we will see how something similar can be done to obtain

electroweak symmetry breaking without a elementary scalar fields.

2.2 New strong dynamics

Motivated by the considerations above, we want to consider theories in which electroweak symmetry breaking is due to the dynamics of elementary fermion fields. Specifically, we will focus on "technicolor" (TC) theories in which dynamical EWSB results from chiral symmetry breaking (χSB) in a new, strongly-interacting sector. We begin by considering quantum chromodynamics (QCD) as a concrete example of χSB due to strong interactions, and show how this process can produce EWSB. Then we need to extend the framework to accommodate fermion masses, which leads us to a discussion of some phenomenological challenges that this approach faces. We conclude this section by considering how at least some of these challenges may be addressed if the running coupling of the theory evolves very slowly, or "walks". Recent reviews of technicolor and related theories include Refs. [93, 94, 95, 96, 97, 98].

2.2.1 Technicolor

It is instructive to begin our discussion of technicolor by considering what would happen if we were to remove $\mathcal{L}_H$ from Eqn. 2.1, but leave the rest of the theory the same (still considering, for simplicity, a single generation) [52, 99]. Then the theory possesses a global $SU(2)_L \times SU(2)_R$ chiral symmetry that is spontaneously broken to the vector subgroup $SU(2)_V$ by the strong QCD interaction [61, 62, 100]. This is described by the appearance of a non-zero vacuum expectation value for the chiral condensate

$$\langle \overline{\psi}\psi \rangle = \langle \overline{\psi}_L \psi_R + \overline{\psi}_R \psi_L \rangle \neq 0. \tag{2.26}$$

Let us see how this spontaneous chiral symmetry breaking produces electroweak symmetry breaking.

Three massless Nambu–Goldstone bosons (the pions π^a) appear as a result of chiral symmetry breaking, in terms of which we can formulate an effective low-energy field theory

known as chiral perturbation theory (χPT) [101, 102]. The leading-order chiral lagrangian including electroweak interactions is

$$\mathcal{L}_\chi = \frac{F^2}{4}\mathrm{Tr}\left[(D_\mu\Sigma)^\dagger D^\mu\Sigma\right] - \frac{1}{4}W^a_{\mu\nu}W^{a\mu\nu} - \frac{1}{4}B_\mu B^\mu, \tag{2.27}$$

where the gauge kinetic terms are the same as in Eqn. 2.2 and

$$\Sigma = \exp\left(\frac{4i}{F}T^a\pi^a\right). \tag{2.28}$$

The flavor matrices T^a are the same as in Eqn. 2.5. Because the pions are exact NGBs ($m_\pi = 0$) in this calculation, F can be identified with the pion decay constant f_π defined by

$$\langle 0|A^a_\mu(x)|\pi^b(p)\rangle = ip_\mu f_\pi \delta^{ab} e^{-ip\cdot x}, \tag{2.29}$$

where p is the momentum of the pion and $A^a_\mu(x)$ is the axial-vector current

$$A^a_\mu(x) = \overline{\psi}(x)\gamma_\mu\gamma^5 T^a\psi(x). \tag{2.30}$$

The covariant derivative for the field Σ is [103]

$$iD_\mu\Sigma = \left(i\partial_\mu + g_2T^aW^a_\mu - g_1T^3B_\mu\right)\Sigma = \left(-\frac{4}{F}T^a\partial_\mu\pi^a + g_2T^aW^a_\mu - g_1T^3B_\mu\right)\Sigma, \tag{2.31}$$

where the $SU(2)_L$ gauge fields W^a_μ act only on the left of Σ.

We now expand $\frac{F^2}{4}\mathrm{Tr}\left[(D_\mu\Sigma)^\dagger D^\mu\Sigma\right]$ much as we expanded $(D_\mu\Phi)^\dagger(D^\mu\Phi)$ in the standard model (Eqn. 2.17). Applying $\left\{T^a, T^b\right\} = \frac{1}{2}\delta^{ab}$ and neglecting terms proportional to $[\Sigma, T^3]$, we have

$$\Delta\mathcal{L}_{mass} = 2(\partial_\mu\pi^a)^2 - F(\partial_\mu\pi^a)W^{a\mu} + \frac{F^2g_2^2}{8}(W^a_\mu)^2 + \frac{F^2g_1^2}{8}B^2_\mu + F(\partial_\mu\pi^3)B^\mu - \frac{Fg_2g_1}{4}W^3_\mu B^\mu. \tag{2.32}$$

By changing variables to

$$A^a_\mu \equiv \left\{W^1_\mu, W^2_\mu, W^3_\mu - \frac{g_1}{g_2}B_\mu\right\}, \tag{2.33}$$

we obtain

$$\Delta\mathcal{L}_{mass} = \frac{F^2 g_2^2}{8}\left(A_\mu^a - \frac{4}{F g_2}\partial_\mu \pi^a\right)\left(A^{a\mu} - \frac{4}{F g_2}\partial^\mu \pi^a\right), \tag{2.34}$$

gauge boson mass terms for the fields $\widetilde{W}_\mu^a = A_\mu^a - \frac{4}{F g_2}\partial_\mu \pi^a$. Accounting for the effects of the field redefinition Eqn. 2.33 on the gauge field kinetic terms produces exactly the same massive $W^\pm$ and Z gauge bosons as in the standard model,

$$\Delta\mathcal{L}_{mass} = \frac{F^2 g_2^2}{4} W_\mu^+ W^{-\mu} + \frac{F^2(g_2^2+g_1^2)}{8} Z_\mu Z^\mu \equiv m_W^2 W_\mu^+ W^{-\mu} + \tfrac{1}{2} m_Z^2 Z_\mu Z^\mu \tag{2.35}$$

$$m_W = \frac{1}{2} g_2 F \qquad\qquad m_Z = \frac{\sqrt{g_2^2+g_1^2}}{2} F = \frac{m_W}{\cos\theta_w}, \tag{2.36}$$

if we identify $F = v = 246$ GeV to match Eqn. 2.19.

Before proceeding, we note a few important features of this calculation. First, the pions were exact Nambu–Goldstone bosons with $m_\pi = 0$. When we work on the lattice, we are not able to directly simulate massless pions, and have to extrapolate to the chiral limit. Less obviously, the pions possessed the appropriate quantum numbers to be "eaten" by the gauge bosons because of the electroweak $SU(2)_L \times U(1)_Y$ charges of the quark fields Q_L, u_R and d_R (Table 2.1). If more than two flavors of the massless strongly-interacting fermions were charged in this way under the electroweak interaction, chiral symmetry breaking would produce more than the three pions eaten by the $W^\pm$ and Z. Phenomenology requires that any additional would-be NGBs obtain masses of $\mathcal{O}(100\text{GeV})$ through interactions with other sectors of the theory; we refer to these massive pseudoscalars as pseudo-Nambu–Goldstone bosons (PNGBs).

Historically, Refs. [104, 105] introduced the idea that a strongly-coupled non-vectorial gauge theory could spontaneously break a global symmetry and obtain massive gauge bosons from the resulting NGBs, while Ref. [106] showed the relation $m_Z \cos\theta_w = m_W = g_2 F/2$ for the case of $SU(2) \times U(1)$. Refs. [14, 15, 16] added the final ingredient of the first technicolor models, the idea of a new, asymptotically-free gauge theory that becomes strongly coupled around the electroweak scale $v = 246$ GeV. At least one pair of N_f

massless technifermions charged under this new interaction form an electroweak doublet, so that chiral symmetry breaking dynamics drive electroweak symmetry breaking.

For the purposes of this dissertation, we will take the technicolor gauge group to be $SU(N_c)$; with $N_c > 2$, the chiral symmetry breaking pattern $SU(N_f)_L \times SU(N_f)_R \to SU(N_f)_V$ produces $N_f^2 - 1$ NGBs. $N_f^2 - 4$ of them must become PNGBs with masses obtained from other interactions, as mentioned above and discussed in more detail below. Notationally, we will use capital letters (T, U, D) to refer to technifermions, and $N_D \geq 1$ to refer to the number of electroweak doublets in the technicolor sector. It is simplest to put every left-handed technifermion into an electroweak doublet, $N_D = N_f/2$, but this is not necessary so long as anomaly cancellation can be satisfied.

2.2.2 Extended technicolor

Technicolor as discussed above addresses most of the criticisms of the standard model raised in Section 2.1.3: no elementary scalar fields have been introduced, the theory is asymptotically free, and there is no hierarchy problem destabilizing the electroweak scale. However, we have yet to see how fermion masses and mixings can be accommodated in the technicolor framework.

In order to avoid the reintroduction of elementary scalar fields, the typical technicolor approach to explaining fermion masses proposes another new gauge interaction under which both technifermions as well as the quarks and leptons are charged, and are in the same representations [107, 108]. (For a brief review of some TC models that do reintroduce scalar fields, bosonic technicolor and supersymmetric technicolor, see Ref. [93] and references therein.) Exchange of ETC gauge bosons then generates quark and lepton masses as illustrated in Fig. 2·1. This extended technicolor (ETC) gauge interaction is also assumed to be asymptotically free, and dynamically broken to $SU(N_c)_{TC} \times SU(3)_C \times SU(2)_L \times U(1)_Y$ at some very high scale $\Lambda_{ETC} \gg v$. This gives the as-yet-unobserved ETC gauge bosons very large masses $M_{ETC} \sim g_{ETC}\Lambda_{ETC}$, where g_{ETC} is the ETC gauge coupling, which we expect to be strong $g_{ETC} \sim 1$ at the scale M_{ETC}.

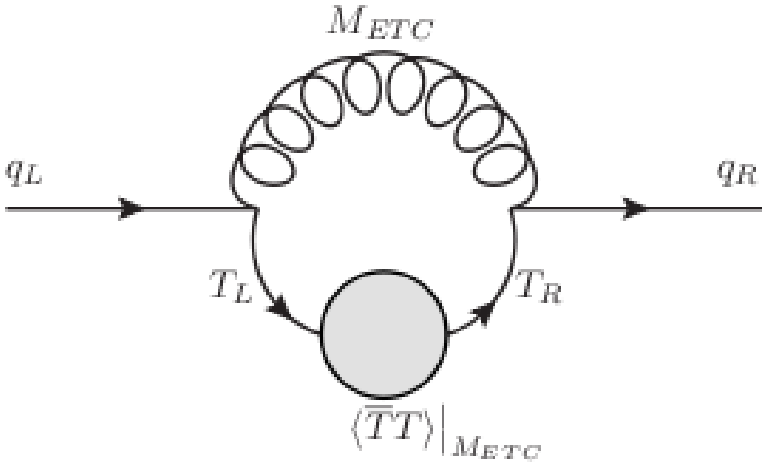

Figure 2·1: Diagram illustrating how extended technicolor theories generate fermion masses through the exchange of massive ETC gauge bosons.

The situation is in fact very complicated. To naturally account for large hierarchies between the various quark and lepton masses, ETC models often assume a sequence of dynamical symmetry breakings at several scales, at least one for each of the three generations [109]. Due to the lack of direct information on ETC dynamics, the strong interactions involved, and the stringent experimental information on quark and lepton masses, mixings, CP violation, etc., no reasonably realistic ETC model exists. This is not surprising, given that ETC seeks to solve the "flavor problem" responsible for the considerable majority of the free parameters in the standard model. For our purposes, we can simply integrate out all the massive ETC gauge bosons, and consider the resulting effective field theory at much lower scales $\Lambda \ll M_{ETC}$.

After integrating out the massive ETC gauge bosons, we are left with effective four-fermion interactions involving technifermions (T), quarks and leptons (q), which we can collect into the generic operators [93, 96]

$$\frac{g_{ETC}^2}{M_{ETC}^2}\left\{\alpha_{ab}(\overline{T}\gamma_\mu t^a T)(\overline{T}\gamma^\mu t^b T) + \beta_{ab}(\overline{T}\gamma_\mu t^a T)(\overline{q}\gamma^\mu t^b q) + \gamma_{ab}(\overline{q}\gamma_\mu t^a q)(\overline{q}\gamma^\mu t^b q)\right\} \qquad (2.37)$$

where t^a label the ETC generators and α_{ab}, β_{ab} and γ_{ab} are dimensionless coefficients. The β_{ab} terms in Eqn. 2.37 connect the quarks and leptons to the technifermions, and produce

generic quark and lepton masses [94]

$$m \simeq \frac{g_{ETC}^2}{M_{ETC}^2} \left\langle \overline{T}T \right\rangle \big|_{M_{ETC}} . \tag{2.38}$$

Here the mass and technifermion condensate $\left\langle \overline{T}T \right\rangle$ are both renormalized at the scale M_{ETC}, since asymptotic freedom implies that the dominant momentum running around the loop is $\mathcal{O}(M_{ETC})$ [110, 111, 112]. We omit the "$|_{M_{ETC}}$" label on m since below M_{ETC} the technicolor and flavor sectors decouple, and the running of m is given by the QCD logarithmic evolution, which we neglect here. At scales $\mu > M_{ETC}$, the quark and lepton masses fall off more rapidly, at least as fast as $1/\mu$ [94].

The scale-dependence of $\left\langle \overline{T}T \right\rangle$ is not as clear-cut, since it depends on the anomalous dimension $\gamma_m(\alpha(\mu))$ of the operator $\overline{T}T$, which in turn depends on the running coupling $\alpha(\mu) = g(\mu)^2/(4\pi)$. In the conventions of naïve dimensional analysis [113, 114], around the electroweak scale $v \ll M_{ETC}$

$$\left\langle \overline{T}T \right\rangle \big|_{\Lambda_{TC}} \simeq 4\pi (v/\sqrt{N_D})^3, \tag{2.39}$$

where $\Lambda_{TC} \simeq 4\pi v/\sqrt{N_D}$ and N_D is the number of electroweak doublets.[1] The evolution of $\left\langle \overline{T}T \right\rangle$ from Λ_{TC} to M_{ETC} is given by its renormalization group equation

$$\left\langle \overline{T}T \right\rangle \big|_{M_{ETC}} = \left\langle \overline{T}T \right\rangle \big|_{\Lambda_{TC}} \exp\left(\int_{\Lambda_{TC}}^{M_{ETC}} \frac{d\mu}{\mu} \gamma_m(\alpha(\mu)) \right) , \tag{2.40}$$

where we ignore all interactions except for technicolor. If technicolor behaves like QCD, then $\gamma_m(\alpha(\mu))$ is negligible for μ much above Λ_{TC}, and we can approximate $\left\langle \overline{T}T \right\rangle \big|_{M_{ETC}} \approx \left\langle \overline{T}T \right\rangle \big|_{\Lambda_{TC}}$. We will revisit this issue in Section 2.2.4 below.

Similar considerations allow us to obtain masses for the pseudo-Nambu–Goldstone

[1] Due to the factor of $v/\sqrt{N_D}$, models with large N_D are known as low-scale technicolor (LSTC). Refs. [115, 116, 117] use the requirement that the technifermions, quarks and leptons all transform together in a few ETC representations [108], to suggest that N_D is generically large. Experimental searches for technihadrons usually consider LSTC models [118, 119, 120].

bosons from the α_{ab} terms in Eqn. 2.37, which connect four technifermions,

$$M_{PNGB}^2 \simeq \frac{g_{ETC}^2}{M_{ETC}^2} \left\langle \overline{T}T\overline{T}T \right\rangle \Big|_{M_{ETC}} . \tag{2.41}$$

For large N_c, we can approximate $\left\langle \overline{T}T\overline{T}T \right\rangle \simeq \left\langle \overline{T}T \right\rangle^2$. Finally, the γ_{ab} terms in Eqn. 2.37, which involve only quark and lepton fields, represent potentially dangerous flavor-changing neutral currents (FCNCs). Stringent constraints on FCNC processes provide some of the most severe phenomenological challenges for extended technicolor.

2.2.3 Challenges

In this section we review some phenomenological challenges facing (extended) technicolor theories as introduced above. In the next section, we consider possible means to address at least some of these difficulties in the framework of walking technicolor.

Flavor-changing neutral currents

Notable flavor-changing neutral current processes include $\mu \to ee\overline{e}$, $\mu \to e\gamma$, $K_L \to \mu e$, and mixing between the neutral mesons $\overline{K}$–K, $\overline{D}$–D, $\overline{B}$–B and $\overline{B}_s$–B_s. Here we qualitatively discuss the implications of these processes for extended technicolor, omitting detailed calculations. The essential difficulty is the ETC prediction that both FCNC observables as well as quark, lepton and PNGB masses are proportional to M_{ETC}^{-2}, since they are all dominated by the operators in Eqn. 2.37. Experimental limits on FCNC processes therefore imply limits on the quark and lepton masses obtainable from Eqn. 2.38 and the PNGB masses obtainable from Eqn. 2.41.

For example, if we assume ETC interactions do not contribute to CP violation, then limits on $\overline{D}$–D mixing [121] imply $M_{ETC}^{(c)} \gtrsim 1.5 \times 10^3$ TeV [122], where $^{(c)}$ indicates that this constraint is specific to the ETC interactions responsible for the charm quark mass. The resulting limit on the charm quark mass is $m_c \lesssim 1$ MeV, far below its physical value. (As discussed below Eqn. 2.38, this mass is defined at the scale $M_{ETC}^{(c)}$, but varies only logarithmically for energy scales down to $\Lambda_{QCD} \sim 1$ GeV where strong QCD effects start

to become important.) If ETC interactions are CP-violating, as they may well be, then constraints on the imaginary part of the $\overline{K}$–K mass matrix lead to the limits $M_{ETC}^{(s)} \gtrsim 10^4$ TeV and $m_s \lesssim 0.1$ MeV. If the theory possesses any PNGBs, they would receive masses of at most $\mathcal{O}$(GeV), far smaller than experimental bounds.

These limits assume that the ETC interactions introduce unsuppressed tree-level FCNCs. At least some ETC contributions to FCNC processes must be present in order for extended technicolor to produce the CKM mixing matrix. While approximate flavor symmetries could suppress these FCNCs, in a way similar to the Glashow–Iliopoulos–Maiani mechanism [123], ETC models attempting to incorporate this feature are (like most ETC models) extremely complicated and little developed [124, 125, 93, 126, 127].

FCNCs are formally a problem of extended technicolor and flavor physics, as opposed to technicolor as a theory of electroweak symmetry breaking. However, because ETC is the natural means to communicate EWSB to the quarks and leptons in the TC framework, FCNCs can be considered a reasonable means of constraining the entire approach.

Precision electroweak observables

Precision electroweak observables are quantities that we can use to search for the effects of physics beyond the standard model, and thereby constrain BSM theories. This approach has received much attention over the past couple of decades, due to the continuing lack of direct evidence that would reveal the physics responsible for electroweak symmetry breaking. The Higgs boson of the standard model remains undiscovered, as do the new particles predicted by supersymmetric theories, technicolor, and other models of BSM physics. Technicolor models, for example, predict a number of so-called technihadrons (bound states of technifermions), the lightest of which include analogs of the ρ, ω and a_1 mesons of QCD. As discussed in Section 2.2.1 above, there may also be a number of massive pseudo-Nambu–Goldstone bosons.

While we expect experiments at the CERN Large Hadron Collider to find evidence for such particles if they do exist [128, 129, 130] (and experiments at the Fermilab Teva-

tron have made progress constraining their possible masses [13, 118, 119, 120]), precision electroweak observables make it possible to constrain BSM theories with already-existing data. These data encompass a variety of electroweak processes (from Z boson decays to neutrino scattering to atomic parity violation [13]), and to make possible simple comparisons between theories and experiment, are typically represented by a small number of parameters.

The most commonly used parameterization of precision electroweak observables as S, T and U was introduced by Peskin and Takeuchi [17, 131, 18], building on the formalism of Refs. [132, 133]. Other equivalent formulations were presented around the same time [134, 135, 136, 137], and such parameterizations can be related to the electroweak chiral lagrangian introduced much earlier [138, 139, 140, 103]. In the remainder of this section we introduce the Peskin–Takeuchi parameterization, and qualitatively review its implications for technicolor. We will have much more to say about the S parameter in Section 4.2 below.

The S, T and U parameters represent the contributions of BSM physics to the vacuum polarization functions shown in Fig. 2·2. In this figure, we imagine that each of the gauge boson propagators appears as an internal line with momentum Q in diagrams describing some scattering process such as $e^+e^- \to e^+e^-$. (In anticipation of working on the lattice, we consider euclidean $Q^2 = -q^2 > 0$.) Because these processes only modify the gauge boson propagators, they are sometimes called "oblique" corrections as opposed to the "direct" (vertex and box) corrections that involve the external fermions not shown in Fig. 2·2.

Fig. 2·2 shows how the diagrams are related to the transverse electroweak vacuum polarization functions $\Pi(Q^2)$, which we can define in terms of current correlators as

$$\Pi_{ij}^{\mu\nu}(Q) \equiv \int d^4x e^{iQ\cdot x} \left\langle J_i^\mu(x) J_j^\nu(0) \right\rangle = \delta^{\mu\nu}\Pi_{ij}(Q^2) - \frac{Q^\mu Q^\nu}{Q^2}[\Pi_{ij}(Q^2) + \Pi_{ij}^L(Q^2)], \quad (2.42)$$

where $\Pi_{ij}(Q^2)$ and $\Pi_{ij}^L(Q^2)$ are the transverse and longitudinal components of $\Pi_{ij}^{\mu\nu}(Q)$,

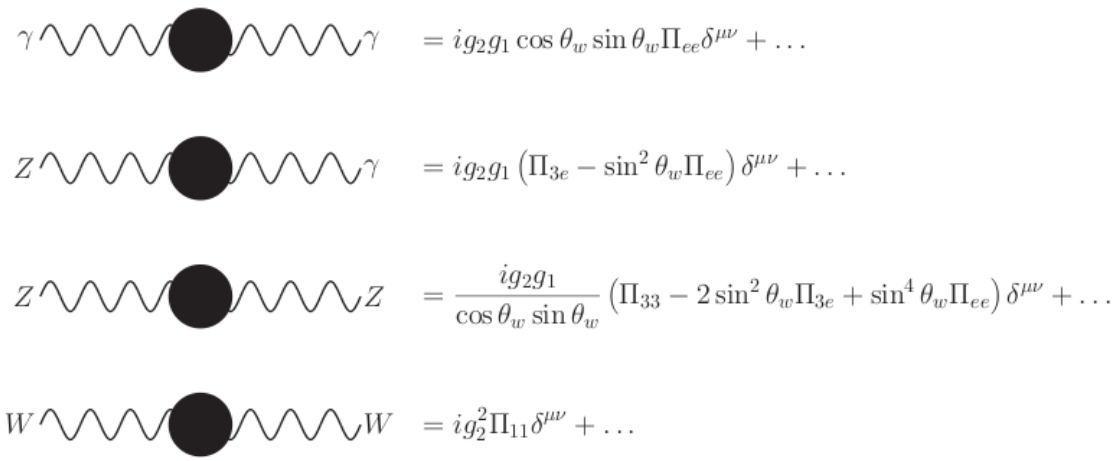

Figure 2·2: Electroweak vacuum polarization amplitudes (oblique corrections), omitting terms that involve higher powers of the small Πs.

respectively.[2] In terms of these functions,

$$S = 16\pi \frac{d}{dQ^2}\left[\Pi_{3e}^{(new)}(Q^2) - \Pi_{33}^{(new)}(Q^2)\right]_{Q^2=0} = 4\pi \frac{d}{dQ^2}\left[\Pi_{VV}^{(new)}(Q^2) - \Pi_{AA}^{(new)}(Q^2)\right]_{Q^2=0} \tag{2.43}$$

$$T = \frac{4\pi}{\sin^2\theta_w \cos^2\theta_w m_Z^2}\left[\Pi_{11}^{(new)}(0) - \Pi_{33}^{(new)}(0)\right] \tag{2.44}$$

$$U = \pi \frac{d}{dQ^2}\left[\Pi_{11}^{(new)}(Q^2) - \Pi_{33}^{(new)}(Q^2)\right]_{Q^2=0}, \tag{2.45}$$

where in the first line we have introduced the vector and axial correlators via

$$\Pi_{33} = \left(\Pi_{VV} + \Pi_{AA}\right)/4 \qquad\qquad \Pi_{3e} = \Pi_{VV}/2. \tag{2.46}$$

Qualitatively, T represents violations of the "custodial" $SU(2)_V$ isospin symmetry that guarantees $m_W = m_Z \cos\theta_w$, while S can be thought of as an isospin-symmetric measure of the size of the sector responsible for electroweak symmetry breaking. The S parameter places the tightest constraints on technicolor theories. Most models predict U to be very small, and in effective field theories based on the standard model it corresponds to a

[2] These conventions follow Ref. [18]; some other authors (including Refs. [141, 142]) define the transverse component of $\Pi_{ij}^{\mu\nu}(Q)$ as $Q^2\Pi^{(1)}(Q^2)$, and the longitudinal component as $Q^2\Pi^{(0)}(Q^2)$.

dimension-eight operator, while S and T correspond to the dimension-six operators [143, 144]

$$\frac{Sg_2g_1}{8\pi v^2}\Phi^\dagger T^a \Phi W^a_{\mu\nu} B^{\mu\nu} \qquad\qquad -\frac{Tg_2g_1\cos\theta_w\sin\theta_w}{2\pi v^2}|\Phi^\dagger D_\mu \Phi|^2 \tag{2.47}$$

where Φ is the scalar doublet introduced in Eqn. 2.12 and v is its vacuum expectation value. Alternately, in chiral perturbation theory we have

$$\frac{S}{16\pi}\mathrm{Tr}\left[T^a W^a_{\mu\nu}\Sigma B^{\mu\nu} T^3 \Sigma^\dagger\right]. \tag{2.48}$$

As an aside, we mention that there are two other dimension-six operators we do not discuss here, which correspond to parameters called Y and W [145].

The superscripts $^{(new)}$ in Eqns. 2.43 through 2.45 are meant to remind us that we are interested only in the contributions from new physics beyond the standard model. Because loops of Higgs bosons can appear in the diagrams of Fig. 2·2, we subtract this contribution to the parameters so that $S = 0$ and $T = 0$ in the standard model. Performing this subtraction requires specifying some "reference" value for the Higgs boson mass, which we take to be $M_H^{(ref)} = 1$ TeV, a typical technihadronic scale. Switching from one $M_H^{(ref)}$ to another changes $\Delta S = \log\left(M_H^{(1)}/M_H^{(2)}\right)/(6\pi)$. Experimentally, for $M_H^{(ref)} = 300$ GeV [13],

$$S = -0.07(10) \qquad\qquad T = 0.12(11) \qquad\qquad U = 0.07(10), \tag{2.49}$$

so we conclude $S \approx -0.15(10)$ for $M_H^{(ref)} = 1$ TeV.

Of course, the point of parameterizing precision electroweak measurements in this way is to compare these experimental results with theoretical predictions. For strongly-interacting theories, however, the diagrams in Fig. 2·2 require non-perturbative treatment to obtain any quantitatively reliable result. Peskin and Takeuchi attempted to circumvent this difficulty by assuming that the dynamics of the strongly-interacting theories closely resembled those of QCD [18]. By taking experimental information on QCD and scaling it up to the

electroweak scale, they found (as always, for $M_H^{(ref)} = 1$ TeV)

$$S \approx 0.3 \frac{N_f}{2} \frac{N_c}{3}, \tag{2.50}$$

in considerable disagreement with the experimental value $S \approx -0.15(10)$.

Non-perturbative calculation of the S parameter using lattice gauge theory is the subject of Section 4.2 in this dissertation, so we will not discuss it here. While lattice gauge theory (the subject of Section 3.1) is the premier method for non-perturbative calculations, a very active field of research focuses on developing and applying relations between certain strongly- and weakly-interacting theories. This approach encompasses gauge–gravity (or AdS/CFT) dualities [146, 147, 148, 149], and electric–magnetic dualities [150, 151], and ideally might permit determination of quantities such as S in strongly-interacting theories through controlled perturbative calculations. While current results from this program are interesting, they remain qualitative and inconclusive [152, 153, 154, 155, 156].

Top quark mass

The difficulty that the large top quark mass $m_t = 172$ GeV poses to (extended) technicolor goes beyond the issue of flavor-changing neutral currents discussed above. The top quark mass is so large that the associated ETC scale ($M_{ETC}^{(t)} \sim 3$ TeV [157]) is comparable to the electroweak scale itself. This calls into question our entire approach of separating the technicolor dynamics responsible for electroweak symmetry breaking from the ETC dynamics responsible for flavor physics.

In addition, the large splitting between the top and bottom quark masses requires that the relevant ETC interactions strongly break isospin symmetry, which could generate excessively large contribution to the T parameter discussed above [158, 159].

The top quark mass is arguably the single greatest challenge facing the (extended) technicolor framework; below we will see that typical walking technicolor theories cannot resolve this issue, and in Section 2.3 we will briefly mention some of the extensions that aim to address it.

2.2.4 Walking technicolor

Let us consider the first challenge discussed in the previous section, the tension between quark and lepton masses on the one hand, and flavor changing neutral currents on the other. Considering the relevant terms in Eqn. 2.37, we see that unlike the FCNC terms, the masses in Eqn. 2.38 include a factor of $\langle \overline{T}T \rangle|_{M_{ETC}}$. In all of the discussions above, we assumed that $\langle \overline{T}T \rangle|_{M_{ETC}} \simeq \langle \overline{T}T \rangle|_{\Lambda_{TC}} \simeq 4\pi(v/\sqrt{N_D})^3$. This is appropriate only for precociously asymptotically free theories such as QCD, where the running coupling and the anomalous dimension $\gamma_m(\alpha(\mu))$ appearing in the $\langle \overline{T}T \rangle$ renormalization group equation (Eqn. 2.40) drop precipitously at energies above the low-energy scale Λ_{IR}.

Thus we see a straightforward way in which achievable quark and lepton masses could be increased without affecting FCNCs: simply suppose that $\gamma_m(\alpha(\mu))$ is large throughout a wide range of scales between Λ_{TC} and M_{ETC}, which implies that $\alpha(\mu)$ itself is large and slowly-varying. Models with a slowly-running coupling of this sort are known as walking theories, and were introduced by Refs. [160, 161, 162, 163, 164, 165]. In this section we discuss the consequences of walking, focusing on the issues discussed in Section 2.2.3 above. In Section 2.3 below, we consider a more systematic framework for walking technicolor, and non-QCD dynamics more generally.

First and most obviously, walking affects the $\langle \overline{T}T \rangle$ renormalization group equation, Eqn. 2.40. If for simplicity we suppose that the anomalous dimension is approximately constant (but non-zero), $\gamma_m(\alpha(\mu)) \simeq \gamma_m$ in the range from Λ_{TC} up to M_{ETC}, we have

$$\langle \overline{T}T \rangle|_{M_{ETC}} = \langle \overline{T}T \rangle|_{\Lambda_{TC}} \exp\left(\int_{\Lambda_{TC}}^{M_{ETC}} \frac{d\mu}{\mu} \gamma_m \right) \simeq \langle \overline{T}T \rangle|_{\Lambda_{TC}} \left(\frac{M_{ETC}}{\Lambda_{TC}} \right)^{\gamma_m}. \tag{2.51}$$

The approximate gap equation for the technifermion propagator (discussed further around Eqn. 2.55 below) requires $\gamma_m \leq 1$. Quark and lepton masses can therefore be enhanced by a potentially large factor, given strange- and charm-quark FCNC constraints implying $M_{ETC}^{(s)}$, $M_{ETC}^{(c)} \sim 10^3$–$10^4 \Lambda_{TC}$. However, the top quark mass is so large that even for $\gamma_m \approx 1$ the associated ETC scale can only be raised from $M_{ETC}^{(t)} \sim 3$ TeV to $M_{ETC}^{(t)} \sim 10$

TeV [157].

Similarly, walking enhances the PNGB masses from Eqn. 2.41 above, $M^2_{PNGB} \propto \langle \overline{T}T\overline{T}T \rangle\big|_{M_{ETC}}$. This enhancement may be so large that these pseudoscalars might not even be well-described as pseudo-Nambu–Goldstone bosons [166]. More significantly, this enhancement of the PNGB mass may kinematically forbid decays of the vector technihadrons ρ_T, ω_T, a_T into two or three pseudoscalars. This has important consequences for collider phenomenology, implying that the technivectors may be very narrow resonances [115, 167, 168, 169, 116, 117].

Finally, qualitative arguments suggest that the S parameter may be reduced in walking theories compared to the QCD-based analysis discussed in Section 2.2.3 above [170, 171, 172]. At a minimum, walking invalidates that analysis, requiring the value of S to be computed non-perturbatively. More speculatively, we can note from Eqn. 2.43 that S depends on the difference between vector and axial vacuum polarization functions. The connection between walking behavior and the conformal window suggests that the spectra of walking theories may exhibit parity doubling [173], i.e., reduced splitting between vector and axial spectral functions, which would decrease S. We now consider more carefully this connection between walking behavior and the conformal window.

2.3 Conformal windows and non-QCD dynamics

In the previous section, we saw that by introducing a large, slowly-running coupling $\alpha(\mu) = g(\mu)^2/(4\pi)$, we could address some of the phenomenological challenges facing technicolor theories. In this section we argue that such walking behavior is not necessarily just wishful thinking, but can be expected from general properties of $SU(N_c)$ gauge theories. In particular, we introduce the concept of the conformal window $N_f^{(c)} \leq N_f < N_f^{(af)}$ for a gauge theory with N_f fermions transforming in representation R, and argue that walking behavior may be realized when N_f is slightly below the critical value $N_f^{(c)}$ that defines the lower edge of the conformal window.

We begin by considering the perturbative β function of $SU(N_c)$ Yang–Mills theory with

N_f massless fermions in representation R [50, 51],

$$\beta(\alpha) = \frac{\partial\alpha}{\partial(\log\mu^2)} = \beta_0\alpha^2 + \beta_1\alpha^3 + \cdots \tag{2.52}$$

$$\beta_0 = -\frac{1}{4\pi}\left(\frac{11}{3}N_c - \frac{4}{3}T(R)N_f\right) \tag{2.53}$$

$$\beta_1 = -\frac{1}{(4\pi)^2}\left[\frac{34}{3}N_c - T(R)N_f\left(\frac{20}{3}N_c + 4C_2(R)\right)\right], \tag{2.54}$$

where $T(R)$ is the trace normalization and $C_2(R)$ the quadratic Casimir. For the fundamental representation $T(R) = 1/2$ and $C_2(R) = (N_c^2 - 1)/(2N_c)$, and we have applied $C_2(Adj) = N_c$ for the adjoint representation. While β_0 and β_1 are universal, all higher-order terms depend on the choice of renormalization scheme.

In order to maintain asymptotic freedom, we require $\beta_0 < 0$, which implies $N_f < 11N_c/(4T(R)) \equiv N_f^{(af)}$. (While some of the first walking technicolor proposals imagined models with nontrivial ultraviolet fixed points [160, 163], this scenario is more speculative, and certain conditions must be satisfied in order to recover results that follow directly from asymptotic freedom, such as Eqns. 2.38 and 2.41 above, or the Weinberg sum rules discussed in Section 4.2.1 [18].) For $N_c = 3$ with fermions in the fundamental representation, this is the familiar $N_f^{(af)} = 16.5$.

Asymptotic freedom allows us to consider the evolution of the coupling down from some high energy scale where α is small and the perturbative expansion reliable. For precociously asymptotically free theories such as QCD, with $N_f \ll N_f^{(af)}$, the coupling stays small until rising precipitously around some low energy scale Λ_{IR},[3] as illustrated schematically in Fig. 2·3. The β function, as a function of α, is always negative and quickly grows large in magnitude as α increases, as shown in Fig. 2·4.

If instead of $N_f \ll N_f^{(af)}$ we consider the other extreme $N_f \lesssim N_f^{(af)}$, then the two-loop β function crosses zero while the coupling is small enough to trust the perturbative expansion in Eqn. 2.52 [19, 20]. Because $\beta_0 < 0$, this indicates an infrared-attractive

[3] We introduced the naïve dimensional analysis convention $\Lambda_{IR} \simeq 4\pi F$ in Section 2.2.2 above. Another approach takes Λ_{IR} to be the dimensional transmutation scale at which the running coupling in a given perturbative scheme diverges [174]. We have in mind $\Lambda_{QCD} \sim 0.1$–1 GeV for QCD, $\Lambda_{TC} \sim 0.1$–1 TeV for technicolor.

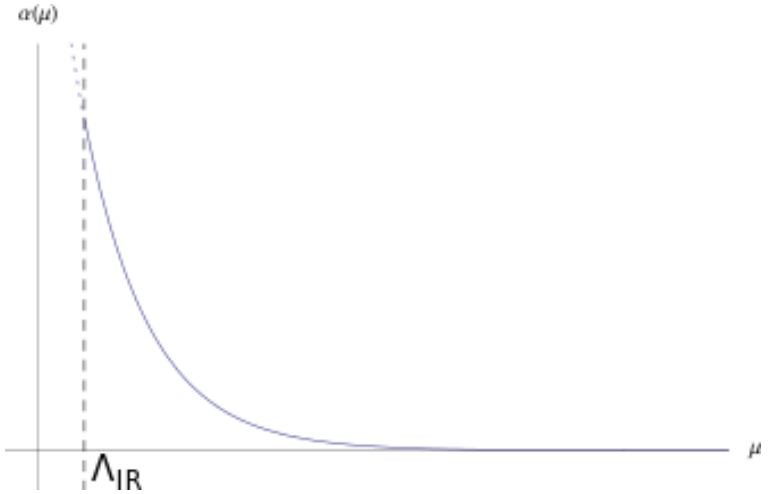

Figure 2·3: Cartoon of the coupling α as a function of energy scale μ for a precociously asymptotically free theory such as QCD.

fixed point (IRFP), illustrated in Fig. 2·4. The theory is conformal in the infrared: chiral symmetry is not broken, all particles are massless, and the coupling flows to a fixed value α_{IR} at low energies, as shown in Fig. 2·5. As N_f decreases away from $N_f^{(af)}$, the IRFP moves to stronger coupling and the perturbative analysis breaks down. Although the value of the coupling associated with the IRFP is scheme-dependent, the *existence* of an IRFP is scheme-independent, as is the value of the mass anomalous dimension γ_m *at* the fixed point.

For small enough N_f less than some critical value $N_f^{(c)}$, spontaneous chiral symmetry breaking occurs before the renormalization group flow reaches an IRFP. If we call the critical coupling associated with chiral symmetry breaking $\alpha_{\chi SB}$, then for N_f slightly below $N_f^{(c)}$ we expect $\alpha_{\chi SB}$ slightly below α_{IR}, that is $0 < (\alpha_{IR} - \alpha_{\chi SB})/\alpha_{IR} \ll 1$. This theory exhibits chiral symmetry breaking as required by technicolor, and we require that it is "close enough" to the IRFP for the fixed point to approximately govern the dynamics of the theory from the scale of chiral symmetry breaking up to some much higher scale where either asymptotic freedom sets in, or new (e.g., extended technicolor) physics becomes relevant. Over this range of scales μ, the mass anomalous dimension $\gamma_m(\mu)$ approximately equals the scheme-independent fixed-point value it would have taken had χSB not occurred

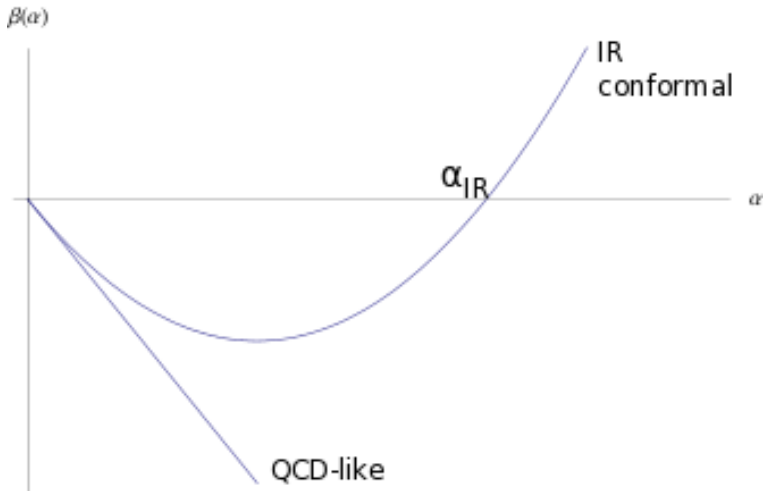

Figure 2·4: Cartoon of the β function as a function of the coupling α for a QCD-like theory (lower line) and an IR-conformal theory (upper line) with IR fixed point where the upper line crosses $\beta = 0$ at α_{IR}.

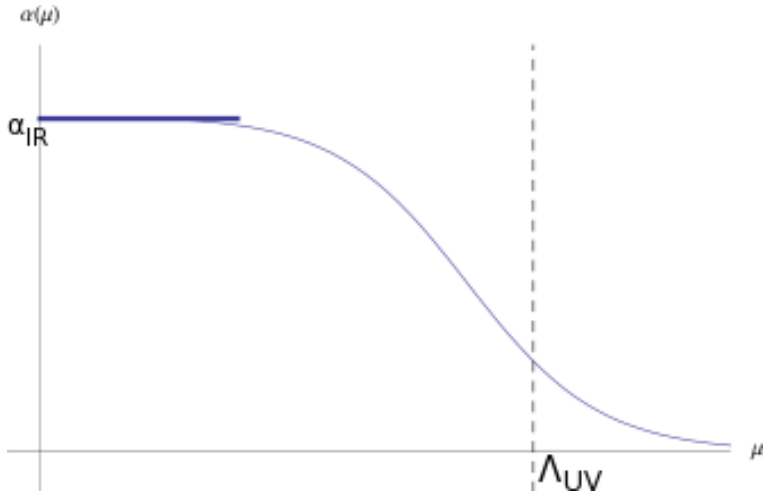

Figure 2·5: Cartoon of the coupling α as a function of energy scale μ for an IR-conformal theory. The IR fixed point at α_{IR} is indicated with a dotted horizontal line.

and affected the dynamics. That is, we have located walking technicolor slightly below the lower edge of the conformal window. We illustrate this scenario in Figs. 2·6 (for the coupling) and 2·7 (for the β function).

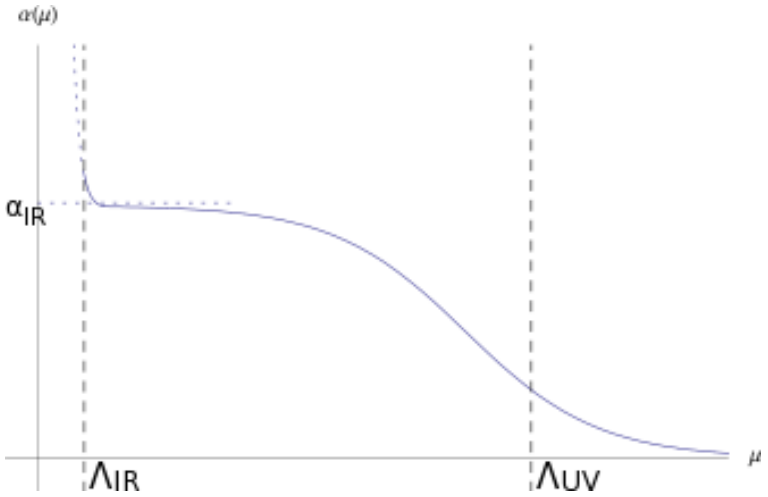

Figure 2·6: Cartoon of the coupling α as a function of energy scale μ for a walking theory in which chiral symmetry breaking occurs at a coupling slightly below the would-be IR fixed point at α_{IR} (dotted horizontal line).

This approach to describing walking dynamics as approximately conformal was emphasized by Refs. [175, 176]. It can be formalized by considering the gap equation for the fermion propagator [177, 164, 112], an approximation that relates the anomalous dimension to the running coupling by

$$\gamma_m(\mu) = 1 - \sqrt{1 - \frac{3C_2(R)}{\pi}\alpha(\mu)}. \tag{2.55}$$

This relation is assumed to break down when chiral symmetry breaking occurs, which identifies $\alpha_{\chi SB} = \frac{\pi}{3C_2(R)}$ and, more importantly, $\gamma(\mu) \approx 1$ over the large range of scales μ for which $\alpha(\mu)$ is close to (but less than) $\alpha_{\chi SB}$. This result realizes the dream of Eqn. 2.51, in that quark and lepton masses can be enhanced by a potentially large factor M_{ETC}/Λ_{TC} without affecting flavor-changing neutral currents.

The issue now becomes locating the lower edge of the conformal window, $N_f^{(c)}$. We will discuss results of lattice searches for $N_f^{(c)}$ in Section 4.1.1 below, but there are also some

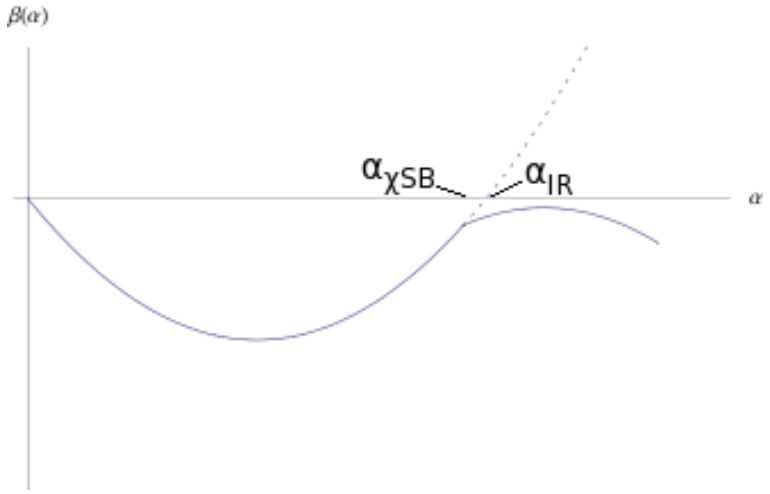

Figure 2·7: Cartoon of the β function as a function of the coupling α for a walking theory in which chiral symmetry breaking occurs at a coupling $\alpha_{\chi\mathrm{SB}}$ slightly below the would-be IR fixed point at α_{IR}.

notable analytical estimates. For instance, Ref. [176] combines the critical coupling $\alpha_{\chi SB}$ from the gap equation with the two-loop perturbative β function to find

$$N_f^{(c)} = \frac{N_c}{T(R)} \left[\frac{66 C_2(R) + 17 N_c}{30 C_2(R) + 10 N_c} \right], \tag{2.56}$$

which becomes $N_f^{(c)} \approx 7.9$ (11.9) for $SU(2)$ ($SU(3)$) gauge theory with fermions in the fundamental representation. However, the result depends fairly strongly on the scheme used for the β function; the $SU(3)$ prediction drops to $N_f^{(c)} \approx 9.9$ in three-loop $\overline{MS}$ perturbation theory [178]. An alternate approach conjectures that the Nambu–Goldstone bosons of the theory in the infrared should have fewer degrees of freedom than the gluons and fermions of the theory in the ultraviolet [179]. This implies $N_f^{(c)} \approx 4N_c$ for $N_c \geq 3$, and $N_f^{(c)} \approx 4$ for $N_c = 2$ (because of the pseudo-reality of $SU(2)$ representations).

Finally, we note that the gap equation requires $\gamma_m \leq 1$. As we saw in Section 2.2.4, $\gamma_m \leq 1$ does not solve the problem posed by the large top quark mass. However, the gap equation is approximate, and $\gamma_m > 1$ is not excluded by this analysis (although unitarity requires $\gamma_m < 2$ [180]). Early models with $\gamma_m > 1$ supposed that the ETC four-fermion interactions were strong enough at the electroweak scale to play a role in the technifermions'

chiral symmetry breaking [181, 182, 183]; this approach resembles the Nambu–Jona-Lasinio model [184, 185] and tends to require significant fine-tuning.

A more recent proposal for obtaining $\gamma_m > 1$ is to consider a theory that would be IR-conformal in isolation (i.e., it is within the conformal window), but is driven to chiral symmetry breaking by other interactions or relevant operators [186, 157, 187, 188]. Recent analytical studies have begun to shed light on the range of behavior that is possible in such theories [189, 190, 191, 192, 193]. There are also approaches to explaining the top quark mass that do not use $\gamma_m > 1$, such as topcolor-assisted technicolor [194] (which proposes new strong gauge interactions specifically for the third generation), and monopole condensation [195].

It is possible that ongoing or future lattice studies may find evidence for theories with $\gamma_m > 1$. We now turn to discuss lattice gauge theory and its application to strongly-interacting theories.

Chapter 3

Lattice gauge theory

Lattice gauge theory (LGT) is a non-perturbative regularization of quantum gauge field theories, in which we discretize euclidean spacetime into a regular grid of sites connected by links. In this document we focus on hypercubic lattices of size $L^3 \times 2L$. In the combined limit that the lattice becomes infinitely large ($L \to \infty$) while the lattice spacing a between sites becomes infinitesimally small ($a \to 0$), we must recover the original gauge theory defined in the continuum.

In addition to regularizing the theory, the fact that the lattice formulation involves a finite number of degrees of freedom permits numerical calculation of observables from the defining path integral. Such numerical computations will be the focus of our discussion. Although these calculations are non-perturbative, they are carried out through stochastic importance sampling, which introduces statistical errors. Additional systematic effects result from considering a discretized theory in a finite volume.

In this section we review the formulation and application of lattice gauge theory, considering lattice QCD ($SU(3)$ gauge theory with $N_f = 2$ light fermions) as a relatively familiar example. After summarizing basic lattice actions and observables, we discuss Monte Carlo lattice simulation procedures, and consider the corresponding statistical and systematic effects. Finally, we focus on a systematic effect that is particularly important to exploring technicolor models on the lattice, the explicit chiral symmetry breaking that arises both from the need to perform simulations at non-zero fermion mass as well as from many common lattice actions themselves. We review domain wall fermions, a formulation that decouples the continuum and chiral limits by adding a fifth dimension to the lattice.

Useful introductions to and reviews of lattice gauge theory include [196, 197, 198, 199,

21, 22, 200]; in addition, several chapters from a forthcoming volume [201] are already available [202, 102, 44, 203, 204, 205, 206, 207].

3.1 Formulation

3.1.1 Euclidean path integral

We begin our discussion of the formulation of lattice gauge theory by considering the euclidean path integral for a generic gauge theory, assuming familiarity with the standard Wick rotation procedure for relating a euclidean theory to the physical theory in Minkowski spacetime. Because we are working in euclidean spacetime, $Q^2 = -q^2 > 0$ and the spacetime index $\mu = 1, \ldots, 4$, where $\mu = 4$ corresponds to the Wick-rotated temporal component. By using periodic boundary conditions, for most of these considerations we can treat the lattice as though it were infinitely large, with fixed lattice spacing $a > 0$. For convenience, we will often use "lattice units" which take $a = 1$.

Under local gauge transformations $\Omega_x \in SU(3)$, the fermions transform as

$$\psi_x \to \Omega_x \psi_x \qquad\qquad \overline{\psi}_x \to \overline{\psi}_x \Omega_x^\dagger. \tag{3.1}$$

The gauge-covariant derivative $\overline{\psi}_{x+a\widehat{\mu}} D_\mu \psi_x$ now connects fermion fields at lattice sites separated by a distance $a > 0$. In order to maintain exact gauge invariance, we associate the gauge fields with the links between neighboring sites by defining

$$U_{x,\mu} = \exp\left[igaA_\mu(x + a\widehat{\mu}/2)\right], \tag{3.2}$$

where $A_\mu(x) = A_\mu^a(x)T^a$ is the continuum gauge field. This notation is common, but potentially confusing, because

$$U_{x,\mu} \to \Omega_x U_{x,\mu} \Omega_{x+a\widehat{\mu}}, \tag{3.3}$$

so we consider $U_{x,\mu}$ the parallel transporter along the link *from* site $(x + a\widehat{\mu})$ *to* site x. The oppositely-directed variable is $U_{x,\mu}^\dagger$, and since $U_{x,\mu} \in SU(3)$, $U_{x,\mu}^\dagger U_{x,\mu} = U_{x,\mu} U_{x,\mu}^\dagger = 1$.

Now that we have defined our variables, we can write down the partition function

$$Z = \mathrm{Tr}\left[\exp(-S)\right] = \int \mathcal{D}U\mathcal{D}\overline{\Psi}\mathcal{D}\Psi \exp\left[-S(U,\Psi,\overline{\Psi})\right], \tag{3.4}$$

where S is the lattice action and the integration is over all configurations of the gauge and fermion fields on the lattice, for example $\int D\Psi \equiv \int \prod_x d\psi_x$. For $\int DU \equiv \int \prod_{x,\mu} dU_{x,\mu}$ we use the gauge-invariant Haar measure, so that no gauge-fixing is required for the functional integral to be well defined. If we take the temporal extent of the lattice to be finite, then we can write

$$Z = \mathrm{Tr}\left[\exp(-aN_tS)\right] = \mathrm{Tr}\left[\widehat{T}^{N_t}\right], \tag{3.5}$$

where $\widehat{T} = \exp(-aS)$ is the transfer matrix operator. Acting on a state in the Hilbert space, $\widehat{T}$ evolves the state through a euclidean time interval a. $\widehat{T}$ must be positive (i.e., have only positive eigenvalues) in order for the theory to describe a unitary Hilbert space with a real hamiltonian [208].

Similarly, the path integral defining the expectation value of an observable O is

$$\begin{aligned}\langle O\rangle &= \frac{1}{Z}\mathrm{Tr}\left[O\exp(-aN_tS)\right] \\ &= \frac{1}{Z}\int \mathcal{D}U\mathcal{D}\overline{\Psi}\mathcal{D}\Psi O(U,\overline{\Psi},\Psi)\exp\left[-S_g(U) - \overline{\Psi}D(U)\Psi\right].\end{aligned} \tag{3.6}$$

We break up the lattice action S into two pieces, S_g for the gauge fields and $S_f = \overline{\Psi}D(U)\Psi$ for the fermions, where $D(U)$ is a lattice Dirac operator. In the next two sections, we will discuss each of S_g and S_f in turn, introducing simple lattice actions that possess a positive transfer matrix.

3.1.2 Lattice gauge action

The simplest gauge action was introduced by Wilson [209], and is most conveniently written in terms of the plaquette variables

$$P_{x,\mu\nu} = \mathrm{Tr}\left[U_{x,\mu}U_{x+\widehat{\mu},\nu}U^{\dagger}_{x+\widehat{\nu},\mu}U^{\dagger}_{x,\nu}\right], \tag{3.7}$$

where $\mu \neq \nu$ and the trace is over color and spin indices that we will not write explicitly. The plaquette corresponds to the unit lattice square bounded by the four links in the trace, with normal vector defined by the direction of the links in the product. $P^{\dagger}_{x,\mu\nu}$ is the oppositely-directed plaquette. Considering for a moment the abelian case $F_{\mu\nu} = \partial_\mu A_\nu - \partial_\nu A_\mu$, and reintroducing the lattice spacing a,

$$\begin{aligned} U_{x,\mu} &= \exp\left[igaA_\mu(x + a\widehat{\mu}/2)\right] \\ \Rightarrow P_{x,\mu\nu} &= e^{iga} \exp\left[A_\mu(x + \tfrac{a}{2}\widehat{\mu}) + A_\nu(x + a\widehat{\mu} + \tfrac{a}{2}\widehat{\nu}) - A_\mu(x + a\widehat{\nu} + \tfrac{a}{2}\widehat{\mu}) - A_\nu(x + \tfrac{a}{2}\widehat{\nu})\right] \\ &\simeq \exp\left[iga^2 F_{\mu\nu}(x + a\widehat{\mu}/2 + a\widehat{\nu}/2)\right], \end{aligned} \tag{3.8}$$

where the final equality becomes exact in the continuum limit $a \to 0$. Therefore, to reproduce a continuum gauge action of the form $F^A_{\mu\nu} F^{A\mu\nu}$ (returning to $SU(3)$), we could imagine a lattice action including terms like

$$2 - e^{igF_{\mu\nu}(x)} - e^{-igF_{\mu\nu}(x)} \simeq 2 - P_{x,\mu\nu} - P^{\dagger}_{x,\mu\nu} = 2 - 2\mathrm{Re}P_{x,\mu\nu}. \tag{3.9}$$

We need to sum over all x and μ, ν with $\mu \neq \nu$ in order to ensure that the action is gauge-invariant. This line of reasoning gives us the plaquette gauge action

$$S_{plaq} = \beta \sum_x \sum_{\mu,\nu;\mu<\nu} \left(1 - \frac{1}{N_c} P_{x,\mu\nu}\right), \tag{3.10}$$

where $\beta \equiv 2N_c/g^2$. As $a \to 0$, $S_{plaq} \to \int d^4x \frac{1}{4} F_{\mu\nu} F^{\mu\nu} + \mathcal{O}(a^2)$.

Given the simple form of the action when expressed in terms of the plaquette variables, it is natural to consider generalizations of Eqn. 3.7 involving additional links in the trace. Like the plaquette, the sum of such variables over lattice sites and orientations would be gauge-invariant. The smallest closed loops after the plaquette involve six links, and so correspond to dimension-six operators that introduce $\mathcal{O}(a^2)$ lattice artifacts in quantities calculated with the plaquette gauge action. However, by explicitly adding one or more of these operators to the lattice action itself, we can hope to tune the coefficients of terms in the action so that these artifacts are reduced in some observables.

Of the three six-link loops, the simplest is the 2×1 rectangle

$$R_{x,\mu\nu} = \mathrm{Tr}\left[U_{x,\mu}U_{x+\widehat{\mu},\mu}U_{x+\widehat{\mu}+\widehat{\nu},\nu}U^\dagger_{x+\widehat{\mu}+\widehat{\nu},\mu}U^\dagger_{x+\widehat{\nu},\mu}U^\dagger_{x,\nu}\right]. \tag{3.11}$$

The other two (the "chair" and "parallelogram" loops) involve links in three dimensions, and we will not consider them. Adding a rectangle term to the plaquette gauge action, we have the generic improved gauge action

$$S_{imp} = \beta\sum_x\left\{c_0\sum_{\mu,\nu;\mu<\nu}\left(1-\frac{1}{N_c}P_{x,\mu\nu}\right)+c_1\sum_{\mu,\nu}\left(1-\frac{1}{N_c}R_{x,\mu\nu}\right)\right\} \tag{3.12}$$

with the normalization $c_0 = 1-8c_1$. Noteworthy choices of the rectangle coefficient c_1 include:

$c_1 = -\dfrac{1}{12}$ (tree-level Lüscher–Weisz [210])

$c_1 = -0.331$ (Iwasaki [211, 212])

$c_1 = -1.4088$ (DBW2: doubly-blocked from Wilson in two-coupling space [213, 214])

The tree-level Lüscher–Weisz action is based on a one-loop perturbative calculation following the Symanzik improvement program [215, 216] (so is sometimes known as the tree-level Symanzik-improved action), while the Iwasaki and DBW2 actions are inspired by the renormalization group.

3.1.3 Lattice fermions and doubling

Wilson [209] also introduced the simplest phenomenologically viable lattice action for fermions. Let us start from the free theory, $S_f = \int d^4x\overline{\psi}(x)\gamma^\mu\partial_\mu\psi(x) + m\overline{\psi}(x)\psi(x)$, and discretize the derivative as the lattice central difference

$$\partial_\mu\psi(x) \to \Delta_\mu\psi_x = \frac{\psi_{x+\widehat{\mu}}-\psi_{x-\widehat{\mu}}}{2} \tag{3.13}$$

(recall $a = 1$ in lattice units). We need to use the link variables $U_{x,\mu}$ to transport the ψ field between neighboring lattice sites, which introduces the gauge fields into the action,

$$S_f = \frac{1}{2}\sum_{x,\mu}\overline{\psi}_x\gamma^\mu\left[U_{x,\mu}\psi_{x+\widehat{\mu}} - U^\dagger_{x-\widehat{\mu}}\psi_{x-\widehat{\mu}}\right] + m\sum_x\overline{\psi}_x\psi_x \equiv \overline{\psi}D_{naive}(m)\psi. \tag{3.14}$$

By performing a Fourier transform, it is straightforward to find the free momentum-space propagator

$$\widetilde{D}^{-1}_{naive}(p,m) = (i\gamma^\mu\sin(p_\mu) + m)^{-1} = \frac{-i\gamma^\mu\sin(p_\mu) + m}{\sum_\mu\sin^2(p_\mu) + m^2}, \tag{3.15}$$

where $p_\mu = 2\pi i x_\mu/N_\mu$ and N_μ is the length of the lattice in direction μ. For small $p_\mu \approx (0,0,0,0)$, we can approximate $\gamma^\mu\sin(p_\mu) \approx \not{p}$ and recover the usual fermion propagator in the continuum. However, the same thing (up to negative signs) happens at fifteen other locations in the Brillouin zone, $p_\mu \approx (0,0,0,\pi)$, $(0,0,\pi,0)$, $\ldots$, (π,π,π,π). The naïve lattice fermion action we have written down therefore describes sixteen degenerate fermions, not just one.

This is known as the "doubling problem", and Wilson addressed it by adding another term to Eqn. 3.14, the "Wilson term" $r\overline{\psi}_x\Delta^2_\mu\psi_x$. This term involves the central difference discretization of the second-derivative,

$$\Delta^2_\mu\psi_x = \frac{\psi_{x+\widehat{\mu}} - 2\psi_x + \psi_{x-\widehat{\mu}}}{2}. \tag{3.16}$$

The Wilson term is a dimension-five operator, so it does not interfere with our recovery of the correct continuum physics as $a \to 0$. Here r is a free dimensionless parameter, and setting $r = 1$ when we insert this term into Eqn. 3.14 produces a pleasantly compact result,

$$\begin{aligned} S_f &= -\frac{1}{2}\sum_{x,\mu}\overline{\psi}_x\left[(1-\gamma^\mu)U_{x,\mu}\psi_{x+\widehat{\mu}} + (1+\gamma^\mu)U^\dagger_{x-\widehat{\mu}}\psi_{x-\widehat{\mu}}\right] + (4+m)\sum_x\overline{\psi}_x\psi_x \\ &\equiv \overline{\psi}D_W(m)\psi. \end{aligned} \tag{3.17}$$

Although the Wilson Dirac operator D_W is not hermitian, it satisfies "γ_5-hermiticity",

which is the statement that $H_W \equiv \gamma_5 D_W$ is a hermitian operator, or

$$D_W^\dagger = \gamma_5 D_W \gamma_5. \tag{3.18}$$

Now the free momentum-space propagator becomes

$$\begin{aligned} \widetilde{D}_W^{-1}(p,m) &= [i\gamma^\mu \sin(p_\mu) + m + \sum_\mu (1-\cos(p_\mu))]^{-1} \\ &= \frac{-i\gamma^\mu \sin(p_\mu) + m + \sum_\mu (1-\cos(p_\mu))}{\sum_\mu \sin^2(p_\mu) + [m + \sum_\mu (1-\cos(p_\mu))]^2}, \end{aligned} \tag{3.19}$$

so that all the doubler modes with any component $p_\mu \approx \pi$ obtain large masses $\propto a^{-1}$.

Unfortunately, the Wilson term explicitly introduces $\overline{\psi}\psi = \overline{\psi}_L\psi_R + \overline{\psi}_R\psi_L$ into the action, thereby breaking the chiral symmetry of the massless lattice theory. (Again, this chiral symmetry breaking vanishes in the continuum limit.) This consequence was generalized into a famous theorem by Nielsen and Ninomiya [40, 41, 42] (building on earlier work by Refs. [217, 218, 219]), which states that in an even number of euclidean dimensions, the fermion operator $\widetilde{D}(p)$ cannot simultaneously satisfy the four conditions [44]

1. $\widetilde{D}(p)$ is a periodic, analytic function of p;
2. $\widetilde{D}(p) \propto \gamma^\mu p_\mu$ for $|p_\mu| \ll 1$;
3. $\widetilde{D}(p)$ is invertible everywhere except $p_\mu = 0$;
4. $\gamma_5 \widetilde{D}(p) + \widetilde{D}(p)\gamma_5 = 0$.

Here the second and third conditions forbid doublers, while the fourth condition is the statement of chiral symmetry. The first condition guarantees that the operator is local in coordinate space.

A tradeoff seems to be necessary between doubling and chiral symmetry. The naïve fermion action possesses both, while the Wilson fermion action possesses neither. In between, staggered fermions [220, 221, 222] retain a portion of the full chiral symmetry, and at the same time reduce doubling from sixteen-fold to four-fold by spreading out the four

spinor components of the fermionic field across the 2^4 hypercube. The resulting lattice action is very computationally efficient, and improved forms of it are still widely used.

However, there are undoubled chiral lattice fermion actions that evade the Nielsen–Ninomiya theorem, one of which we will consider in Section 3.3 below. In particular, Ginsparg and Wilson showed that a remnant of chiral symmetry remains on the lattice [43],

$$\gamma_5 D(0) + D(0)\gamma_5 = 2D(0)\gamma_5 D(0) \tag{3.20}$$

where $D(m = 0)$ is the massless lattice Dirac operator. The Ginsparg–Wilson relation can be considered a redefinition of what is meant by a chiral rotation [223],

$$\gamma_5 D(0) + D(0)\widehat{\gamma}_5 = 0, \tag{3.21}$$

where $\widehat{\gamma}_5 = \gamma_5(1 - 2D(0))$. Unfortunately, the lattice Dirac operators that exactly realize this modified chiral symmetry at non-zero lattice spacing are extremely expensive to use in the numerical simulations we discuss below. The outstanding example is the overlap operator [224, 225, 226, 227, 228]

$$D_{ov}(m) = \left(M_5 + \frac{m}{2}\right) + \left(M_5 - \frac{m}{2}\right)\gamma_5 \text{sign}\left[\gamma_5 D_W(-M_5)\right] \tag{3.22}$$

where $0 < M_5 < 2$ is a large mass parameter and numerically evaluating the operator sign function

$$\text{sign}\left[X\right] = \frac{X}{\sqrt{X^\dagger X}} \tag{3.23}$$

is the cause of its computational expense.

3.2 Simulation procedures

Now that we have presented the basic formulation of lattice gauge theory, let us consider how we carry out numerical lattice simulations. In practice, we divide the work into two pieces. First, we apply importance sampling Monte Carlo techniques to generate an ensemble of gauge field configurations from the path integral for our lattice action. Then

we analyze these stored gauge configurations to calculate observables of interest.

This division of the work into configuration generation on the one hand, and configuration analysis on the other, is motivated by the different computational requirements of each piece of the simulation. Configuration generation through the hybrid Monte Carlo algorithm we discuss below involves running long molecular dynamics evolutions in order to generate independent (uncorrelated) samples of the gauge fields. Because this evolution must run for many molecular dynamics steps, it is most efficient to perform the calculation on the largest available supercomputing resources, to minimize the time to solution. Once gauge configurations have been generated, however, they can trivially be analyzed in parallel. Therefore it is most efficient to perform the analysis of each configuration on the smallest computing resource that can handle the calculation.

In the next two sections we discuss each of these steps in turn, and then consider the systematic effects inherent in lattice simulations.

3.2.1 Configuration generation

To use importance sampling Monte Carlo to simulate the euclidean theory described by Eqn. 3.6, we must be able to interpret the factor e^{-S} as a probability distribution. This requires that the action be positive. For the gauge action $S_g \sim F_{\mu\nu}F^{\mu\nu}$, this condition is easy to satisfy. The fermion action $S_f = \overline{\Psi}D\Psi$ is quadratic in the anti-commuting fermionic fields, so this piece of the action can be reformulated in terms of more tractable bosonic "pseudofermion" fields Φ,

$$\int \mathcal{D}\overline{\Psi}\mathcal{D}\Psi \exp\left[-\overline{\Psi}D\Psi\right] \propto \det[D] \propto \int \mathcal{D}\Phi^\dagger\mathcal{D}\Phi \exp\left[-\Phi^\dagger D^{-1}\Phi\right] \tag{3.24}$$

(any constant factor from the gaussian integral on the left will be re-absorbed into the gaussian integral on the right). In order to ensure positivity, we restrict ourselves to even numbers of fermions N_f. In this case, γ_5-hermiticity implies $\det[D]^2 = \det[D^\dagger D]$, and our measure becomes

$$\exp\left[-S_g - \Phi^\dagger(D^\dagger D)^{-1}\Phi\right],$$

which is positive definite (because we assume a non-zero fermion mass $m > 0$), and can therefore be treated as a probability distribution. Increasing N_f only requires adding more pairs of pseudofermion fields to this expression. (See Refs. [229, 230] for an example of a more complicated algorithm that is not restricted to even N_f.)

The complication introduced by the pseudofermion fields is the need to invert $D^\dagger D$, typically a large, sparse matrix. These inversions (calculated iteratively using an algorithm such as conjugate gradient [231]) form the bulk of the computational expense of lattice gauge theory simulations. In addition, because the inverse (or equivalently the determinant) must be recomputed globally after any change in the gauge fields, local updating schemes are inefficient. Instead, we want to use some global updating scheme that generates a new configuration by changing all the link variables simultaneously. In the remainder of this section, we briefly summarize the hybrid Monte Carlo (HMC) algorithm [232, 233], some form of which is currently used in nearly all lattice gauge theory simulations [234, 203]).

We divide the Markov step of the HMC algorithm into three pieces. First we generate gaussian random values for the pseudofermion fields Φ, as well as a real auxiliary field π_μ that we add to the action via

$$1 = \int \mathcal{D}\pi e^{-\pi^2/2}. \tag{3.25}$$

This π_μ plays the role of a fictitious momentum that is conjugate to the gauge field, producing an effective hamiltonian $H_{eff} = \frac{1}{2}\pi^2 + S_g + \Phi^\dagger (D^\dagger D)^{-1}\Phi$. The next piece of the algorithm is hamiltonian evolution of π_μ and the gauge field over a short trajectory of length τ in a "molecular dynamics time". During this evolution we keep Φ fixed. We perform this evolution through inexact integration of Hamilton's equations, which divides τ into N_τ steps of length $\delta\tau = \tau/N_\tau$, and introduces $\delta\tau$-dependent numerical errors $\left\langle \Delta H_{eff}^2 \right\rangle^{1/2} > 0$. The first-order Verlet (leapfrog) method is a simple example of such an integration algorithm, though higher-order methods such as the Omelyan integrator are used in practice [235, 236].

Note that the molecular dynamics evolution involves the force (Lie derivative)

$$\frac{d\pi}{d\tau} = -\frac{\partial S_g}{\partial U} - \Phi^\dagger \frac{\partial (D^\dagger D)^{-1}}{\partial U} \Phi = -\frac{\partial S_g}{\partial U} - \left[(D^\dagger D)^{-1} \Phi \right]^\dagger \frac{\partial D^\dagger D}{\partial U} \left[(D^\dagger D)^{-1} \Phi \right], \tag{3.26}$$

which requires the expensive computation of the inverse at each step in the evolution. After carrying out the N_τ steps in the integration, we stochastically correct for the numerical errors by performing a Metropolis (Rosenbluth–Teller) accept/reject test [237, 238], the third and final piece of the algorithm. So long as the integrator is reversible and preserves phase-space volume (i.e., is symplectic), this acceptance test guarantees that the algorithm maintains detailed balance and will approach the correct fixed-point distribution.

Repeating the Markov step outlined above produces an ensemble of gauge configurations. These configurations are not completely independent, to an extent that depends on our choice of molecular dynamics integrator and evolution parameters, an issue we will return to in Section 3.2.3. For now, let us consider how we analyze these configurations to measure some observables of interest.

3.2.2 Configuration analysis

Assuming that we have used the HMC algorithm described above to generate an ensemble of gauge configurations, in this section we discuss the analysis of these configurations. While observables involving only the gauge fields (such as the plaquette averaged over the lattice) are generally inexpensive to compute and can be useful to monitor the HMC evolution, typically we are most interested in the behavior of the valence fermions. Therefore in this section we focus on fairly simple but illustrative observables, including meson masses and decay constants as well as the chiral condensate $\langle \overline{\psi}\psi \rangle$.

Treating the euclidean action as a hamiltonian, a generic two-point correlation function has the form

$$C_{ij}(t) = \frac{1}{Z} \mathrm{Tr} \left[O_i(t) O_j(0) e^{-N_t H} \right] = \frac{1}{Z} \sum_m \langle m | e^{Ht} O_i e^{-Ht} O_j e^{-N_t H} | m \rangle, \tag{3.27}$$

where $|m\rangle$ are a complete set of energy eigenstates, $e^{-N_t H} |m\rangle = e^{-N_t E_m}$. Inserting another

complete set of states produces

$$C_{ij}(t) = \frac{1}{Z}\sum_{m,n}\langle m|O_i|n\rangle\langle n|O_j|m\rangle e^{-E_n t}e^{-E_m(N_t-t)}. \tag{3.28}$$

In the case $i = j$, if we consider $t \gg 1$ and $N_t - t \gg 1$ (and subtract the vacuum expectation value $|\langle 0|O_i|0\rangle|^2$ if it non-zero), then the correlator C_{ii} will be dominated by the lightest state with the appropriate quantum numbers, whose energy we identify as its mass M,

$$C(t) \approx A\left(\exp\left[-Mt\right] + \exp\left[-M(N_t - t)\right]\right). \tag{3.29}$$

Fig. 3·1 shows an example of this approximation to the correlation function describing propagation of a (flavor non-singlet) meson from a source at time t_0 to a sink at time t,

$$\begin{aligned} C_\Gamma(|t-t_0|) &= \left\langle \sum_{\mathbf{x}} \mathrm{Tr}\left[\left\{\overline{\psi}(\mathbf{x},t)\Gamma T^a \psi(\mathbf{x},t)\right\}\left\{\overline{\psi}(\mathbf{0},t_0)\Gamma T^b \psi(\mathbf{0},t_0)\right\}\right]\right\rangle \\ &= -\left\langle \sum_{\mathbf{x}} \mathrm{Tr}\left[D^{-1}(\mathbf{0},t_0;\mathbf{x},t)\Gamma T^a D^{-1}(\mathbf{x},t;\mathbf{0},t_0)\Gamma T^b\right]\right\rangle, \end{aligned} \tag{3.30}$$

where the sum over the spatial volume of the lattice projects out the zero-momentum component of the correlator. We write the second line to emphasize that measuring valence fermion observables requires additional inversions of the lattice Dirac operator, against some source(s) placed on the gauge configurations being analyzed. ($D^{-1}(y;x) = \gamma_5\left(D^{-1}(x;y)\right)^\dagger\gamma_5$ is the fermion propagator from site x to site y, and in the future we will generally use translation invariance to write it as $D^{-1}(y-x)$.) As in Section 2.2.1, the flavor matrices T^a are normalized so that $\mathrm{Tr}\left[T^a T^b\right] = \frac{1}{2}\delta^{ab}$ (similar traces over color and spin are not explicitly written). The Γ is some product of γ matrices. For example, the pseudoscalar channel corresponds to $\Gamma = \gamma_5$ and $\gamma_4\gamma_5$ (because the pseudoscalar mass is nonzero on the lattice, these two currents are related by the axial Ward–Takahashi identity we will discuss in Section 3.3.3 below); the vector channel corresponds to $\Gamma = \gamma_i$ and the axial channel to $\Gamma = \gamma_i\gamma_5$, for $i = 1, 2, 3$. The specific correlator shown in Fig. 3·1 uses $\Gamma = \gamma_5$.

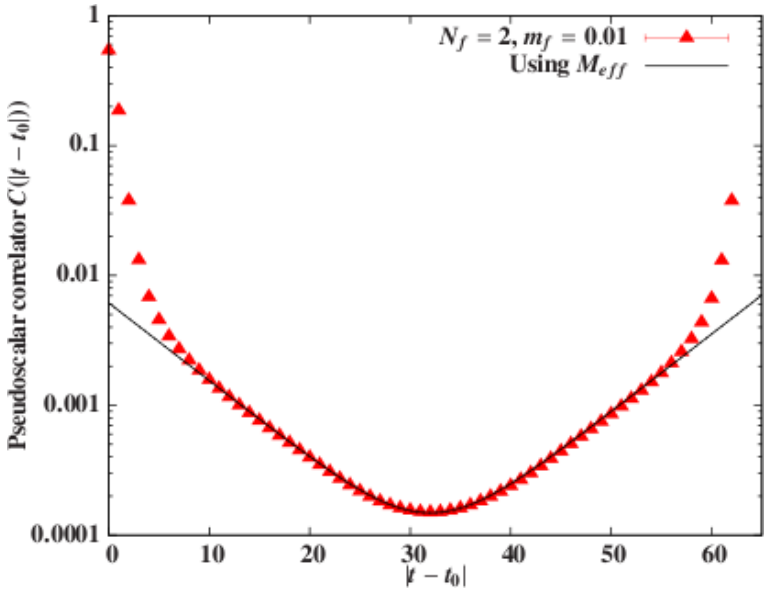

Figure 3·1: Comparing pseudoscalar $C(t)$ data with the approximation of Eqn. 3.29 (solid black line), using M_{eff} from the plateau in Fig. 3·2 for $32^3 \times 64$ LSD Collaboration ensembles with $N_f = 2$ and $m_f = 0.01$ (cf. Section 4.1.2 for details of ensembles and measurements). The dotted lines showing the statistical error are too close to the solid line to see.

We see in Fig. 3·1 that the asymptotic form of Eqn. 3.29 only seems to describe the correlator well for $10 \lesssim |t - t_0| \lesssim 55$. We can be more precise by considering the "effective mass" formula

$$m_{eff}(t) = \log\left[\frac{C(t)}{C(t+1)}\right]. \tag{3.31}$$

According to Eqn. 3.29, for $1 \ll |t - t_0| \ll N_t$ this function should show a "plateau", i.e., $m_{eff}(t)$ should be approximately constant for a range of t, at a value we take to be the effective mass M_{eff} of the state. Because $C(t)$ typically reaches a minimum around $|t - t_0| \approx N_t/2$ (as in Fig. 3·1), $m_{eff}(t)$ crosses zero, breaking the plateau into two disconnected pieces. A simple modification that evades this issue is to consider instead

$$\frac{C(t-1) + C(t+1)}{2C(t)} \to \cosh(M_{eff}), \tag{3.32}$$

which possesses a long plateau shown in Fig. 3·2. Obtaining such long plateaus is the main motivation for working on $L^3 \times 2L$ lattices with temporal extent longer than the spatial

length.

In practice, these effective mass plateaus are used simply to determine the proper range of t to use in a direct fit to Eqn. 3.29 or more complicated forms involving additional exponentials. However, for the simple case shown in Fig. 3·2, the effective mass result $M_P^2 = 0.01904(22)$ is very close to the Lattice Strong Dynamics (LSD) Collaboration result obtained by a simultaneous fit to eight correlators including both $\Gamma = \gamma_5$, $\gamma_4\gamma_5$, and using four different combinations of sources and sinks, $M_P^2 = 0.01873(20)$. Baryon masses can be obtained in essentially the same way, although the operators and contractions required are more complicated, and the resulting correlators are noisier, with much shorter plateaus.

Meson decay constants are also measured from the same two-point correlation functions we have been considering. Let us rewrite Eqn. 2.29 as

$$F_P = \frac{\langle 0|A_0^a(\mathbf{x},t)|\pi^a(p=0)\rangle}{M_P}, \tag{3.33}$$

where we do not sum over the flavor index ^{a}, which is present to indicate that these operators are flavor non-singlet. Because $\langle 0|A_0^a(x)|\pi^a(p=0)\rangle$ is precisely the ground state that we expect to dominate $\langle \sum_{\mathbf{x}} A_0^a(\mathbf{x},t)A_0^a(\mathbf{0},t_0)\rangle$ for $1 \ll |t-t_0| \ll N_t$, we can determine the decay constants from the coefficient A in Eqn. 3.29. For example,

$$\left\langle \sum_{\mathbf{x},i} V_i^a(\mathbf{x},t)V_i^b(\mathbf{0},0) \right\rangle \rightarrow \frac{3}{2}\delta^{ab} Z_V^2 F_V^2 M_V \left[e^{-M_V t} + e^{-M_V(N_t-t)}\right], \tag{3.34}$$

where the factor of $\frac{3}{2}$ comes from the sum over spatial components i and the trace over flavor matrices. Note that measuring the decay constant F requires previous determination of the corresponding mass M, and in some cases the renormalization factor Z that we discuss in Section 3.3.3 below.

Finally, the chiral condensate $\langle\overline{\psi}\psi\rangle$ involves the complication that it directly connects sources and sinks at the same lattice site,

$$\langle\overline{\psi}\psi\rangle = -\frac{1}{4N_cV}\left\langle \sum_x \overline{\psi}(x)\psi(x) \right\rangle = \frac{1}{4N_cV}\left\langle \sum_x D^{-1}(x;x) \right\rangle = \frac{1}{4N_cV}\left\langle \mathrm{Tr}\left[D^{-1}(m)\right]\right\rangle, \tag{3.35}$$

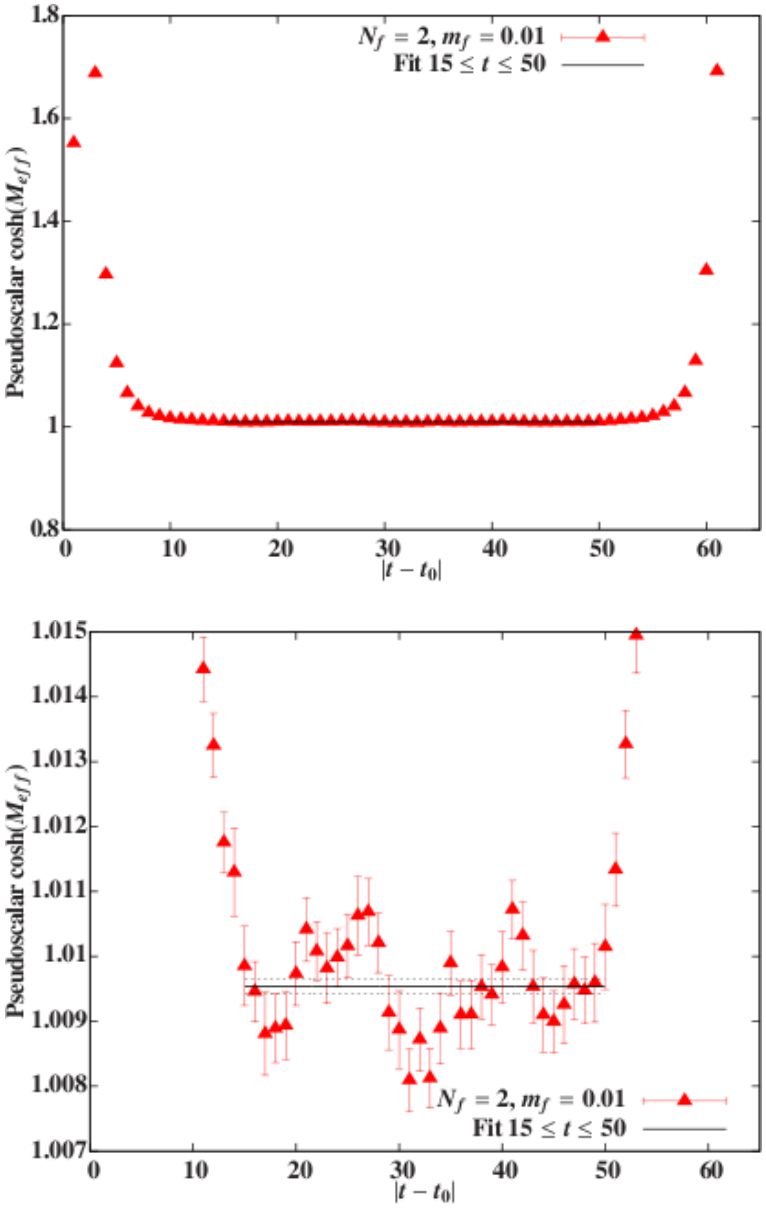

Figure 3·2: Jackknife fit results for the ratio $[C(t-1)+C(t+1)]/[2C(t)]$ of pseudoscalar correlators, and $\cosh(M_{eff})$ (solid black line), for the same ensembles as Fig. 3·1. The bottom panel zooms in on the plateau in the range $15 \leq |t - t_0| \leq 50$. The dotted lines show the statistical error in $\cosh(M_{eff})$.

where the first negative sign is a phase convention inserted to make $\langle\overline{\psi}\psi\rangle > 0$ (for $m > 0$). The factor of $4N_c$ accounts for the implicit traces over color and spin. This is the simplest example of a quark-line disconnected diagram, which on its face seems to require a number of inversions proportional to the lattice volume V. In practice, we estimate the result stochastically, by performing the inversions using only N_{sc} random sources η. Typically, each η uses a unitary random number (e.g., an element of $U(1)$ or Z_2) for each color, spin and spatial degree of freedom, so that $\eta^*_{a\alpha}(x)\eta_{b\beta}(y) = \delta_{ab}\delta_{\alpha\beta}\delta_{xy}$ [239]. For $\langle\overline{\psi}\psi\rangle$ this straightforward approach suffices, and only a few random sources are needed to estimate $\langle\overline{\psi}\psi\rangle$ with reasonably small error. This is because the chiral condensate is usually very large in lattice simulations; the explicit chiral symmetry breaking due to non-zero fermion mass introduces a contribution $\propto m/a^2$, which would diverge in the continuum limit $a \to 0$.

3.2.3 Systematic effects

Now that we have reviewed the basic features of numerical lattice gauge theory simulations, let us consider some of the shortcomings of this approach. These include autocorrelations in the measurements that we perform, as well as systematic effects from working with massive fermions in a finite, discrete spacetime.

In principle these issues can be addressed by performing long-running simulations at various lattice spacings a, on lattices of various sizes $\sim L^4$, and with various pseudoscalar masses M_P^2, in order to perform controlled extrapolations to the continuum ($a \to 0$), infinite-volume ($L \to \infty$) and chiral ($M_P^2 \to 0$) limits. Due to practical limitations in computing power, often only chiral extrapolations are performed, while simulations at different L or a (if they are performed at all) are used to estimate the magnitude of the corresponding systematic effects.

In this section we consider in turn autocorrelations, discretization errors, finite volume effects, and issues related to chiral extrapolations (both for lattice QCD and for studies motivated by dynamical electroweak symmetry breaking). Our goal is to briefly summarize the relevant issues and estimate the severity of the resulting systematic effects.

Autocorrelations

Because the gauge configurations produced by the HMC algorithm are not completely independent, there are autocorrelations between the measurements performed on them. That is, the value of each observable measured on a given configuration is correlated with the value measured on preceding and subsequent configurations. These autocorrelations can depend strongly on the observable, on the evolution algorithm, on the lattice action, and on the simulation parameters (lattice size, lattice spacing and fermion mass).

The straightforward statistical issue introduced by autocorrelations is the risk of underestimating statistical errors. We address this by performing measurements on only a subset of the configurations in the ensemble, and combining these measurements into blocks (sometimes called bins) as described in Section 4.1.2 below. These blocks are the data used in our analyses, which are all performed with jackknife procedures [240]. Given N blocks of measurements, we construct N jackknife samples by removing a single block from the data set and averaging over the rest. Referring to the data x_i in the Jth jackknife sample as $x_i^{(J)}$,

$$x_i^{(J)} = \frac{1}{N-1} \sum_{k \neq J} x_i(k). \tag{3.36}$$

Analyses performed using data sample $x_i^{(J)}$ produce output parameters $a_\alpha^{(J)}$. The overall result of the jackknife procedure is

$$\overline{a_\alpha} = \frac{1}{N} \sum_{J=1}^{N} a_\alpha^{(J)} \tag{3.37}$$

with standard deviation

$$\sigma_\alpha = \sqrt{\frac{N-1}{N} \sum_{J=1}^{N} \left(a_\alpha^{(J)} - \overline{a_\alpha} \right)^2}. \tag{3.38}$$

In general, this standard deviation suffices to quantify uncertainties, but in one case we will propagate errors using the covariance matrix $C_{\alpha\beta}$ given by

$$C_{\alpha\beta} = \frac{N-1}{N} \sum_{J=1}^{N} \left(a_\alpha^{(J)} - \overline{a_\alpha} \right) \left(a_\beta^{(J)} - \overline{a_\beta} \right). \tag{3.39}$$

Ref. [203] encourages recomputing the covariance matrix for each jackknife sample, which requires considering the jackknife samples of the jackknife samples (that is, samples formed by discarding all possible pairs of blocks from the full data set). This allows estimation of the statistical fluctuations (of order $N^{-3/2}$) in Eqn. 3.39.

A related danger is that autocorrelations can grow dramatically as the lattice spacing a decreases, especially autocorrelations in observables related to topology [241]. This critical slowing down can undermine the statistical reliability of all observables (not just those related to the topology), particularly for the small ensembles and small lattice spacings used by the LSD Collaboration. At a minimum, insufficient topological evolution implies that the theory is not being correctly sampled by the Monte Carlo simulation. Because we expect the topology to be fixed in the infinite-volume limit, we may be able to treat errors resulting solely from fixed topology as finite-volume effects [242].

Discretization errors

By discretization errors we refer to deviations of lattice measurements from the corresponding continuum values that are proportional to the lattice spacing a. As discussed in Section 3.1.2 above, much effort has gone into designing "improved" lattice actions that reduce or eliminate leading $\mathcal{O}(a)$ discretization errors [215, 216], and we use modern $\mathcal{O}(a^2)$-accurate actions in our simulations.

In practice, the lattice spacing does not appear as a tunable parameter in the lattice action. Instead one adjusts the gauge coupling β, and the scale-dependence of the running coupling relates a change in the coupling to a change in the lattice spacing. The scale can be translated into physical units through any well-known and reliably-calculated dimensionful quantity, such as the mass of the lightest vector state $M_{V0} \equiv \lim_{M_P^2 \to 0} M_V$. Modern lattice QCD simulations [29] typically use $(2M_{V0})^{-1} \lesssim a \lesssim (4M_{V0})^{-1}$ (specializing to lattice QCD, $M_{V0} = m_\rho = 770$ MeV, this is $0.125 \lesssim a \lesssim 0.065$ fm, or $1.5 \lesssim a^{-1} \lesssim 3$ GeV), with discretization errors below the percent level. LSD Collaboration simulations are performed at small $a \approx (5M_{V0})^{-1}$ (for QCD, $a \approx 0.055$ fm or $a^{-1} \approx 3.6$ GeV), and

should therefore suffer from small discretization errors.

As mentioned in the previous section, it can be dangerous to reduce the lattice spacing too much, because this increases autocorrelations and requires longer simulations to produce the same number of independent measurements. Additional considerations imply that the total cost of generating an independent gauge configuration using an algorithm like hybrid Monte Carlo scales with a large negative power of a^{-6}–a^{-7}. For example, maintaining the same physical volume requires that the size of the lattice scales as a^{-4} (see Refs. [243, 244] for the remainder of the accounting). Reducing the physical volume leads to additional systematic effects, which we now discuss.

Finite volume effects

The danger of working on a finite spacetime with (anti-)periodic boundary conditions is that observables may be affected by signals propagating all the way around the lattice. In order for these unphysical contaminations to be negligible, the linear length L of the lattice must be several times larger than the longest correlation length of the system, which is generally the inverse mass M_P^{-1} of the lightest pseudoscalar meson (the pseudo-Nambu–Goldstone boson in theories exhibiting chiral symmetry breaking). Fortunately, these finite volume effects are exponentially suppressed by $M_P L$ for the observables we consider [245], and the conventional wisdom for lattice QCD is that $M_P L \gtrsim 4$ reduces finite-volume errors in the spectrum to the percent level or less.

While this general argument is not specific to QCD, we should expect to encounter more severe finite volume effects in "walking" theories for which the coupling evolves more slowly as the energy scale changes. Lattice simulations require that the coupling be relatively weak at the scale of the inverse lattice spacing a^{-1}, to avoid a transition into a strongly-coupled lattice phase without a well-defined continuum limit. Walking behavior involves a large separation between a^{-1} and the scale of chiral symmetry breaking, which implies that the lattice volume must grow very large in order to contain the low-energy physics of interest.

In the context of walking technicolor, for example, the separation between the ultra-

violet scale where asymptotic freedom sets in and the infrared scale of chiral symmetry breaking is expected to be $M_{ETC}/\Lambda_{TC} \sim 10^3$–$10^4$. It is very unlikely that the lattices used in numerical simulations will exceed $L/a \lesssim 10^2$ in the foreseeable future. Lattice studies of walking (and IR-conformal) theories are therefore likely to require step-scaling and renormalization group techniques such as those summarized in Section 4.1.1 below, in addition to zero-temperature simulations performed by the LSD Collaboration.

Such considerations were part of the motivation for the LSD Collaboration to proceed cautiously from $N_f = 2$ QCD toward the $SU(3)$ conformal window, as discussed further in Section 4.1.2 below. Comparison with lattice QCD gives some confidence that finite volume effects are small on all of our ensembles with $M_P L > 4$, and direct confirmation of this expectation is underway. However, for a given lattice size L, satisfying this condition limits the range of masses we are able to study, introducing other systematic effects that we now discuss.

Chiral extrapolations

With few exceptions, lattice gauge theory simulations are performed with unphysically heavy particles, and chiral extrapolations are performed to connect numerical results to continuum physics. In QCD, results are extrapolated (and, increasingly, interpolated) to the physical point $m_\pi \approx 135$ MeV, $m_K \approx 494$ MeV, $m_\Omega \approx 1.672$ GeV, etc. In theories that aim to model dynamical electroweak symmetry breaking, the situation is more complicated. In principle, two of the N_f flavors of strongly-interacting fermions must be extrapolated to the chiral limit $m = 0$ so that three exactly massless ($M_P^2 = 0$) Nambu–Goldstone bosons are available to be eaten by the $W^\pm$ and Z. The other $N_f - 2$ flavors must remain massive so that no unphysically light pseudo-NGBs appear in the spectrum.

In practice, such elaborate extrapolations are not performed as part of current lattice calculations exploring technicolor theories, including those we discuss in Section 4. Instead, all N_f fermions are taken to be degenerate. Some quantities (such as the mass M_V of the lightest vector state) are well-behaved in the limit $M_P^2 \to 0$ with $N_f^2 - 1$ NGBs; others

(such as the S parameter) diverge in this limit if $N_f > 2$. In this situation we are forced to keep $M_P^2 > 0$ and estimate the effects of the two-flavor extrapolation by comparison with the $N_f = 2$ theory.

For quantities related to the chiral symmetry breaking process itself (in particular M_P, F_P and $\langle\overline{\psi}\psi\rangle$), it is important to exploit chiral perturbation theory (χPT [101, 246]) to ensure that the chiral extrapolation uses the proper functional form (in particular accounting for so-called chiral logarithms) [102]. Not surprisingly given our introduction of technicolor in terms of a chiral lagrangian, Eqn. 2.27, it is possible to relate the S parameter to one of the low energy constants of next-to-leading order χPT, $L_{10}^r(\mu)$. The relation is

$$S(\mu, M_H^{(ref)}) = \frac{1}{12\pi}\left[-192\pi^2\left(L_{10}^r(\mu) + \frac{1}{384\pi^2}\left\{\log\left[\frac{m_K^2}{\mu^2}\right] + 1\right\}\right) + \log\left[\frac{\mu^2}{M_H^{(ref)}}\right] - \frac{1}{6}\right], \tag{3.40}$$

where μ is a (techni)hadronic renormalization scale (such as the mass of the lightest vector meson state) and $M_H^{(ref)}$ is the reference Higgs boson mass. The kaon mass m_K appears because $L_{10}^r(\mu)$ is a parameter of three-flavor χPT; a related two-flavor formulation of χPT uses the low-energy constant

$$\ell_5^r(\mu) = L_{10}^r(\mu) + \frac{1}{384\pi^2}\left(\log\left[\frac{m_K^2}{\mu^2}\right] + 1\right), \tag{3.41}$$

and a scale-invariant quantity $\overline{\ell}_5$ can be defined by cancelling out the μ-dependence of $\ell_5^r(\mu)$,

$$\overline{\ell}_5 = -192\pi^2\ell_5^r(\mu) - \log\left[\frac{m_\pi^2}{\mu^2}\right]. \tag{3.42}$$

While χPT cannot reliably be applied to chiral extrapolations of LSD Collaboration data (due to large M_P^2 and $N_f > 2$ [1, 2]), this approach is used to calculate S in scaled-up QCD by Refs. [141, 142]. These studies fit low-M_P^2, low-Q^2 data for $\Pi_{V-A}(Q^2) \equiv$

$\Pi_{VV}(Q^2) - \Pi_{AA}(Q^2)$ (cf. Eqn. 2.43) to the χPT expression

$$\Pi_{V-A}(M_P^2, Q^2) = -F_P^2 - Q^2 \left[8L_{10}^r(\mu) + \frac{1}{24\pi^2} \left(\log \left[\frac{M_P^2}{\mu^2} \right] + \frac{1}{3} - H(x) \right) \right] \tag{3.43}$$
$$H(x) = (1+x) \left[\sqrt{1+x} \log \left(\frac{\sqrt{1+x}-1}{\sqrt{1+x}+1} + 2 \right) \right],$$

where $x \equiv 4M_P^2/Q^2$.

3.3 Chiral lattice fermions

In addition to the explicit chiral symmetry breaking due to non-zero fermion mass, we saw above in Section 3.1.3 that simple discretizations of the fermion action also introduce χSB to evade the doubling problem. This has several unwelcome consequences. Without chiral symmetry on the lattice, the input (bare) fermion mass m_f may receive additive (not just multiplicative) renormalization, so that the chiral limit $M_P^2 \to 0$ is not known *a priori* in terms of m_f. In addition (assuming that the lattice gauge action is $\mathcal{O}(a^2)$-accurate), lattice fermion actions that preserve chiral symmetry on the lattice automatically result in discretization errors only quadratic in a, smaller than the $\mathcal{O}(a)$ discretization errors that can occur from actions that break chiral symmetry [247]. Finally, lack of chiral symmetry allows operators to mix that would not if the action were chiral, which can complicate analyses and obscure signals. Qualitatively, because we are interested in applying lattice gauge theory to models of electroweak symmetry breaking that result from spontaneous χSB, we should make every effort to ensure that explicit chiral symmetry breaking does not contaminate our investigations.

We also saw in Section 3.1.3 that lattice fermion can exactly possess a (modified) chiral symmetry at non-zero lattice spacing, described by the Ginsparg–Wilson relation, Eqn. 3.20. There we wrote down the overlap operator, Eqn. 3.22, and in this section we consider a related formulation, the domain wall fermion (DWF) action introduced by Refs. [45, 46, 47]. Originally motivated by the connection between anomalies in $2n$ dimensions and currents in $2n+1$ dimensions, the DWF formulation adds a fifth dimension

to the lattice, of length L_s. Actually, the fifth "dimension" consists of L_s copies of the same four-dimensional gauge field, connected by the action we describe below.

However, the DWF operator can just as well be understood as an approximation (specifically the polar approximation [248, 249, 250]) to the sign function in the overlap operator,

$$\text{sign}_{L_s}[H_5] = \frac{(1+H_5)^{L_s} - (1-H_5)^{L_s}}{(1+H_5)^{L_s} + (1-H_5)^{L_s}} \tag{3.44}$$

where $H_5 = \gamma_5 D_W(-M_5)$ is used to form the transfer matrix that describes the propagation of fermion modes along the fifth dimension,

$$\widehat{T}_5 = \frac{1-H_5}{1+H_5}. \tag{3.45}$$

As $L_s \to \infty$, the approximation $\text{sign}_{L_s}[H_5]$ becomes exact, and in that limit domain wall fermions possess exact chiral symmetry at finite lattice spacing.

Our goal in this section is not to review the fascinating field of chiral symmetry on the lattice (for that purpose, see Ref. [44]), but primarily to establish our notational conventions and introduce some DWF concepts that will play a role in the calculations we discuss in Section 4. We begin with the formulation of the domain wall operator.

3.3.1 Domain wall formulation

Our notation and implementation of domain wall fermions largely follows the work of the RBC and UKQCD Collaborations, Refs. [48, 251, 252, 253, 254, 247]. We label the L_s copies of the gauge field along the fifth dimension with the index $s = 0, \cdots, L_s - 1$. Although domain wall fermions only possess exact chiral symmetry in the limit $L_s \to \infty$, we take the length of the fifth dimension L_s to be finite, and periodically identify $s = L_s$ with $s = 0$. In numerical simulations, $L_s \sim \mathcal{O}(10)$, and we will discuss the "residual" chiral symmetry breaking due to finite L_s in Section 3.3.2 below.

The domain wall fermion action is $S_f = \overline{\Psi} D_{DWF}(m)\Psi + \Phi^\dagger D_{DWF}(m=1)\Phi$, where $\Psi(x,s)$ and $\Phi(x,s)$ are five-dimensional fermion and Pauli–Villars regulator fields, respectively. The domain wall Dirac operator $D_{DWF}(m)$ is built from the four-dimensional

Wilson Dirac operator $D_W(m)$,

$$
\begin{aligned}
[D_W(-M_5)]_{x,y} &= (4-M_5)\delta_{x,y} - \frac{1}{2}\left[(1+\gamma^\mu)U^\dagger_{x,\mu}\delta_{x,y+\mu} + (1-\gamma^\mu)U_{x,\mu}\delta_{x+\mu,y}\right] \\
[D_{DWF}(m_f)]_{s,s'} &= [D_W(-M_5)+1]\,\delta_{s,s'} + P_L\left[(1+m_f)\delta_{s,L_s-1}\delta_{s',0} - \delta_{s+1,s'}\right] \\
&\quad + P_R\left[(1+m_f)\delta_{s,0}\delta_{s',L_s-1} - \delta_{s,s'+1}\right].
\end{aligned}
\tag{3.46}
$$

Here $P_R = \frac{1}{2}(1+\gamma_5)$, $P_L = \frac{1}{2}(1-\gamma_5)$ and $0 < M_5 < 2$ can be considered the height of the domain wall. In the form of an $L_s \times L_s$ matrix, we can write the operator $D_{DWF}(m)$ as

$$
\begin{pmatrix}
D_W(-M_5)+1 & -P_L & 0 & \cdots & mP_R \\
-P_R & D_W(-M_5)+1 & -P_L & \cdots & 0 \\
0 & -P_R & D_W(-M_5)+1 & \cdots & 0 \\
\vdots & \vdots & \vdots & \ddots & \vdots \\
mP_L & 0 & 0 & \cdots & D_W(-M_5)+1
\end{pmatrix}. \tag{3.47}
$$

In the fifth dimension the Pauli–Villars operator $D_{DWF}(1)$ has anti-periodic boundary conditions, but the in the limit of zero fermion mass $m \to 0$, the Dirac operator $D_{DWF}(m)$ has Dirichlet boundary conditions. D_{DWF} is γ_5-hermitian if we also reflect around the midpoint of the fifth dimension,

$$
D^\dagger_{DWF} = \gamma_5 \mathcal{R} D_{DWF} \mathcal{R} \gamma_5, \tag{3.48}
$$

where $\mathcal{R}_{s,s'} = \delta_{s,L_s-1-s'}$. This still satisfies the condition $\det[D_{DWF}] = \det\left[D^\dagger_{DWF}\right]$ needed to show the positivity of the action.

Qualitatively, we see that m couples the left and right walls, and we can understand Eqns. 3.46 and 3.47 to represent light, chiral lattice modes localized near the domain walls. The doublers (and additional modes from the enlarged dimensionality of the operator) propagate in the fifth dimension, and obtain large masses from the Wilson term in the action. As L_s increases, so does the number of these heavy modes, which the Pauli–Villars regulator fields cancel in the limit $L_s \to \infty$.

Although the domain wall fermion formulation introduces a fifth dimension, it describes four-dimensional physics. Adopting the notation of Ref. [48], we define the four-dimensional fermion fields $q(x)$ as the chiral projections of the five-dimensional fermion fields $\Psi(x,s)$ on the domain walls at $s=0$ and $s=L_s-1$,

$$q(x) = P_L\Psi(x,0) + P_R\Psi(x,L_s-1) \qquad \overline{q}(x) = \overline{\Psi}(x,L_s-1)P_L + \overline{\Psi}(x,0)P_R. \tag{3.49}$$

Since $P_R\gamma_5 = \gamma_5 P_R = P_R$ and $P_L\gamma_5 = \gamma_5 P_L = -P_L$, the flavor non-singlet pseudoscalar operator is

$$P^a(x) = \overline{q}(x)\gamma_5 T^a q(x) = \overline{\Psi}(x,0)P_R T^a \Psi(x,L_s-1) - \overline{\Psi}(x,L_s-1)P_L T^a\Psi(x,0), \tag{3.50}$$

where the flavor matrices $T^a = \frac{1}{2}\tau^a$ are normalized so that $\mathrm{Tr}\left[T^aT^b\right] = \frac{1}{2}\delta^{ab}$. A similar "midpoint" pseudoscalar operator is defined by shifting $s \to s + L_s/2$ (recall that $s = L_s$ is periodically identified with $s=0$):

$$J^a_{mid}(x) = \overline{\Psi}(x,L_s/2)P_R T^a\Psi(x,L_s/2-1) - \overline{\Psi}(x,L_s/2-1)P_L T^a\Psi(x,L_s/2). \tag{3.51}$$

We use $J^a_{mid}(x)$ to determine the residual chiral symmetry breaking due to finite L_s. At low energies

$$J^a_{mid} = m_{res}P^a(x) + \mathcal{O}(a^2), \tag{3.52}$$

where the residual mass m_{res} quantifies chiral symmetry breaking as we now discuss.

3.3.2 Residual chiral symmetry breaking

As explained above, the chiral symmetry of domain wall fermions only becomes exact in the limit $L_s \to \infty$. For the low-energy observables that we are interested in, at scales small compared to the inverse lattice spacing a^{-1}, the residual chiral symmetry breaking due to finite L_s can be represented as an additive renormalization m_{res} of the input fermion mass m_f. (Of course, $m_f > 0$ itself breaks chiral symmetry.) The chiral limit can then be obtained as $m \equiv m_f + m_{res} \to 0$.

For the $N_f = 2$ simulations discussed in Section 4 (which have large cutoff a^{-1} and relatively small $L_s = 16$), the residual mass m_{res} is exponentially suppressed by L_s, dominated by a term $\propto e^{-\lambda_c L_s}/L_s$. Here λ_c is the "mobility edge", adapted to lattice QCD from condensed matter physics by Ref. [255]. At stronger coupling (smaller a^{-1}) or larger L_s, an additional contribution to m_{res} that is $\propto 1/L_s$ becomes important [254]. This contribution arises from eigenmodes of $\log \widehat{T}_5$ that have localized four-dimensional support and have eigenvalues near zero, $|\lambda| < \lambda_c$. ($\widehat{T}_5$ is the transfer matrix defined in Eqn. 3.45 above.) Such near-zero modes are believed to be lattice artifacts ("dislocations") localized to a few lattice spacings a; however, they contribute to the effects of chiral symmetry breaking on low-energy observables. Because we must increase the coupling to match low-energy scales for $N_f > 2$, such effects may become more important as N_f increases, cf. Section 4.1.2.

While we will not discuss further the analytic dependence of m_{res} on L_s (or on other DWF parameters such as M_5), we summarize here our non-perturbative calculation of m_{res}. We consider the ratio

$$R(|t-t_0|) = \frac{\left\langle \sum_{\mathbf{x}} \mathrm{Tr}\left[J^a_{mid}(\mathbf{x},t) P^b(\mathbf{0},t_0) \right] \right\rangle}{\left\langle \sum_{\mathbf{x}} \mathrm{Tr}\left[P^a(\mathbf{x},t) P^b(\mathbf{0},t_0) \right] \right\rangle} = \frac{\left\langle \sum_{\mathbf{x}} J^a_{mid}(\mathbf{x},t) P^a(\mathbf{0},t_0) \right\rangle}{\left\langle \sum_{\mathbf{x}} P^a(\mathbf{x},t) P^a(\mathbf{0},t_0) \right\rangle}, \tag{3.53}$$

which measures the pseudoscalar coupling to the midpoint operator (Eqn. 3.51), normalized by the pseudoscalar correlator itself [48, 251, 252, 253]. We explicitly write the trace in Eqn. 3.53 to emphasize that the flavor index ^{a} in the final expression is not summed over, but indicates that these operators are flavor non-singlet.

Similarly to the effective masses discussed in Section 3.2.2 above, for $1 \ll t \ll N_t$ the ratio $R(t)$ should be approximately constant, and we identify m_{res} as the value of this plateau, as illustrated in Fig. 3·3. As discussed above, the physical domain wall fermion modes are localized around the left ($s = 0$) and right ($s = L_s - 1$) walls in the fifth dimension as chiral symmetry improves. Improving this localization reduces $R(t)$ and m_{res}, since $P^a(x)$ is defined on the walls while $J^a_{mid}(x)$ is defined halfway between them. Similarly, the ratio vanishes in the limit $L_s \to \infty$, which reflects our statement that the domain wall fermion formulation possesses exact chiral symmetry in this limit, even at

non-zero lattice spacing.

3.3.3 Local and conserved currents

We conclude our brief overview of domain wall fermions by considering the vector and axial currents that appear in the calculation of the S parameter. Here we actually have two options. The simple approach is to use $q(x)$ from Eqn. 3.49 in the usual continuum expressions,

$$\begin{aligned} V_\mu^a(x) &= \overline{q}(x)\gamma_\mu T^a q(x) \\ &= \overline{\Psi}(x, L_s-1)\gamma_\mu P_R T^a \Psi(x, L_s-1) + \overline{\Psi}(x,0)\gamma_\mu P_L T^a \Psi(x,0) \end{aligned} \tag{3.54}$$

$$\begin{aligned} A_\mu^a(x) &= \overline{q}(x)\gamma_\mu\gamma_5 T^a q(x) \\ &= \overline{\Psi}(x, L_s-1)\gamma_\mu P_R T^a \Psi(x, L_s-1) - \overline{\Psi}(x,0)\gamma_\mu P_L T^a \Psi(x,0). \end{aligned} \tag{3.55}$$

We refer to $V_\mu^a(x)$ and $A_\mu^a(x)$ as "local" currents because they involve $q(x)$ and $\overline{q}(x)$ at the same site x. Ref. [47] introduced the corresponding conserved currents $\mathcal{V}_\mu^a(x)$ and $\mathcal{A}_\mu^a(x)$, which are built from the point-split current

$$j_\mu^a(x,s) = \overline{\Psi}(x+\widehat{\mu}, s)\frac{1+\gamma_\mu}{2}U_{x,\mu}^\dagger T^a \Psi(x,s) - \overline{\Psi}(x,s)\frac{1-\gamma_\mu}{2}U_{x,\mu} T^a \Psi(x+\widehat{\mu}, s) \tag{3.56}$$

by summing over the fifth dimension,

$$\mathcal{V}_\mu^a(x) = \sum_{s=0}^{L_s-1} j_\mu^a(x,s) \qquad \mathcal{A}_\mu^a(x) = \sum_{s=0}^{L_s-1} \text{sign}\left(s - \frac{L_s-1}{2}\right) j_\mu^a(x,s). \tag{3.57}$$

Because $j_\mu^a(x,s)$ is point-split, we should think of $\mathcal{V}_\mu^a(x)$ and $\mathcal{A}_\mu^a(x)$ as the currents carried by the link between x and $(x+\widehat{\mu})$, properly located at $(x+\widehat{\mu}/2)$.

$\mathcal{V}_\mu^a(x)$ is conserved in the sense that its divergence vanishes,

$$\Delta_\mu \mathcal{V}^{a\mu}(x) = \sum_{s=0}^{L_s-1} \Delta_\mu j^{a\mu}(x,s) = 0. \tag{3.58}$$

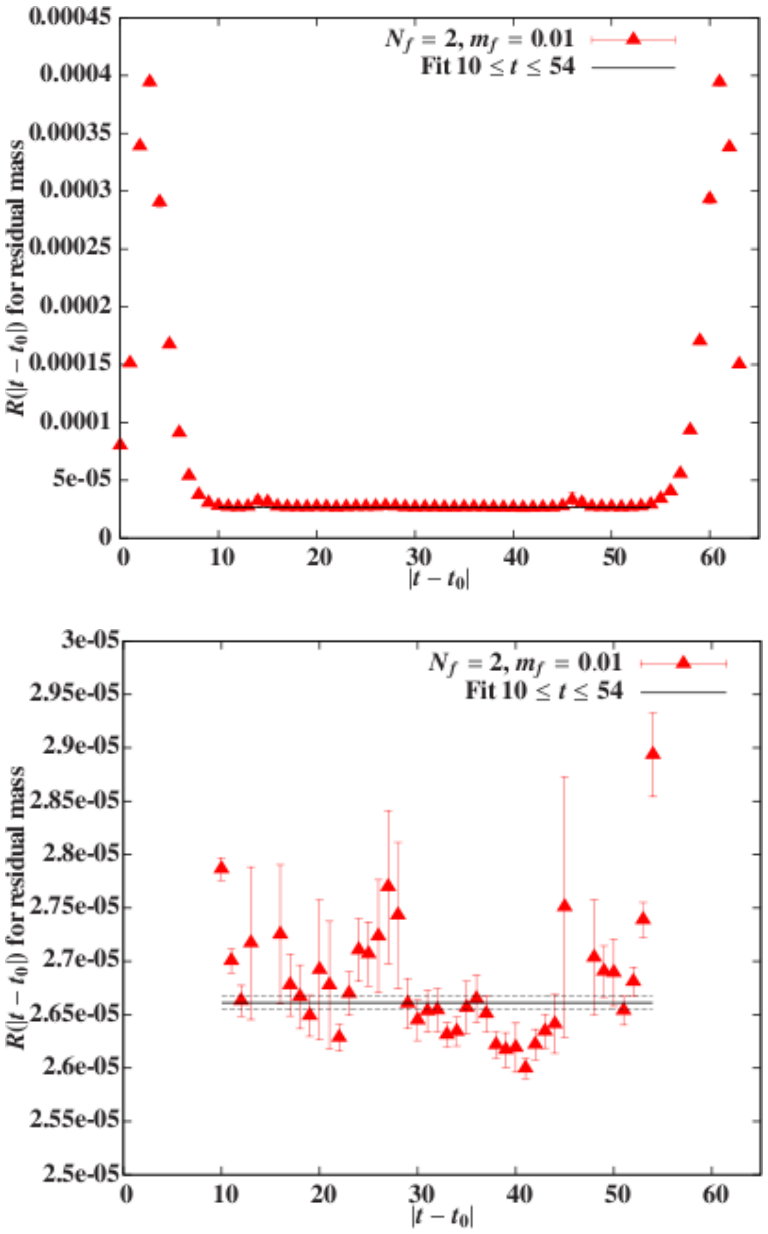

Figure 3·3: Jackknife fit results for $R(|t - t_0|)$ and m_{res} (solid black line) from $32^3 \times 64$ LSD Collaboration ensembles with $N_f = 2$ and $m_f = 0.01$ (cf. Section 4.1.2 for details of ensembles and measurements). The bottom panel zooms in on the plateau in the range $10 \leq t \leq 54$. The dotted lines show the statistical error in m_{res}.

Here Δ_μ is the lattice finite difference operator with five-dimensional continuity equation

$$\Delta_\mu j^{a\mu}(x,s) = \begin{cases} -j_5^a(x,0) - mP^a(x) & s = 0 \\ j_5^a(x,s-1) - j_5^a(x,s) & 0 < s < L_s - 1 \\ j_5^a(x,L_s-2) + mP^a(x) & s = L_s - 1 \end{cases} \tag{3.59}$$

where for notational convenience we have defined

$$j_5^a(x,s) \equiv \overline{\Psi}(x,s+1)P_R T^a \Psi(x,s) - \overline{\Psi}(x,s)P_L T^a \Psi(x,s+1). \tag{3.60}$$

Note that $j_5^a(x,L_s-1) = P^a(x)$ and $j_5^a(x,L_s/2-1) = J^a_{mid}(x)$. When acting on a four-dimensional operator,

$$\Delta_\mu f(x) = f(x) - f(x-\widehat{\mu}), \tag{3.61}$$

so the local current $V_\mu^a(x)$ is not conserved. We can also discuss current conservation in terms of the Ward–Takahashi identity [256, 257]

$$\Delta_\mu \left\langle \mathcal{V}^{a\mu}(x) O(y) \right\rangle = i \left\langle \delta^a O(y) \right\rangle . \tag{3.62}$$

Similarly, $\mathcal{A}_\mu^a(x)$ is "partially" conserved (i.e., conserved in the chiral limit),

$$\Delta_\mu \mathcal{A}^{a\mu}(x) = 2m_f P^a(x) + 2J^a_{mid}(x) \approx 2(m_f + m_{res})P^a(x) \tag{3.63}$$

$$\Delta_\mu \left\langle \mathcal{A}^{a\mu}(x) O(y) \right\rangle = 2m_f \left\langle P^a(x) O(y) \right\rangle + 2 \left\langle J^a_{mid}(x) O(y) \right\rangle + i \left\langle \delta^a O(y) \right\rangle , \tag{3.64}$$

which follows from Eqns. 3.57 and 3.59. If the operator $O(x)$ is a flavor non-singlet defined on the walls (i.e., built from the fields $q(x)$ and $\overline{q}(x)$), then $\langle J^a_{mid}(x)O(y)\rangle$ vanishes in the limit $L_s \to \infty$ [47].

While $\mathcal{V}_\mu^a(x)$ and $\mathcal{A}_\mu^a(x)$ approach the corresponding continuum currents with unit normalization as $a \to 0$,[1] the continuum limits of the non-conserved local currents $V_\mu^a(x)$ and

[1] According to Ref. [258], the conserved axial current receives an additional multiplicative renormalization $Z_\mathcal{A}$ from the effects of finite L_s, which is expected to be negligible in practice, $Z_\mathcal{A} - 1 \propto m_{res}^2$. Although Ref. [247] argues that $Z_\mathcal{A} - 1 \propto m_{res}$, this is still a small (sub-percent level) effect, though it may become more important for larger N_f, cf. Section 4.1.2.

$A^a_\mu(x)$ may differ from the true currents by a multiplicative renormalization constant Z. More generally, we can define Z_V and Z_A for the vector and axial currents, respectively, which relate

$$\mathcal{A}^a_\mu(x) = Z_A A^a_\mu(x) + \mathcal{O}(a^2) \qquad\qquad \mathcal{V}^a_\mu(x) = Z_V V^a_\mu(x) + \mathcal{O}(a^2) \tag{3.65}$$

at finite lattice spacing. While $Z_A = Z_V$ in the chiral limit, these two renormalization factors can differ in simulations at non-zero lattice spacing and fermion mass.

We can determine Z_V and Z_A non-perturbatively, much as we calculate m_{res} above. The basic idea is to consider a correlator involving one conserved current and one local current, normalized by the corresponding correlator with only local currents. The cleanest signal comes from coupling the temporal component of the axial current with the pseudoscalar operator,

$$C(|t - t_0 + 1/2|) = \left\langle \sum_{\mathbf{x}} \mathcal{A}^a_4(\mathbf{x}, t) P^a(\mathbf{0}, t_0) \right\rangle \tag{3.66}$$

$$L(|t - t_0|) = \left\langle \sum_{\mathbf{x}} A^a_4(\mathbf{x}, t) P^a(\mathbf{0}, t_0) \right\rangle \tag{3.67}$$

(recall that $\mathcal{A}^a_4(\mathbf{x}, t)$ is located at $(x + \widehat{t}/2)$, and we do not sum over the flavor index ^{a}). Then, like $R(t)$ in Eqn. 3.53, $C(t)/L(t)$ is approximately constant for $1 \ll t \ll N_t$, and this constant can be identified with Z_A. This procedure can be improved by constructing arithmetic averages of $C(|t - t_0 + 1/2|)$ and $L(|t - t_0|)$, to account for the fact that they are not at exactly the same location. Ref. [48] argues that the ratio

$$Z_A(t) = \frac{1}{2}\left\{ \frac{C(t + 1/2) + C(t - 1/2)}{2L(t)} + \frac{2C(t + 1/2)}{L(t) + L(t + 1)} \right\} \tag{3.68}$$

eliminates $\mathcal{O}(a)$ discretization effects and also reduces $\mathcal{O}(a^2)$ effects. We show an example of the $Z_A(t)$ plateau in Fig. 3·4 for LSD Collaboration ensembles with $N_f = 2$ and $m_f = 0.01$.

Fig. 3·4 also shows a plateau for Z_V, which we calculate non-perturbatively in a slightly different way. Because $Z_A = Z_V$ in the chiral limit, independently measuring the two Z

factors can provide another measure of residual chiral symmetry breaking and its effects on observables. In addition, because our calculation of Z_V differs from that of Z_A, we may be able to estimate the magnitude of $\mathcal{O}(a)$ discretization effects by comparing our results for the two Z factors, especially in the chiral limit.

Straightforwardly changing Eqn. 3.68 from axial currents to the vector case would replace $P^a(x)$ with the (flavor non-singlet) scalar operator $\overline{q}(x)T^a q(x)$, and we find the resulting correlators to be very noisy. Empirically, we find cleaner signals for Z_V from the ratio

$$Z_V(|t-t_0|) = \frac{\langle \sum_{\mathbf{x}} \mathcal{V}_i^a(\mathbf{x},t) V_i^a(\mathbf{0},t_0)\rangle}{\left\langle \sum_{\mathbf{x}} V_j^a(\mathbf{x},t) V_j^a(\mathbf{0},t_0)\right\rangle}, \tag{3.69}$$

where we sum over the spatial indices i and j, but not the flavor index ^{a}. The ratio in Eqn. 3.69 also gives reasonable results for Z_A when we replace $\mathcal{V}_i^a(x)$ and $V_i^a(x)$ with $\mathcal{A}_i^a(x)$ and $A_i^a(x)$. We refer to these results as $Z_A^{(i)}$ to distinguish them from Z_A as calculated by Eqn. 3.68.

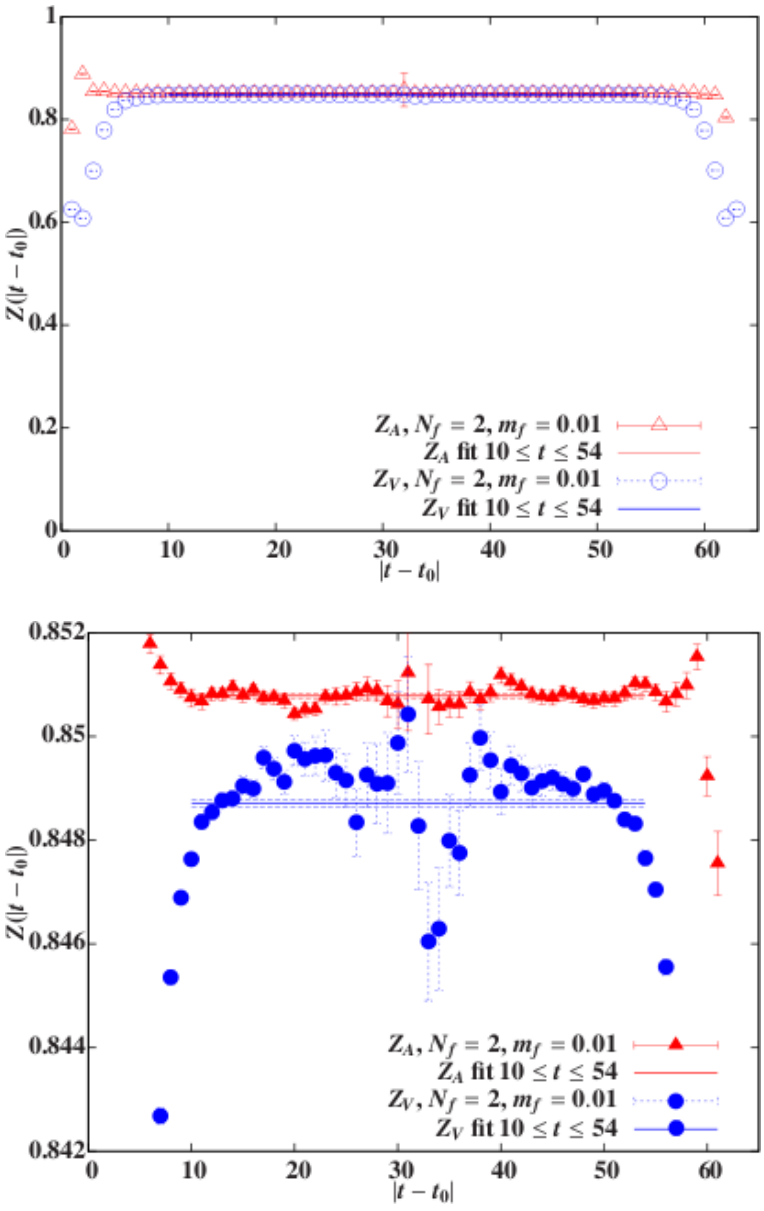

Figure 3·4: Jackknife fit results for $Z_A(|t-t_0|)$ and $Z_V(|t-t_0|)$ as well as Z_A and Z_V (solid lines) from $32^3\times 64$ LSD Collaboration ensembles with $N_f = 2$ and $m_f = 0.01$ (cf. Section 4.1.2 for details of ensembles and measurements). The bottom panel zooms in on the plateaus in the range $10 \leq t \leq 54$. The dotted lines show the statistical errors in the Z factors.

Chapter 4

Lattice strong dynamics

We now bring together the two preceding discussions, by considering the application of lattice gauge theory (Section 3) to models of dynamical electroweak symmetry breaking (Section 2). Although technicolor theories are the immediate motivation for these studies, even if strong dynamics are not directly responsible for EWSB, this work will help improve our very limited understanding of strongly-interacting gauge theories beyond QCD. Because theories of physics beyond the standard model generally involve strongly-coupled dynamics (if in some cases only at very high energies such as the scale of supersymmetry breaking), improving our understanding of strong interactions may prove invaluable to future efforts to unravel BSM physics.

Lattice studies beyond QCD have generated a great deal of interest and activity in recent years, and we begin this section with a brief overview of the field. We review the goals and status of the work, as well as some of the unique challenges that face lattice studies attempting to explore walking or IR-conformal dynamics. Although we sketch the current state of results, detailed discussions of all the models and methods under consideration is well beyond the scope of this document. Recent reviews include Refs. [35, 36, 37, 38, 39].

The remainder of Section 4.1.2 focuses on the program and initial results of the Lattice Strong Dynamics (LSD) Collaboration. To address some of the challenges of studying non-QCD theories on the lattice, LSD Collaboration explorations are grounded on the relatively firm footing of lattice QCD. That is, we study SU(3) gauge theories and systematically increase the number N_f of fermions in the fundamental representation, from $N_f = 2$ (lattice QCD) to $N_f = 6$ and $N_f = 10$. By matching the scales used in these studies, we can search for deviations from QCD-like behavior, and from expectations based on scaling

QCD results with N_f.

After briefly reviewing $N_f = 6$ (and some preliminary $N_f = 10$) LSD Collaboration results on the enhancement of the chiral condensate $\langle\overline{\psi}\psi\rangle$ relative to lattice QCD [1, 4], we consider the corresponding results for the masses and decay constants of the lightest vector and axial mesons. This leads us to a detailed discussion of our lattice calculation of the electroweak S parameter [3, 4]. For $N_f = 2$, we find $S = 0.311(21)$, in agreement with the initial estimate $S = 0.32(3)$ made by scaling up experiment QCD spectrum data to the electroweak scale [18]. For $N_f = 6$ and $N_f = 10$ we find results for S that can be well below the value obtained by simply scaling QCD dynamics by a factor of $N_f/2$. We conclude the section by discussing the systematic effects entering these results for the S parameter, and future directions both for this calculation and for the LSD Collaboration program as a whole.

4.1 General considerations

We begin our discussion of lattice studies of theories beyond QCD by briefly summarizing the current state of the field, focusing on the goals and recent results of these explorations, as well as the particular challenges they face. We then introduce the program of the LSD Collaboration and discuss some if its initial results.

4.1.1 Overview of the field

Goals

Although attempts to apply lattice gauge theory techniques to questions related to dynamical electroweak symmetry breaking date back to the mid-1980s [259, 260, 261, 262, 263, 264, 265, 266, 267, 268], only in recent years have algorithmic advancements and steadily increasing computational resources begun to produce reliable results that have attracted great interest.

Beginning with Refs. [269, 270], most studies have focused on delineating the conformal window for the theories with the fewest degrees of freedom (and therefore the minimal

computational requirements), specifically $SU(2)$ and $SU(3)$ gauge theories with fermions in the fundamental, adjoint or two-index symmetric representations. A related goal, for those theories that appear to exhibit walking or IR-conformal behavior, is to determine the mass anomalous dimension γ_m, with particular interest in identifying any theories with $\gamma_m \gtrsim 1$. Next, with the CERN Large Hadron Collider beginning direct exploration of the TeV scale, predictions for the particle spectra of TeV-scale strongly-interacting theories are of great interest. These calculations can also be used to calculate the S parameter in these theories, and search for any theories with S small enough to satisfy phenomenological constraints.[1] Finally, lattice simulations may observe more speculative possibilities such as pseudo-dilatons [274].

Status

In Table 4.1, we attempt to compactly summarize the conclusions of recent lattice searches for conformal windows, specifying whether the cited studies indicate an infrared fixed point in the continuum chiral limit (IRFP), are better described by chiral symmetry breaking (χSB), or could be consistent with both possibilities. (We also note in the table where asymptotic freedom is lost, to reveal the range of possibilities.) This classification omits a vast amount of information, and we encourage direct consultation of the cited sources and references therein.

There is general consensus that both $SU(3)$ gauge theory with $N_f = 16$ fundamental fermions and $SU(2)$ gauge theory with $N_f = 2$ adjoint fermions are IR-conformal. Similarly, $SU(3)$ gauge theories with $N_f \leq 8$ fermions in the fundamental representation are thought to exhibit chiral symmetry breaking. With the exception of Refs. [290, 291], studies of $SU(2)$ gauge theories with fermions in the fundamental representation have focused on simulations performed at large temperatures and baryonic density (chemical potential), rather than directly searching for the conformal window.

[1] Studying the spectrum and S is most natural in theories exhibiting chiral symmetry breaking, though recent conjectures on the S parameter of "mass-deformed" IR-conformal theories may benefit from comparison with lattice studies [271, 155, 272, 273].

Table 4.1: Lattice studies of the IR behavior of $SU(N_c)$ gauge theories with N_f fermions in the specified representation.

N_c	N_f	**Rep.**	**Result**	**Ref.**
2	2	Adj.	IRFP	[275, 276, 277, 278, 279, 280, 281]
			Unclear	[282, 283, 284, 285, 278, 286]
2	3	Adj.	Asymptotic freedom lost	
2	2	Fund.	χSB	[287, 288]
2	4	Fund.	χSB	[289]
2	6	Fund.	Unclear	[290]
2	8	Fund.	Unclear	[291]
2	11	Fund.	Asymptotic freedom lost	
3	4	Fund.	χSB	[292, 293, 294]
3	6	Fund.	χSB	[1], this work
3	8	Fund.	χSB	[270, 295, 296, 294, 297, 298]
3	9	Fund.	χSB	[294]
3	10	Fund.	IRFP	[299]
3	12	Fund.	χSB	[294, 297, 300, 301]
			IRFP	[270, 295, 302]
			Unclear	[298, 303]
3	16	Fund.	IRFP	[266, 267, 293, 294, 304]
3	17	Fund.	Asymptotic freedom lost	
3	2	Sym.	χSB	[300]
			Unclear	[305, 306, 307, 308, 309]
3	4	Sym.	Asymptotic freedom lost	

The case of $SU(3)$ gauge theory with $N_f = 2$ fermions transforming in the two-index symmetric (sextet) representation illustrates the potential sensitivity of these studies to the method used: initial signs of an IRFP reported by Ref. [307] vanished when those authors improved their action to reduce lattice artifacts [309]. The current disagreement regarding the IR behavior of $SU(3)$ gauge theory with $N_f = 12$ fermions in the fundamental representation is also likely due (at least in part) to the different methods used by the various studies. It is not clear at this time which of these methods may prove most reliable.

Detailed discussion of the many methods employed in these studies is well beyond the scope of this document, but we mention that the most common lattice technique to search for signs of an IRFP is to use step-scaling techniques that measure some definition of the running coupling over a wide range of scales. The Schrödinger functional scheme for the coupling [310, 311, 312] is widely used, as are definitions of the coupling from the potential between static charges [313, 314, 304].[2] Monte Carlo renormalization group techniques operate similarly [315, 316, 317], applying blocking transformations to change the scale. The spectrum or thermodynamical phase diagram of the theory can also be compared to the behavior expected from either IR conformality or chiral symmetry breaking [318, 319, 320, 273].

Although $SU(2)$ gauge theory with $N_f = 2$ fermions in the adjoint representation appears to possess an IR fixed point in the continuum chiral limit, measurements of the mass anomalous dimension at this fixed point have consistently found γ_m to be significantly smaller than the $\gamma_m \gtrsim 1$ that appears to be needed for the simplest theories of walking technicolor to remain viable. Using a variety of different methods, Refs. [277, 279, 280, 281] all find $\gamma_m \lesssim 0.6$. Studies of $SU(3)$ gauge theory with $N_f = 2$ fermions in the two-index symmetric representation also find $\gamma_m \lesssim 0.6$ [319, 309]. For $SU(3)$ gauge theory with $N_f = 16$ fermions in the fundamental representation, the theory is weakly coupled and γ_m negligible; Ref. [298] finds a very small $\gamma_m = 0.06(2)$ for $N_f = 12$ as well. So far,

[2] We reiterate the points made in Section 2.3, that although the value of the coupling associated with an IRFP is scheme-dependent, the *existence* of an IRFP, and the mass anomalous dimension γ_m *at* that IRFP, are scheme-independent.

the only hint of a large $\gamma_m \gtrsim 1$ comes from the $SU(2)$ theory with $N_f = 6$ fermions in the fundamental representation. Here Ref. [290] reports $0.135 < \gamma_m < 1.03$, but large uncertainties make it unclear whether or not the theory possesses an IRFP at all.

Challenges

One challenge that our discussion above clearly reveals is the large number of possible models that could be candidates for physics beyond the standard model, or could be theoretically interesting in their own right. It is not practical (or possible) to study all of these models in detail. Instead, our strategy (guided by experiment and model-building) must be to map out isolated islands in the theoretical sea, and attempt to understand how the properties of a given theory depend on its most basic features: the gauge group and matter content.

Another difficulty is that, unlike lattice QCD, we do not have extensive experimental information to guide us. Without this means of assessing the systematic effects of working in a finite, discrete spacetime, we are obligated to carefully ensure that our lattice calculations provide reliable information about continuum physics. This produces a significant increase in computational cost; the LSD Collaboration, for instance, uses computationally expensive domain wall fermions due to the closer connection to continuum physics possessed by this chiral lattice formulation, as opposed to cheaper Wilson or staggered fermions. Similarly, the different methods employed by the various groups studying lattice gauge theories beyond QCD cannot be evaluated by how well they reproduce experimental information; more care must be taken to understand and resolve any discrepancies in results obtained by different methods.

Additional costs arise from the larger number of degrees of freedom possessed by most of these theories compared to lattice QCD. Besides the linear growth in the number of inversions required as N_f increases, the additional fermions contribute to the total forces entering into hybrid Monte Carlo simulations, requiring that the HMC step size be reduced by a factor of roughly $\sqrt{N_f}$. The total cost of the simulations therefore increases $\propto N_f^{3/2}$.

Finally, and perhaps most significantly, the walking or IR-conformal dynamics that we aim to study present challenges to lattice methods by their very nature. As discussed in Section 3.2.3, the emergence of widely separated scales that is associated with walking behavior demands very large lattices (or the use of step-scaling techniques) for results to be reliable.

4.1.2 Lattice Strong Dynamics Collaboration program

The challenges just discussed play a significant role shaping the strategy of the LSD Collaboration. As mentioned, we exploit the good chiral and flavor symmetries of domain wall fermions, despite the associated computational expense. More broadly, we ground our entire program of exploration on the relatively well understood case of lattice QCD, using it as a baseline to help us observe and understand new features of other strongly-interacting theories. Our initial studies of $SU(3)$ gauge theories systematically increase the number N_f of degenerate fermions in the fundamental representation, from the $N_f = 2$ of lattice QCD to $N_f = 6$ and $N_f = 10$. The $N_f = 10$ studies are ongoing, and all $N_f = 10$ results presented here are **preliminary** and may change prior to publication. Additional LSD Collaboration studies of $SU(2)$ gauge theories with $N_f = 2$, 4 and 6 are underway but will not be discussed here. (In particular, we make no claim in Table 4.1 above regarding the IR behavior implied by our $N_f = 10$ or $SU(2)$ studies.)

Although we use only a single lattice spacing, we take care to match this scale between all three sets of simulations (with $N_f = 2$, $N_f = 6$ and $N_f = 10$) as described below. The point of this scale matching is to permit the most direct comparisons possible between our results for the different theories. Our main simulations (producing the results discussed below) are performed on $32^3 \times 64$ lattices, and additional simulations on $16^3 \times 32$ and $24^3 \times 32$ lattices permit (ongoing) numerical checks of finite volume effects. Because our calculations are exploratory, aiming for 10% accuracy, only short runs are performed at 5–6 different input fermion masses $0.005 \leq m_f \leq 0.03$ for each N_f.

Simulation details

LSD Collaboration simulations use domain wall fermions with the Iwasaki improved gauge action (Eqn. 3.12), using lattice volume $32^3 \times 64$, fifth-dimension length $L_s = 16$ and domain wall height $M_5 = 1.8$ (cf. Eqn. 3.46). Gauge configuration generation is performed using the HMC algorithm implemented in the Columbia Physics System,[3] which provides a well-optimized multilevel [321] symplectic integrator with Hasenbusch preconditioning [322] and chronological inversion. Our computations are performed primarily on the BlueGene/L supercomputer at Lawrence Livermore National Laboratory, with additional resources provided by the USQCD Collaboration, the NSF Teragrid, and Boston University.

The first step in our studies is matching the scale at which we perform simulations. This is done by means of $16^3 \times 32$ simulations carried out with a range of $\beta = 2N_c/g^2$, where g is the bare coupling. Because the additional dynamical fermions in the path integral have the effect of "smoothing out" the gauge field over many lattice spacings [251], the gauge coupling must be increased (β decreased) for larger N_f. Although the transition into the strongly-coupled lattice phase is similarly shifted to lower β, the effects of additional fermions are less significant at the scale of one or two lattice spacings (as revealed by the dramatic growth in m_{res} discussed below), and we must carefully ensure that our simulations are well away from this strong-coupling transition. Here we are helped by our use of a very small lattice spacing, $a \approx (5M_{V0})^{-1}$ (where $M_{V0} \equiv \lim_{M_P^2 \to 0} M_V$ and M_V is the mass of the lightest vector state), which was originally chosen to maximize the range of scales available for the coupling to evolve on these lattices. The β used in our simulations are

$$N_f = 2 : \beta = 2.7 \qquad N_f = 6 : \beta = 2.1 \qquad N_f = 10 : \beta = 1.95. \tag{4.1}$$

In the context of technicolor, the proper dimensionful quantity to use to determine the scale is the pseudoscalar decay constant in the chiral limit, $\lim_{M_P^2 \to 0} F_P = v = 246$ GeV. In

[3] http://qcdoc.phys.columbia.edu/cps.html

practice, the short runs on small lattices that we use to match scales do not allow reliable chiral extrapolations of F_P; instead we must consider these data at $M_P^2 > 0$, along with the more accessible observable M_{V0}. In our $N_f = 6$ simulations, not only these two quantities, but also the nucleon mass and Sommer scale [323] match their $N_f = 2$ values [1, 4], which we consider "accidental" and unlikely to persist for $N_f = 10$. We estimate that the scale as defined by F_P as well as that defined by M_{V0} are matched to within our 10% target accuracy across all three simulations (though the $N_f = 10$ results are preliminary), cf. Figs. 4·8 and 4·10.

Finally, as discussed in Section 3.2.3 above, a disadvantage to performing simulations at such a small lattice spacing is that the evolution of the topology can be very slow, especially at small M_P^2. In our simulations for both $N_f = 2$ and $N_f = 6$, we find that the topological charge evolves sufficiently to provide a reasonable sampling of different topological sectors for all $m_f \geq 0.01$. However, topological evolution is not sufficient for $m_f = 0.005$, or for most of our $N_f = 10$ simulations, and the resulting systematic effects are under investigation [1, 4].

Measurement details and analysis overview

Table 4.2 lists the $32^3 \times 64$ LSD Collaboration ensembles used in the analyses presented below. For each ensemble, we begin performing measurements after a thermalization time of several hundred molecular dynamics trajectories. The initial gauge configuration in each ensemble is usually chosen to be random (a disordered start labelled by "dis" in Table 4.2), or is set to unity, $U(x) = 1$ (an ordered start labelled by "ord"). In one case, the $N_f = 2$ $m_f = 0.005$ ensemble labelled "thm", a new Monte Carlo Markov chain was started from a thermalized configuration selected from the disordered-start $N_f = 2$ $m_f = 0.005$ ensemble. Instead of starting a $N_f = 10$ ensemble with $m_f = 0.005$ from a completely random gauge configuration, we set $U(x) = 1$ on one half of the lattice ($0 \leq t \leq 31$) and use a random gauge field on the other half ($32 \leq t \leq 63$), a mixed start labelled "mix".

Thermalization times may vary for different observables, and for $N_f = 2$ and $N_f = 6$

we choose the thermalization cuts shown in Table 4.2 by requiring that all of $\langle\overline{\psi}\psi\rangle$, the plaquette, pseudoscalar correlators and vector correlators reach a thermalized state. For those N_f and m_f where we generate both ordered- and disordered-start ensembles, we also monitor the convergence of observables to common values. Similarly, the $N_f = 10$ $m_f = 0.005$ mixed-start ensemble allows us to monitor thermalization by comparing observables computed on each 32^4 subvolume, to see how the initially ordered and disordered domains evolve. Thermalization generally occurs more quickly as m_f increases.

Because $N_f = 10$ simulations are ongoing, thermalization analyses have not yet been finalized. We choose preliminary $N_f = 10$ thermalization cuts by examining pseudoscalar and vector masses M_P and M_V calculated from measurements over a range of 100 trajectories (e.g., trajectories 300 through 400, 320 through 420, etc.), as a function of the first trajectory included in the range. We place the thermalization cut around the point where M_P and M_V begin to fluctuate around a stable value, as opposed to evolving monotonically, as illustrated in Fig. 4·1. Although the LSD Collaboration is currently generating five ordered-start $N_f = 10$ ensembles at the same values of m_f as the mixed- and disordered-start ensembles listed in Table 4.2, only two of these ensembles have accumulated a significant number of trajectories, and even these do not yet appear to be thermalized, as illustrated in Fig. 4·2. We therefore omit these ordered-start $N_f = 10$ ensembles from this preliminary analysis.

Once a given ensemble is thermalized, we perform measurements on every fifth trajectory, alternating the time t_0 at which we place the source. Specifically, we use point sources at $t_0 = 0$ and 32 on trajectories numbered with multiples of 10 (N_{traj} mod 10 = 0), and point sources at $t_0 = 16$ and 48 on alternating trajectories (N_{traj} mod 10 = 5). The fifth column of Table 4.2 lists the resulting total number of measurements for each ensemble. For $N_f = 2$ and $N_f = 6$, LSD Collaboration results for meson masses and decay constants presented below do not include measurements on the alternating trajectories, but add measurements using gauge-fixed wall sources placed at $t_0 = 0$ and 32 on every tenth trajectory.

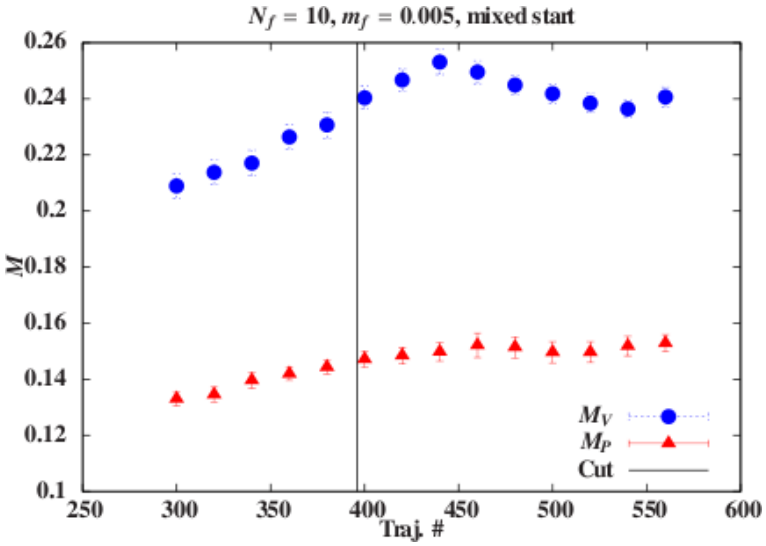

Figure 4·1: M_P and M_V for the mixed-start $N_f = 10$ $m_f = 0.005$ ensemble, calculated from measurements over the 100 trajectories starting from the trajectory number indicated on the horizontal axis.

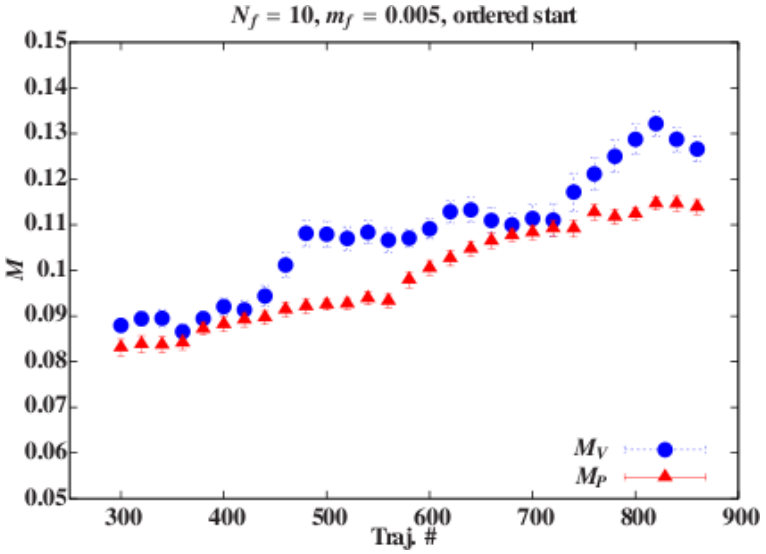

Figure 4·2: M_P and M_V for the ordered-start $N_f = 10$ $m_f = 0.005$ ensemble, calculated from measurements over the 100 trajectories starting from the trajectory number indicated on the horizontal axis.

Table 4.2: LSD Collaboration ensembles, thermalization cuts and blocks used in analyses.

N_f	m_f	**Start**	**Traj**	N	L_B	N_B
2	0.005	dis	515–1260	300	30	
		ord	405–820	168	30	
		thm	5–1080	432	30	
		Tot:		900	30	75
2	0.010	dis	535–2450	768	30	
		ord	535–950	168	30	
		Tot:		936	30	78
2	0.015	dis	510–1495	396	30	33
2	0.020	dis	705–1420	288	30	24
2	0.025	ord	205–830	252	30	21
2	0.030	ord	225–610	156	30	13
6	0.005	dis	605–1200	240	30	
		ord	435–1180	300	30	
		Tot:		540	30	45
6	0.010	dis	405–820	168	30	
		ord	425–510	36	30	
			675–1270	240	30	
		Tot:		444	30	37
6	0.015	dis	415–950	216	30	18
6	0.020	dis	415–800	156	30	13
6	0.025	dis	410–825	168	30	14
6	0.030	dis	505–760	104	20	13
10	0.005	mix	405–520	48	30	
			550–665	48	30	
		Tot:		92	30	8
10	0.010	dis	405–790	156	30	13
10	0.015	dis	340–755	168	30	14
10	0.020	dis	325–890	228	30	19
10	0.025	dis	310–755	180	30	15

The point of performing measurements only on every fifth trajectory, and at varying t_0, is to minimize autocorrelations between the measurements, as discussed in Section 3.2.3 above. To address remaining autocorrelations, we average the measurements over blocks (sometimes called "bins") of length $L_B = 20$–30 trajectories (8–12 measurements per block), treating each block as a single measurement in our subsequent jackknife analyses. Although larger block lengths are more effective at removing autocorrelations, increasing L_B reduces the statistics available for analyses.

We choose L_B by calculating M_P and M_V with a variety of $10 \leq L_B \leq 60$, and comparing the statistical error bars and the stability of the reults. We find stable results with comparable error bars for all L_B in this range. An example is shown in Fig. 4·3, which plots M_P against L_B for the $N_f = 10$ ensemble with $m_f = 0.01$. Details of this study for $N_f = 2$ and $N_f = 6$ will be presented in Ref. [4]; blocking parameters for $N_f = 10$ are preliminary.

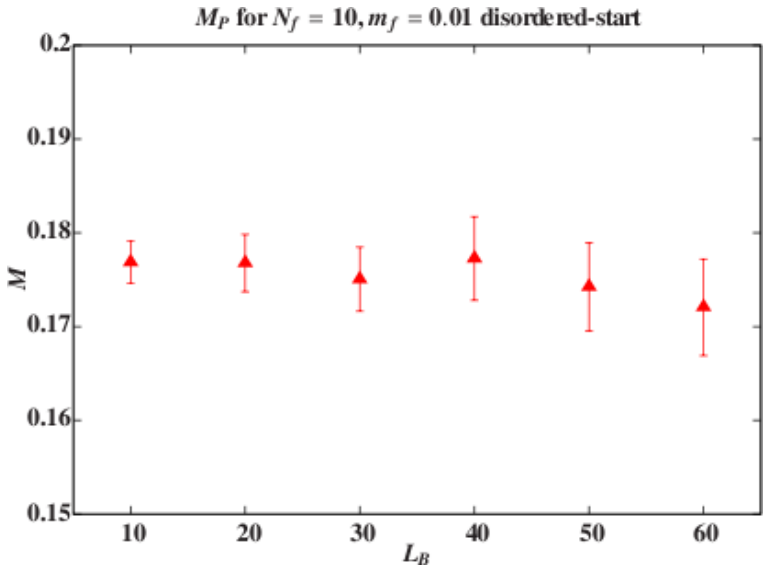

Figure 4·3: M_P for $N_f = 10$ with $m_f = 0.01$, as a function of block length L_B.

In cases where we have generated multiple ensembles with the same N_f and m_f, we analyze all of their blocks together as a single data set. The last column of Table 4.2 shows the number of blocks N_B for each N_f and m_f.

Residual mass and renormalization factors

We calculate the residual mass m_{res} as discussed in Section 3.3.2, fitting the ratio

$$R(|t-t_0|) = \frac{\left\langle \sum_{\mathbf{x}} \mathrm{Tr}\left[J^a_{mid}(\mathbf{x},t) P^b(\mathbf{0},t_0) \right] \right\rangle}{\left\langle \sum_{\mathbf{x}} \mathrm{Tr}\left[P^a(\mathbf{x},t) P^b(\mathbf{0},t_0) \right] \right\rangle} = \frac{\left\langle \sum_{\mathbf{x}} J^a_{mid}(\mathbf{x},t) P^a(\mathbf{0},t_0) \right\rangle}{\left\langle \sum_{\mathbf{x}} P^a(\mathbf{x},t) P^a(\mathbf{0},t_0) \right\rangle}, \tag{4.2}$$

to a constant in the range $10 \leq t \leq 54$. Our results are plotted versus M_P^2/M_{V0}^2 in Fig. 4·4 and tabulated in Table 4.3. (As discussed in the next section below, plotting versus M_P^2/M_{V0}^2 provides a more directly physical comparison between theories with different N_f, since the relation between M_P^2 and the fermion mass m is strongly N_f-dependent.)

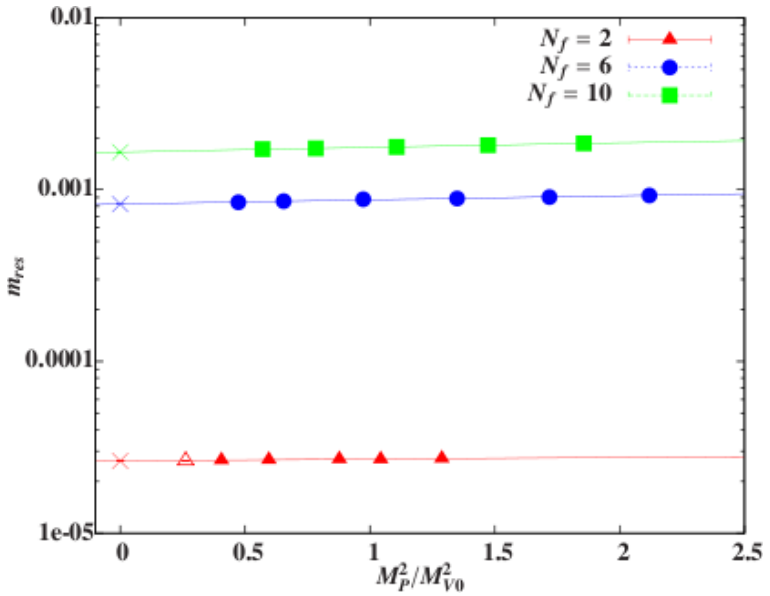

Figure 4·4: m_{res} for $N_f = 2$, $N_f = 6$ and (preliminary) $N_f = 10$. Because the empty point has $M_P L < 4$, it may suffer from non-negligible finite-volume effects, and is omitted from the linear $M_P^2 \to 0$ extrapolation ($\times$). Error bars are smaller than the symbols.

While m_{res} varies little with M_P^2/M_{V0}^2, as expected, we observe significant increases in m_{res} as N_f increases. Following the argument of Ref. [251], we can ascribe this qualitative behavior to the fact that we must significantly increase the bare coupling (decrease β) in order to match the scale a^{-1} between the simulations with different N_f, as discussed in Section 4.1.2. Increasing N_f has little effect on short-distance lattice dislocations, which we

Table 4.3: m_{res} and Z factors for $N_f = 2$, $N_f = 6$ and (preliminary) $N_f = 10$, using fit range $10 \leq t \leq 54$. The final lines for each N_f show the results of linear $M_P^2 \to 0$ extrapolations. The $N_f = 2$ extrapolations labelled "$M_P L > 4$" only include the five heaviest data points that satisfy this condition.

N_f	m_f	M_P^2/M_{V0}^2	$m_{res} \cdot 10^5$	Z_A	Z_V	$Z_A^{(i)}$
2	0.005	0.2615	2.636(7)	0.85078(7)	0.84895(7)	0.84775(13)
2	0.010	0.4053	2.661(6)	0.85079(5)	0.84872(6)	0.84709(15)
2	0.015	0.5950	2.674(7)	0.85104(7)	0.84835(8)	0.84651(20)
2	0.020	0.8771	2.699(8)	0.85146(7)	0.84815(8)	0.84623(30)
2	0.025	1.0427	2.694(7)	0.85166(6)	0.84766(9)	0.84624(23)
2	0.030	1.2877	2.723(9)	0.85233(6)	0.84771(12)	0.84584(23)
2	–	$\to 0$	2.627(8)	0.85021(13)	0.84925(11)	0.84801(23)
2	–	$M_P L > 4$	2.636(8)	0.85007(14)	0.84919(17)	0.84753(18)
6	0.005	0.4729	84.34(19)	0.72676(6)	0.72204(7)	0.72099(11)
6	0.010	0.6546	85.59(47)	0.72689(12)	0.72100(8)	0.71853(17)
6	0.015	0.9729	87.80(29)	0.72675(5)	0.72061(10)	0.71666(26)
6	0.020	1.3487	88.70(29)	0.72684(6)	0.71952(17)	0.71571(41)
6	0.025	1.7190	90.45(35)	0.72734(4)	0.71871(14)	0.71460(38)
6	0.030	2.1191	92.34(37)	0.72760(8)	0.71772(9)	0.71297(52)
6	–	$\to 0$	82.28(38)	0.72625(20)	0.72300(8)	0.72300(77)
10	0.005	0.570	171.8(4)	0.70727(9)	0.70209(6)	0.70098(12)
10	0.010	0.783	173.7(4)	0.70707(11)	0.70184(7)	0.70049(15)
10	0.015	1.107	177.0(2)	0.70729(5)	0.70116(5)	0.69910(14)
10	0.020	1.473	181.1(3)	0.70735(5)	0.70020(4)	0.69689(15)
10	0.025	1.856	185.7(3)	0.70765(6)	0.69916(7)	0.69394(19)
10	–	$\to 0$	165.1(11)	0.70690(17)	0.70358(21)	0.70436(65)

expect to contribute to chiral symmetry breaking (i.e., increase m_{res}), from the discussion in Section 3.3.2.

Table 4.3 also includes our results for the renormalization constant Z, calculated in the three ways described in Section 3.3.3. To review, Z_V and $Z_A^{(i)}$ are both calculated from a simple ratio,

$$Z_V(|t-t_0|) = \frac{\langle \sum_{\mathbf{x}} \mathcal{V}_i^a(\mathbf{x},t) V_i^a(\mathbf{0},t_0)\rangle}{\left\langle \sum_{\mathbf{x}} V_j^a(\mathbf{x},t) V_j^a(\mathbf{0},t_0)\right\rangle} \tag{4.3}$$

(and similarly for $Z_A^{(i)}$), while Z_A is built from the more elaborate expression

$$\begin{aligned} C(|t-t_0+1/2|) &= \left\langle \sum_{\mathbf{x}} \mathcal{A}_4^a(\mathbf{x},t) P^a(\mathbf{0},t_0)\right\rangle \\ L(|t-t_0|) &= \left\langle \sum_{\mathbf{x}} A_4^a(\mathbf{x},t) P^a(\mathbf{0},t_0)\right\rangle \\ Z_A(t) &= \frac{1}{2}\left\{ \frac{C(t+1/2)+C(t-1/2)}{2L(t)} + \frac{2C(t+1/2)}{L(t)+L(t+1)}\right\} \end{aligned} \tag{4.4}$$

that accounts for the fact that the conserved and local currents are not defined at exactly the same location. Results from these three different definitions are plotted in Fig. 4·5 for $N_f = 6$, which has the most significant disagreement between the three Z factors in the chiral limit $M_P^2 \to 0$.

At non-zero M_P^2, disagreement between the three Z factors comes from both chiral symmetry breaking effects as well as the different ingredients in the calculation of each. For example, we expect discretization errors for Z_V and $Z_A^{(i)}$ to be $\mathcal{O}(a)$, while the ratios in Eqn. 4.4 are designed so that even a piece of the $\mathcal{O}(a^2)$ discretization errors for Z_A will cancel out. In addition, because the correlators $\langle \mathcal{A}_i^a(x) A_i^a(0)\rangle$ and $\langle A_i^a(x) A_i^a(0)\rangle$ are the noisiest of those involved in these calculations, we expect $Z_A^{(i)}$ to have the largest statistical errors.

In the chiral limit $M_P^2 \to 0$, the remaining disagreement between our results for Z_A, Z_V and $Z_A^{(i)}$ can be used to estimate the $\mathcal{O}(a)$ discretization effects, which we find to be small (half a percent or less). Because systematic effects should be smallest for Z_A as calculated from Eqn. 4.4, we take the chiral extrapolation of Z_A as the common renormalization factor

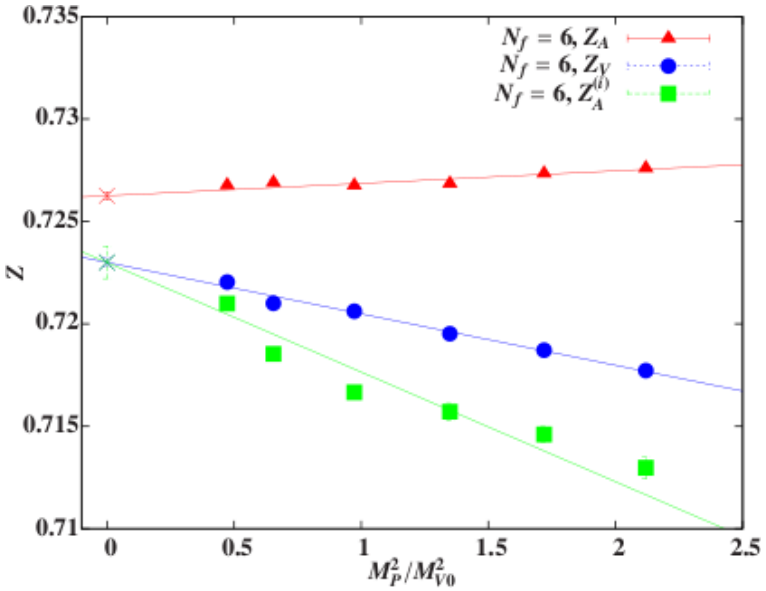

Figure 4·5: Comparison of Z factors for $N_f = 6$, with linear $M_P^2 \to 0$ extrapolations ($\times$). Note the small vertical scale.

Z used in the calculation of the S parameter below. We plot Z_A and its linear $M_P^2 \to 0$ extrapolations in Fig. 4·6.

Light meson spectrum and condensate enhancement

The first physical result reported by the LSD Collaboration for the $N_f = 6$ theory was the enhancement of the chiral condensate $\langle \overline{\psi}\psi \rangle$ at the scale of the lattice cutoff a^{-1} [1]. By virtue of the Gell-Mann–Oakes–Renner relation (equivalent to leading-order chiral perturbation theory) [324, 101],

$$\frac{M_P^2}{2m} = \frac{\langle \overline{\psi}\psi \rangle}{F_P^3} \quad \text{in the limit } m, M_P^2 \to 0 \tag{4.5}$$

our matching of the pseudoscalar decay constant F_P between the simulations with different N_f relates the enhancement of the condensate to a stronger dependence of the pseudoscalar mass-squared M_P^2 on the renormalized fermion mass m. This effect is plotted in Fig. 4·7, and is the reason we plot other results versus M_P^2/M_{V0}^2 to ensure a more directly physical comparison between theories with different N_f.

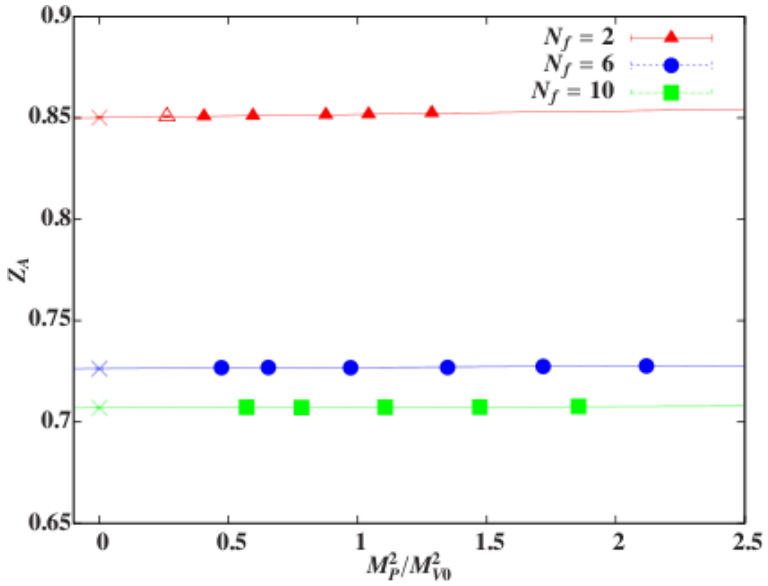

Figure 4·6: Z_A for $N_f = 2$, $N_f = 6$ and (preliminary) $N_f = 10$. Because the empty point has $M_P L < 4$, it may suffer from non-negligible finite-volume effects, and is omitted from the linear $M_P^2 \to 0$ extrapolation ($\times$). Error bars are smaller than the symbols.

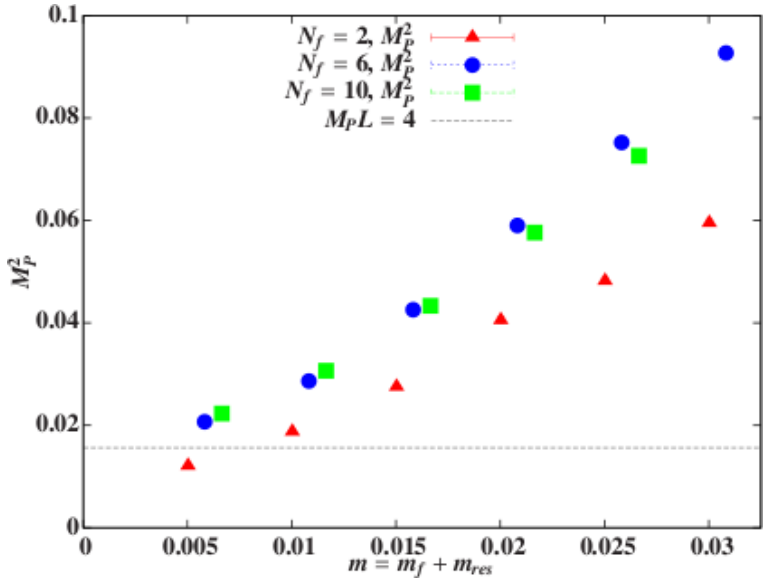

Figure 4·7: Pseudoscalar mass-squared M_P^2 plotted versus $m = m_f + m_{res}$ for $N_f = 2$, $N_f = 6$ and (preliminary) $N_f = 10$. Error bars are smaller than the symbols.

Data for M_P^2 are also presented in Table 4.4, which additionally includes results for the masses M_V and M_A of the lightest vector and axial states. (M_A has not yet been reliably measured for the $N_f = 10$ theory.) As mentioned in Secs. 2.2.4 and 2.3, parity doubling between the vector and axial spectral functions has been conjectured as a possible means to reduce the S parameter in walking theories. In Fig. 4·8 we compare M_V and M_A plotted versus M_P^2/M_{V0}^2 for $N_f = 6$ and $N_f = 2$, and in Fig. 4·9 we plot the ratio M_A/M_V. For $N_f = 2$, our results for the ratio are roughly consistent with the physical $m_{a1}/m_\rho = 1.59(5)$ of QCD [13], if we omit from the chiral extrapolation the lightest $N_f = 2$ point, which has $M_P L < 4$ and may suffer from non-negligible finite-volume effects as a result.

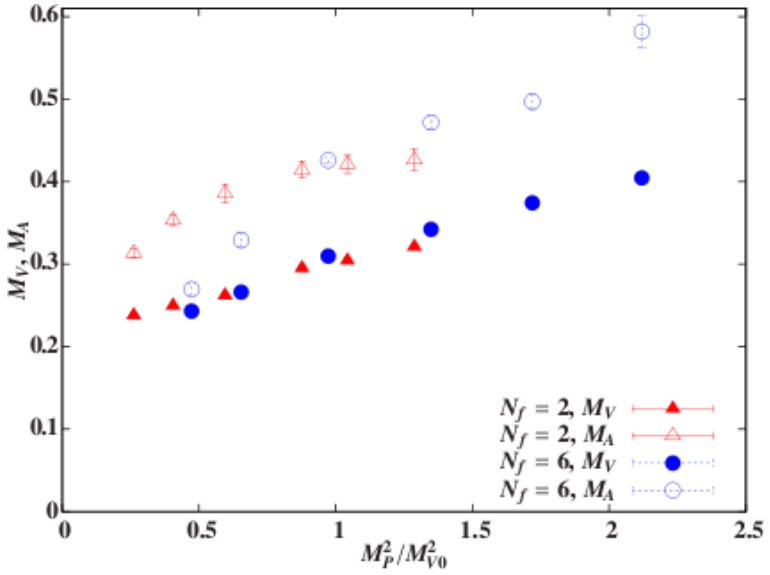

Figure 4·8: Masses of the lightest vector (M_V, filled) and axial (M_A, empty) states, plotted versus M_P^2/M_{V0}^2 for $N_f = 2$ and $N_f = 6$.

For $M_P^2 \lesssim M_{V0}^2$, Fig. 4·9 indicates a substantial decrease in M_A/M_V for $N_f = 6$, moving toward unity. In order to achieve parity doubling, the corresponding vector and axial decay constants F_V and F_A must also be comparable. We plot these results for $N_f = 2$ and $N_f = 6$ in Fig. 4·11 and tabulate their values in Table 4.5, which also includes results for F_P plotted in Fig. 4·10. We do not report chiral extrapolations of these data. A particular difficulty for F_P that was raised in Section 3.2.3 is the need to perform chiral

Table 4.4: LSD Collaboration results for the masses of the lightest pseudoscalar, vector and axial states, for $N_f = 2$ and $N_f = 6$. Some preliminary results for $N_f = 10$ are also included. Chiral extrapolations are linear in $M_P^2 \to 0$, and for $N_f = 2$ the lightest ($m_f = 0.005$) data are omitted from the extrapolations, as described in the text.

N_f	m_f	M_P^2	M_V	M_A	M_A/M_V
2	0.005	0.01208(33)	0.2379(26)	0.3132(58)	1.316(25)
2	0.010	0.01873(20)	0.2495(22)	0.3533(67)	1.416(27)
2	0.015	0.02750(40)	0.2620(26)	0.3857(113)	1.472(42)
2	0.020	0.04053(61)	0.2951(33)	0.4142(99)	1.404(44)
2	0.025	0.04819(67)	0.3043(37)	0.4211(110)	1.384(32)
2	0.030	0.05951(67)	0.3210(30)	0.4264(131)	1.328(38)
2	–	$\to 0$	0.2150(31)	0.3201(107)	1.476(40)
6	0.005	0.02069(55)	0.2430(44)	0.2695(71)	1.109(19)
6	0.010	0.02864(23)	0.2661(30)	0.3289(84)	1.236(31)
6	0.015	0.04257(45)	0.3096(23)	0.4259(37)	1.376(16)
6	0.020	0.05901(43)	0.3422(25)	0.4717(77)	1.378(26)
6	0.025	0.07521(34)	0.3742(22)	0.4969(88)	1.328(22)
6	0.030	0.09271(45)	0.4045(35)	0.5818(200)	1.438(51)
6	–	$\to 0$	0.2092(31)	0.2253(78)	1.123(23)
10	0.005	0.02229(29)	0.2426(49)	–	–
10	0.010	0.03064(120)	0.2531(71)	–	–
10	0.015	0.04332(43)	0.2776(57)	–	–
10	0.020	0.05764(65)	0.3083(33)	–	–
10	0.025	0.07262(56)	0.3370(52)	–	–
10	–	$\to 0$	0.1978(31)	–	–

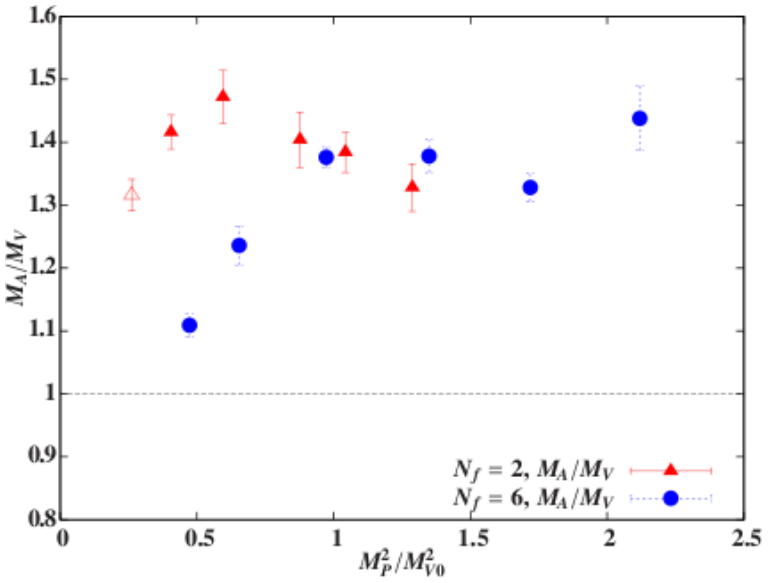

Figure 4·9: Ratio of axial and vector masses M_A/M_V plotted versus M_P^2/M_{V0}^2 for $N_f = 2$ and $N_f = 6$. Because the empty point has $M_P L < 4$, it may suffer from non-negligible finite-volume effects.

perturbation theory fits jointly for all of M_P^2, F_P and $\langle\overline{\psi}\psi\rangle$. While such fits function for $N_f = 2$, they fail for $N_f = 6$, due both to the larger M_P of the $N_f = 6$ simulations, as well as the N_f-dependence of next-to-leading and next-to-next-to-leading order coefficients in χPT expansions [325].

Although the signs of parity doubling that we observe for $N_f = 6$ are suggestive, they are not yet conclusive and should be viewed with caution. Similar parity doubling was discovered to be caused by finite volume effects in an early $N_f = 8$ study [265], and a careful analysis by Ref. [292] also found these observables to be more sensitive to finite volume effects, considering the $N_f = 4$ theory compared to $N_f = 2$. In the next section we report more compelling results from direct lattice calculation of the S parameter itself.

4.2 Electroweak S parameter

We now focus on our calculation of the S parameter on the LSD Collaboration ensembles listed in Table 4.2 above. We first review the S parameter, expanding on the introduction presented in Section 2.2.3 and providing details of the lattice calculation. We then

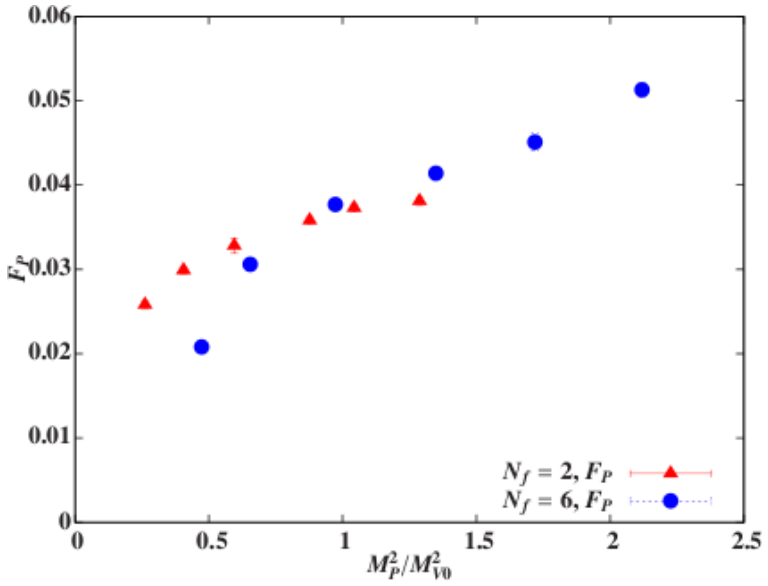

Figure 4·10: Pseudoscalar decay constant F_P plotted versus $m = m_f + m_{res}$ for $N_f = 2$ and $N_f = 6$ and (preliminary) $N_f = 10$. Error bars are smaller than the symbols.

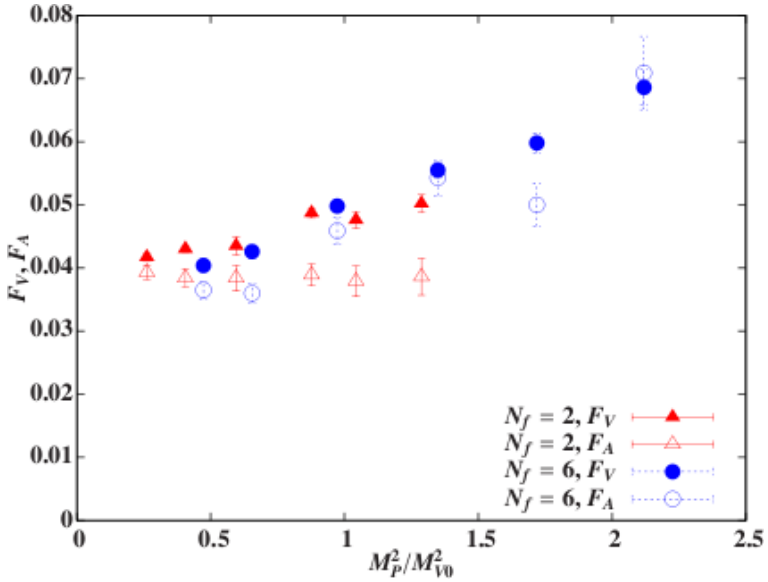

Figure 4·11: Vector (filled) and axial (empty) decay constants F_V and F_A plotted versus M_P^2/M_{V0}^2 for $N_f = 2$ and $N_f = 6$.

Table 4.5: LSD Collaboration results for the decay constants of the lightest pseudoscalar, vector and axial states, for $N_f = 2$ and $N_f = 6$.

N_f	m_f	M_P^2/M_{V0}^2	F_P	F_V	F_A
2	0.005	0.2615	0.0258(5)	0.0417(6)	0.0393(11)
2	0.010	0.4053	0.0299(4)	0.0430(5)	0.0384(14)
2	0.015	0.5950	0.0328(9)	0.0435(14)	0.0384(20)
2	0.020	0.8771	0.0358(5)	0.0487(8)	0.0389(17)
2	0.025	1.0427	0.0373(5)	0.0476(13)	0.0379(24)
2	0.030	1.2877	0.0381(5)	0.0502(14)	0.0386(29)
6	0.005	0.4729	0.0208(7)	0.0404(10)	0.0365(14)
6	0.010	0.6546	0.0306(8)	0.0426(10)	0.0360(15)
6	0.015	0.9729	0.0377(5)	0.0498(10)	0.0459(22)
6	0.020	1.3487	0.0414(8)	0.0555(13)	0.0543(28)
6	0.025	1.7190	0.0451(11)	0.0598(16)	0.0500(34)
6	0.030	2.1191	0.0513(9)	0.0686(28)	0.0709(58)

summarize our analysis and results, which for $N_f = 2$ and $N_f = 6$ were first presented in Ref. [3].

4.2.1 Formulation

We introduced the S parameter in Section 2.2.3 as the difference between the vector and axial vacuum polarization functions due to new physics. Let us reformulate Eqn. 2.43 as

$$S = 4\pi N_D \Pi'_{V-A}(0) - \Delta S_{SM}(M_P^2), \tag{4.6}$$

where $\Pi_{V-A}(Q^2) \equiv \Pi_{VV}(Q^2) - \Pi_{AA}Q^2$ and we define $\Pi'(Q^2)$ through [18]

$$\Pi(Q^2) \equiv \Pi(0) + Q^2\Pi'(Q^2), \tag{4.7}$$

so that only at $Q^2 = 0$

$$\Pi'(Q^2) = \left.\frac{d\Pi(Q^2)}{dQ^2}\right|_{Q^2=0}. \tag{4.8}$$

Because the lattice measurement of Π as a current correlation function on a given gauge configuration involves only a single pair of fermions, we include in Eqn. 4.6 the kinematic factor N_D, the number of electroweak doublets in the theory $1 \leq N_D \leq N_f/2$. We emphasize that the gauge configurations on which these measurements are performed account for

the dynamics of all N_f flavors of fermions. Finally, $\Delta S_{SM}(M_P^2)$ is the contribution of the standard model (SM) Higgs sector, subtracted so that $S = 0$ in the SM. This subtraction will also take into account the effects of working at non-zero fermion mass on the lattice, $M_P^2 > 0$; we discuss it further in Section 4.2.2 below.

In our lattice calculation, we use current correlators composed of a conserved domain wall current and a local current (cf. Section 3.3.3),

$$\begin{aligned}\Pi_{VV}^{\mu\nu}(x) &= Z\left\langle \mathrm{Tr}\left[\mathcal{V}^{a\mu}(x)V^{b\nu}(0)\right]\right\rangle \\ &= \frac{Z}{2}\left\langle \sum_{s=0}^{L_s-1}\left\{ \left(D^{-1}_{L_s-1-s}(x)\right)^\dagger \gamma_5 \frac{1-\gamma^\mu}{2} U_{x,\mu} D_s^{-1}(x+\widehat{\mu})\gamma^\nu\gamma_5 \right.\right. \\ &\qquad \left.\left. - \left(D^{-1}_{L_s-1-s}(x+\widehat{\mu})\right)^\dagger \gamma_5 \frac{1+\gamma^\mu}{2} U^\dagger_{x,\mu} D_s^{-1}(x)\gamma^\nu\gamma_5 \right\}\right\rangle \end{aligned} \tag{4.9}$$

$$\begin{aligned}\Pi_{AA}^{\mu\nu}(x) &= Z\left\langle \mathrm{Tr}\left[\mathcal{A}^{a\mu}(x)A^{b\nu}(0)\right]\right\rangle \\ &= \frac{Z}{2}\left\langle \sum_{s=0}^{L_s-1}\Gamma_5(s)\left\{ \left(D^{-1}_{L_s-1-s}(x)\right)^\dagger \gamma_5 \frac{1-\gamma^\mu}{2} U_{x,\mu} D_s^{-1}(x+\widehat{\mu})\gamma^\nu \right.\right. \\ &\qquad \left.\left. - \left(D^{-1}_{L_s-1-s}(x+\widehat{\mu})\right)^\dagger \gamma_5 \frac{1+\gamma^\mu}{2} U^\dagger_{x,\mu} D_s^{-1}(x)\gamma^\nu \right\}\right\rangle, \end{aligned} \tag{4.10}$$

where $\Gamma_5(s) = \mathrm{sign}\,[s-(L_s-1)/2]$, and the overall factors of $\frac{1}{2}$ come from the normalization of the flavor matrices $\mathrm{Tr}\left[T^aT^b\right] = \frac{1}{2}\delta^{ab}$. (Translation invariance lets us label the generic source point as the origin, for notational convenience.) $D_s^{-1}(x)$ is the five-dimensional domain wall propagator from the domain walls to fifth-dimensional index s. We determine the common renormalization factor Z non-perturbatively as described in Section 4.1.2 above.

Ref. [142] emphasizes that using at least one conserved current in the correlators ensures that lattice artifacts cancel in the V–A difference, which we will verify in Section 4.2.2 below. Correlators built from two conserved currents would not require renormalization, making determination of Z unnecessary for this calculation. However, because the conserved currents are involve sums over the fifth dimension, the resulting correlators would require calculating propagators from every fifth-dimensional index s to every other s', in-

creasing computational costs by a factor of $L_s \sim \mathcal{O}(10)$.

Because the conserved currents are point-split, the appropriate Fourier transform is

$$\Pi^{\mu\nu}_{VV}(Q) = \sum_x e^{iQ\cdot(x+\widehat{\mu}/2)}\Pi^{\mu\nu}_{VV}(x) = \delta^{\mu\nu}\Pi_{VV}(Q^2) - \frac{\widehat{Q}^\mu\widehat{Q}^\nu}{\widehat{Q}^2}[\Pi_{VV}(Q^2) + \Pi^L_{ij}(Q^2)], \quad (4.11)$$

and similarly for Π_{AA}, where $\widehat{Q}^\mu = 2\sin(Q^\mu/2)$ is the lattice momentum corresponding to $Q^\mu = 2\pi n^\mu/L$ with n^μ an integer four-vector labelling each lattice site. Note that we take the transverse and longitudinal correlators themselves to be functions of Q^2 even though we use $\widehat{Q}^\mu$ to define the decomposition of $\Pi^{\mu\nu}(Q)$,

$$\Pi^L(Q^2) = -\frac{\widehat{Q}^\mu\widehat{Q}^\nu}{\widehat{Q}^2}\Pi^{\mu\nu}(Q) \qquad \Pi(Q^2) = \frac{1}{3}\left[\Pi^{\mu\mu}(Q) + \Pi^L(Q^2)\right]. \quad (4.12)$$

At small momenta, $Q^\mu \approx \widehat{Q}^\mu$.

We now have all the necessary ingredients to calculate S. Before doing so, we reformulate the calculation in terms of a dispersive integral over the vector and axial spectral functions R_V and R_A. Thinking in terms of R_V and R_A can provide more opportunities to apply physical intuition, and it will also allow us to see a concrete form of the standard model subtraction (in the chiral limit $\Delta S_{SM}(M_P^2 = 0)$). The connection between the current correlators and the spectral functions is

$$R(s) = 12\pi \mathrm{Im}\Pi'(s) \quad (4.13)$$

so that

$$\Pi_{V-A}(Q^2) = Q^2\Pi'_{V-A}(Q^2) - \Pi_{AA}(0) = \frac{Q^2}{12\pi}\int_0^\infty \frac{ds}{\pi}\left[\frac{R_V(s) - R_A(s)}{s+Q^2}\right] - F_P^2 \quad (4.14)$$

(again in the chiral limit $M_P^2 = 0$). For an asymptotically free theory, $\Pi_{V-A}(Q^2) \sim 1/Q^4$

as $Q^2 \to \infty$, which produces the first and second Weinberg sum rules [326]

$$\frac{1}{3\pi}\int_0^\infty ds\,[R_V(s) - R_A(s)] = 4\pi F_P^2 \tag{4.15}$$

$$\frac{1}{3\pi}\int_0^\infty ds\,[sR_V(s) - sR_A(s)] = 0. \tag{4.16}$$

To obtain the S parameter, we take the derivative with respect to Q^2, in the limit $Q \to 0$,

$$S = \frac{1}{3\pi}\int_0^\infty \frac{ds}{s}\left\{N_D\,[R_V(s) - R_A(s)] - \frac{1}{4}\left[1 - \left[1 - \frac{(M_H^{(ref)})^2}{s}\right]^3 \theta(s - (M_H^{(ref)})^2)\right]\right\}, \tag{4.17}$$

where the last term is the SM subtraction $\Delta S_{SM}(0)$. Without the standard model subtraction, this "zeroth" Weinberg sum rule has the form of the Das–Mathur–Okubo sum rule [327]. On the lattice, $M_P^2 > 0$ implies a non-zero infrared cutoff on these spectral integrals, and changes the asymptotic behavior of $\Pi_{V-A}(Q^2)$ to $\Pi_{V-A}(Q^2) \sim 1/Q^2$ at large Q^2 [328, 329].

4.2.2 Results

We now discuss our results for the S parameter calculated from Eqn. 4.6, considering in turn the conserved–local current correlators $\Pi_{V-A}(Q^2)$, the Padé fits used to extract $\Pi'_{V-A}(0)$, and the standard model subtraction $\Delta S_{SM}(M_P)$. After discussing the systematic uncertainties entering our final analyses, we relate our results for S to the vector and axial spectra discussed above.

Current correlators

Because the conserved–local current correlators we use were implemented specifically for this calculation, the first order of business is to confirm that the currents we calculate are actually conserved. We verify the conservation of $\mathcal{V}_\mu^a$ by checking the Ward identity

$$\widehat{Q}_\mu \Pi_{VV}^{\mu\nu}(Q) = 0, \tag{4.18}$$

which is illustrated in the top panel of Fig. 4·12.[4] Note that the conserved current always corresponds to the index $^{\mu}$ in the correlator, so Eqn. 4.18 is the Fourier transform of Eqn. 3.62. This figure also shows the corresponding quantity $\widehat{Q}_\mu \Pi^{\mu\nu}_{AA}(Q)$ for the axial correlator, which is consistent with partial conservation of the axial current (PCAC), Eqn. 3.63.

The bottom panel of Fig. 4·12 confirms that these results are nontrivial tests of current conservation, by contrasting them with the corresponding quantities from correlators that use only local currents,

$$\widetilde{\Pi}^{\mu\nu}_{VV}(Q) = Z^2 \sum_x e^{iQ\cdot x} \left\langle \mathrm{Tr}\left[V^{a\mu}(x) V^{b\nu}(0) \right] \right\rangle . \tag{4.19}$$

Next, we confirm the claim made in Section 4.2.1 above, that using at least one conserved domain wall current in the correlators ensures that lattice artifacts cancel in the V–A difference $\Pi_{V-A}(Q^2)$. The quantity $\Pi^{\mu\nu}_{VV}(Q)\widehat{Q}_\nu$ is just such a lattice artifact: the local current corresponding to the index $^{\nu}$ in the correlator is not conserved at non-zero lattice spacing (even though it is proportional to the conserved current in the continuum). The top panel of Fig. 4·13 shows that even though $\Pi^{\mu\nu}_{VV}(Q)\widehat{Q}_\nu \neq 0$ and $\Pi^{\mu\nu}_{AA}(Q)\widehat{Q}_\nu \neq 0$, these lattice artifacts cancel in the difference

$$\left[\Pi^{\mu\nu}_{VV}(Q) - \Pi^{\mu\nu}_{AA}(Q)\right] \widehat{Q}_\nu \approx 0. \tag{4.20}$$

Again, this does not hold if we use only local currents in the correlators, shown in the bottom panel of Fig. 4·13.

We now discuss our extraction of the S parameter from the transverse conserved–local correlator $\Pi_{V-A}(Q^2)$. First, we note from Fig. 4·14 that the magnitude of $\Pi_{V-A}(Q^2)$ for $Q^2 \leq 0.2$ is comparable to the magnitude of the lattice artifacts in the local–local V–A correlator shown in the bottom panel of Fig. 4·13. The use of conserved–local correlators appears crucial to the success of our calculation.

[4] Here we average all $\widehat{Q}\cdot\Pi(Q)$ that involve Q_μ with the same magnitude Q^2. The product is therefore a function of Q^2, which is the horizontal axis of all plots in this section.

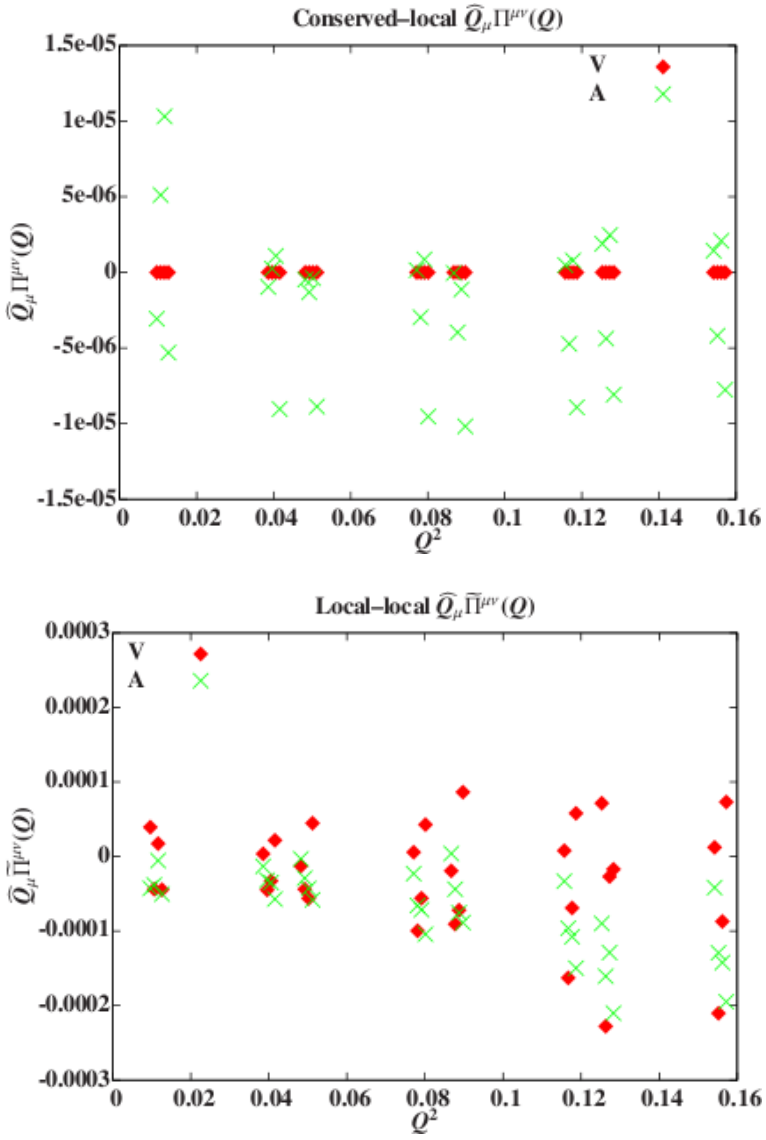

Figure 4·12: Top panel: vector Ward identity (V) and PCAC (A) for conserved–local correlators $\Pi^{\mu\nu}(Q)$ measured on a $N_f = 2$ lattice with $m_f = 0.02$. Bottom panel: the corresponding quantities for correlators $\widetilde{\Pi}^{\mu\nu}(Q)$ that use only local currents (note the vertical scale). The horizontal displacements around each Q^2 value distinguish different components ν.

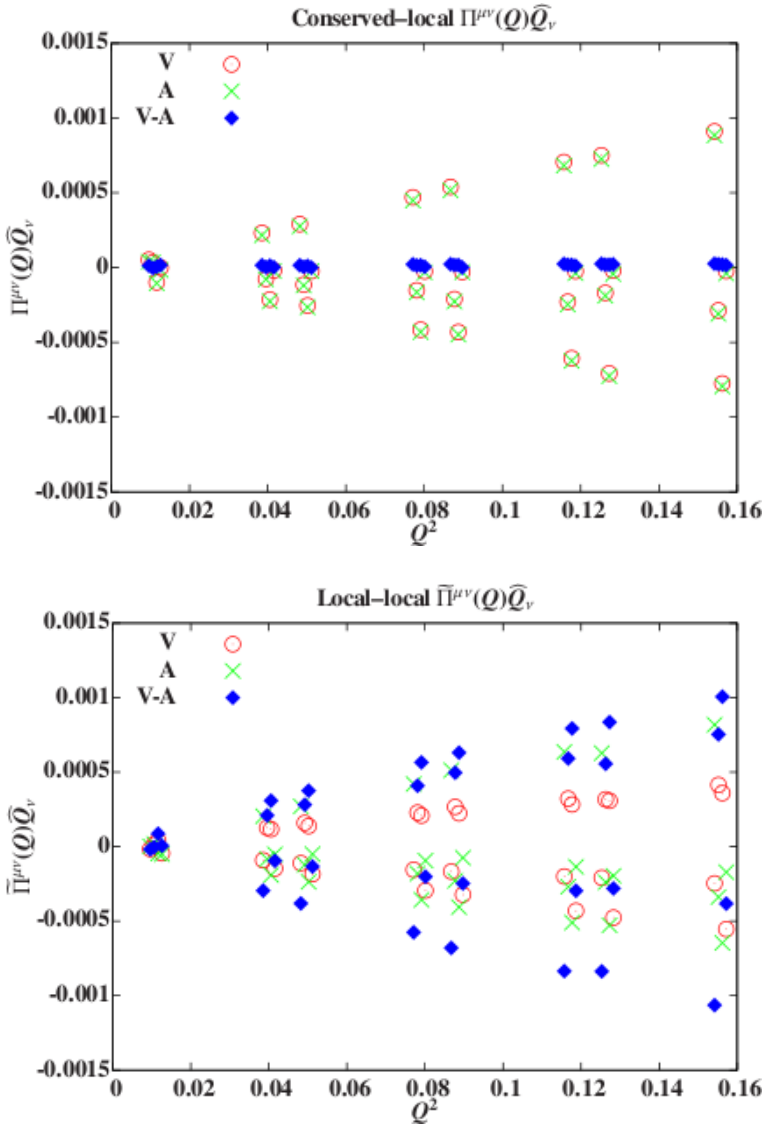

Figure 4·13: Lattice artifacts $\Pi^{\mu\nu}\widehat{Q}_\nu \neq 0$ cancel in the V–A difference for conserved–local correlators $\Pi^{\mu\nu}(Q)$ (top panel), but not for correlators $\widetilde{\Pi}^{\mu\nu}(Q)$ using only local currents (bottom panel). The horizontal displacements around each Q^2 value distinguish different components μ.

Padé fits

To analyze the V–A current correlator, Refs. [141, 142] perform fits to chiral perturbation theory expressions for the low-energy constant L_{10} (or equivalently ℓ_5) discussed in Section 3.2.3. These authors find that they are only able to include in the chiral fits the single $\Pi_{V-A}(Q^2)$ data point with the smallest Q^2 in each of their ensembles. Due to the larger scale a^{-1}, the larger input fermion mass m_f, and (for $N_f > 2$) the enhanced chiral condensate $\langle\overline{\psi}\psi\rangle$ characterizing LSD Collaboration simulations compared to those of Refs. [141, 142], such χPT fits are not viable a viable option.

Instead we fit $\Pi_{V-A}(Q^2)$ to a four-parameter Padé approximant of the form

$$\Pi_{V-A}(Q^2) = \frac{a_0 + a_1 Q^2}{1 + b_1 Q^2 + b_2 Q^4}. \tag{4.21}$$

This functional form has the correct asymptotic behavior $\Pi_{V-A}(Q^2) \sim Q^{-2}$ at large Q^2 (since $M_P^2 > 0$, as discussed below Eqn. 4.17). We can further motivate Eqn. 4.21 by considering the dispersion relation Eqn. 4.14. If we suppose that the vector and axial spectral functions $R_{V,A}$ are each saturated by the lightest state in the corresponding channel, approximated as δ functions

$$R_V(s) = 12\pi^2 F_V^2 \delta(s - M_V^2) \qquad\qquad R_A(s) = 12\pi^2 F_A^2 \delta(s - M_A^2), \tag{4.22}$$

then the dispersion relation becomes

$$\begin{aligned}\Pi_{V-A}^{(pole)}(Q^2) &= -F_P^2 + \frac{Q^2 F_V^2}{M_V^2 + Q^2} - \frac{Q^2 F_A^2}{M_A^2 + Q^2} \\ &= \frac{-F_P^2 M_V^2 M_A^2 - Q^2(F_P^2(M_V^2 + M_A^2) - F_V^2 M_A^2 + F_A^2 M_V^2) - Q^4(F_P^2 - F_V^2 + F_A^2)}{M_V^2 M_A^2 + Q^2(M_V^2 + M_A^2) + Q^4}.\end{aligned} \tag{4.23}$$

Applying the first Weinberg sum rule (Eqn. 4.15) with this approximation for $R_{V,A}$,

$$F_P^2 = F_V^2 - F_A^2, \tag{4.24}$$

immediately reproduces the form of Eqn. 4.21.

We perform an independent fit for each value of N_f and m_f listed above in Table 4.2, using the fit range $Q^2 < 0.4$. We include in this analysis the jackknife estimate of the covariance matrix $C_{\alpha\beta}$ discussed in Section 3.2.3 above. Fit results describe the data well throughout the entire range of Q^2, as shown in Figs. 4·14, 4·15 and 4·16 for $N_f = 2$, $N_f = 6$ and $N_f = 10$, respectively. Fit results and statistical errors for the slope $4\pi\Pi'_{V-A}(0)$ are plotted versus M_P^2/M_{V0}^2 in Fig. 4·17, and tabulated in Table 4.6. Adding more parameters to the rational function in Eqn. 4.21 (such as an a_2Q^4 term in the numerator or a b_3Q^6 term in the denominator) does not significantly affect results.

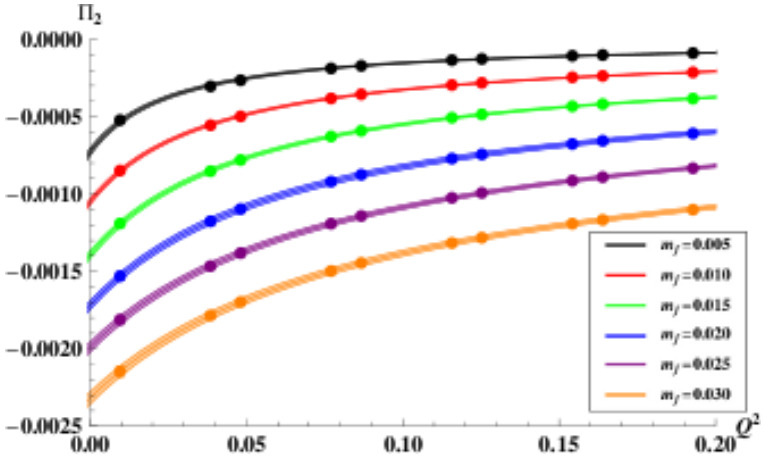

Figure 4·14: $\Pi_{V-A}(Q^2)$ data and Padé fits for $N_f = 2$ ensembles with $m_f = 0.005, \ldots, 0.03$ from top to bottom.

Our fits are stable as the Q^2 fit range is varied somewhat, which we illustrate in Figs. 4·18 and 4·19 for the case of $N_f = 2$ simulations with $m_f = 0.01$. Fig. 4·18 plots fit results for $4\pi\Pi'_{V-A}(0)$ versus the largest Q^2_{Max} included in the fit range $Q^2 \leq Q^2_{Max}$, while Fig. 4·19 shows the corresponding χ^2 per degree of freedom (averaged over the fits for all jackknife samples). The steady upward trend in $\Pi'_{V-A}(0)$ as Q^2_{Max} increases is small, and all results match those from our chosen fit range $Q^2 < 0.4$ within uncertainties. Because the data are strongly correlated in Q^2, the χ^2 per degree of freedom is not a reliable measure of the goodness of fit. We can only require $\chi^2/dof \ll 1$, which is satisfied by all the fits as the Q^2 fit range varies.

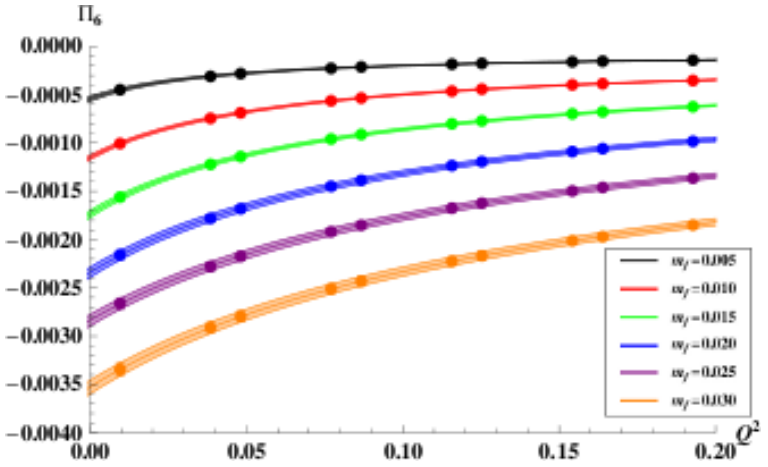

Figure 4·15: $\Pi_{V-A}(Q^2)$ data and Padé fits for $N_f = 6$ ensembles with $m_f = 0.005, \ldots, 0.03$ from top to bottom.

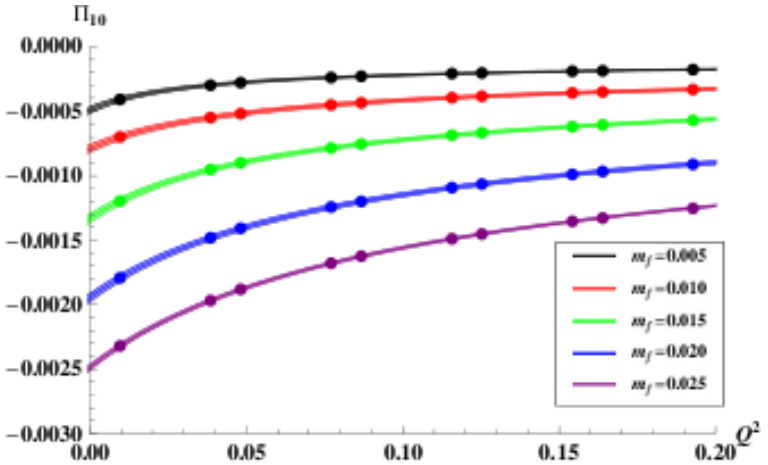

Figure 4·16: Preliminary $\Pi_{V-A}(Q^2)$ data and Padé fits for $N_f = 10$ ensembles with $m_f = 0.005, \ldots, 0.025$ from top to bottom.

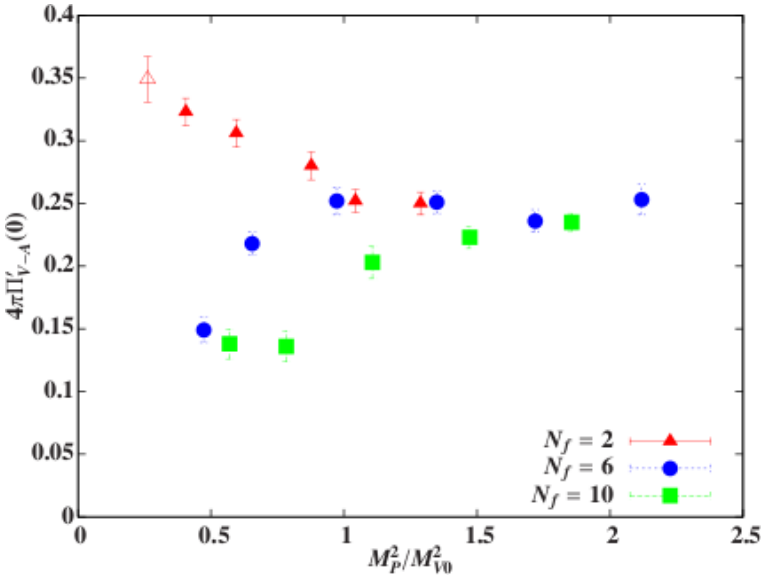

Figure 4·17: $4\pi\Pi'_{V-A}(0)$ for $N_f = 2$, $N_f = 6$ and (preliminary) $N_f = 10$. Because the empty point has $M_P L < 4$, it may suffer from non-negligible finite-volume effects.

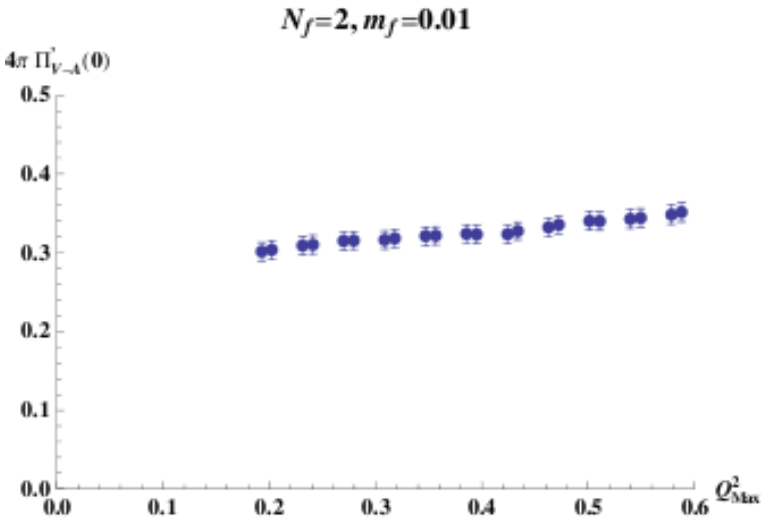

Figure 4·18: Q^2 fit range dependence of Padé fit results for $4\pi\Pi'_{V-A}(0)$, for $N_f = 2$ ensembles with $m_f = 0.01$.

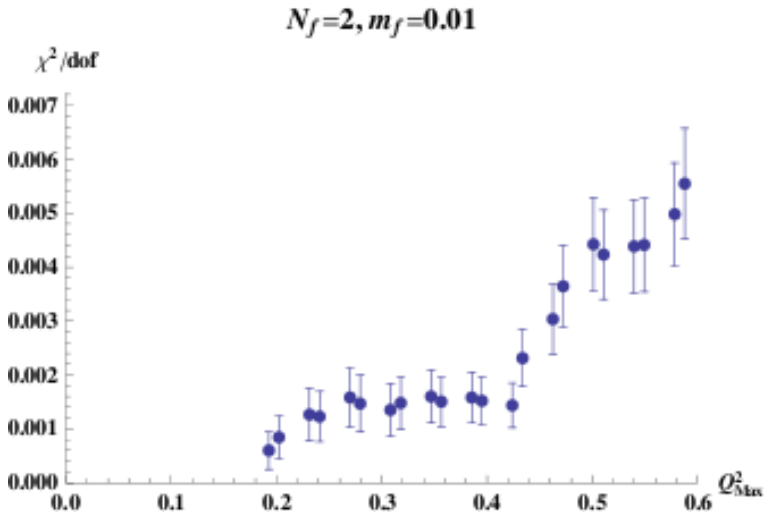

Figure 4·19: Q^2 fit range dependence of χ^2 per degree of freedom from Padé fits for $N_f = 2$ ensembles with $m_f = 0.01$.

Because the standard model subtraction $\Delta S_{SM}(M_P^2)$ has no explicit dependence on N_f, our $4\pi\Pi'_{V-A}(0)$ data already suggest that for $M_P^2 \lesssim M_{V0}^2$, our results for the S parameter in the $N_f = 6$ and $N_f = 10$ theories will be significantly smaller than what we would get by scaling up the $N_f = 2$ values by a factor of $N_f/2$. In the heavy-fermion limit $M_P^2 \gg M_{V0}^2$, the theories should all be effectively quenched. That is, the effects of the very massive technihadrons should become negligible, and the results for all N_f should approach a common value. This is consistent with our results for $4\pi\Pi'_{V-A}(0)$, which all appear to be approaching a common limit of approximately 0.25 for $M_P^2 > M_{V0}^2$.

S parameter

Now that we have in hand results for $4\pi\Pi'_{V-A}(0)$, the last remaining piece of the S parameter calculation from Eqn. 4.6 is the standard model subtraction $\Delta S_{SM}(M_P)$. We begin with the spectral integral of Eqn. 4.17, using $4M_P^2 > 0$ as the infrared cutoff. Further, we take the reference mass to be our usual technihadronic scale, $M_H^{(ref)} = M_{V0} \sim 1$ TeV. This

gives

$$\Delta S_{SM}(M_P) = \frac{1}{12\pi} \int_{4M_P^2}^{\infty} \frac{ds}{s} \left[1 - \left(1 - \frac{M_{V0}^2}{s} \right)^3 \theta(s - M_{V0}^2) \right] \tag{4.25}$$

$$= \begin{cases} \dfrac{1}{12\pi} \left(\dfrac{11}{6} + \log \left[\dfrac{M_{V0}^2}{4M_P^2} \right] \right) & \text{for } 4M_P^2 < M_{V0}^2, \\ \\ \dfrac{1}{12\pi} \left(\dfrac{3M_{V0}^2}{4M_P^2} - \dfrac{3M_{V0}^4}{32M_P^4} + \dfrac{M_{V0}^6}{192M_P^6} \right) & \text{for } 4M_P^2 \geq M_{V0}^2. \end{cases} \tag{4.26}$$

Our results for $\Delta S_{SM}(M_P)$ as well as the S parameter itself (with $N_D = N_f/2$) are tabulated in Table 4.6, for $N_f = 2$, $N_f = 6$ and (preliminary) $N_f = 10$. We see that in all cases $\Delta S_{SM}(M_P)$ is small compared to $4\pi\Pi'_{V-A}(0)$, with $\Delta S_{SM}(M_P) \lesssim 0.04$ for all ensembles with $M_P L > 4$.

Because $\Delta S_{SM}(M_P)$ is so small, the behavior of the S parameter itself is determined primarily by the results for $\Pi'_{V-A}(0)$ discussed in the previous section. In the heavy-fermion limit $M_P^2 \gg M_{V0}^2$, we see the expected scaling $S \propto N_D$, where we take $N_D = N_f/2$. For $M_P^2 \lesssim M_{V0}^2$, however, our $N_f = 6$ and $N_f = 10$ results for the S parameter are well below $N_f/2$ times the $N_f = 2$ value.

For chirally-broken theories with $2 < N_f < N_f^c$ below the conformal window, S diverges logarithmically in M_P^2/M_{V0}^2 as $M_P^2 \to 0$ and the $N_f^2 - 4$ uneaten pseudo-Nambu–Goldstone bosons become massless. (For an IR-conformal theory, $M_{V0} \sim 1/L$ vanishes in the continuum limit, and it would not make sense to plot our results against M_P^2/M_{V0}^2.) We illustrate the chiral divergence in Fig. 4·20 by including fits to the simple linear form accounting for the chiral logarithms,

$$S_{fit} = A + BM_P^2 + \frac{1}{12\pi} \left(\frac{N_f^2}{4} - 1 \right) \log \left[\frac{M_{V0}^2}{M_P^2} \right]. \tag{4.27}$$

For each N_f, we include in the fit only the three lightest data points that satisfy $M_P L > 4$; this limits the fit range to $M_P^2 \lesssim M_{V0}^2$. This fit allows us to estimate the value of M_P^2/M_{V0}^2 at which this chiral effect should become visible in our results. For $N_f = 6$, this occurs at a

PNGB mass too low to simulate while satisfying the condition $M_P L > 4$ with $L = 32$. It is possible that the lightest $N_f = 10$ point shows signs of chiral effects from the 96 expected PNGBs, but these results are preliminary and may change prior to publication.

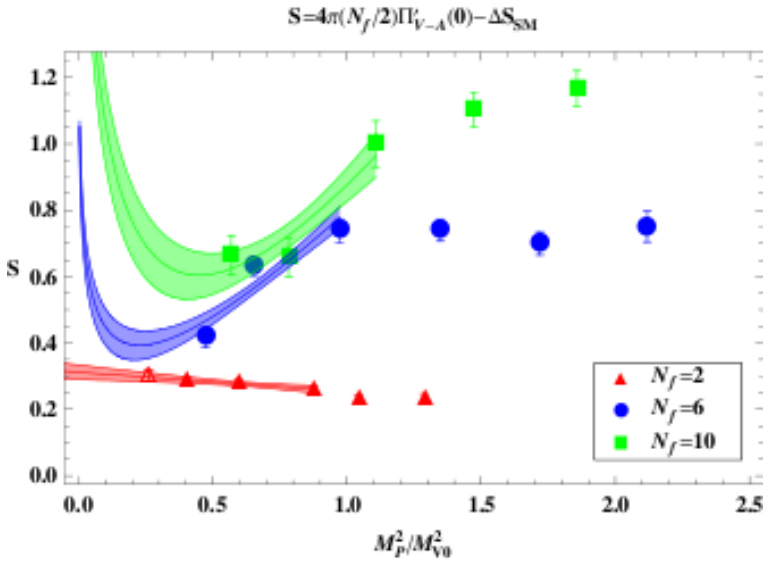

Figure 4·20: S parameter for $N_f = 2$, $N_f = 6$ and (preliminary) $N_f = 10$. The empty point has $M_P L < 4$. The independent linear fits use the three lightest solid points for each N_f, and account for expected chiral logarithmic divergences as described in the text.

In a realistic context, the $N_f^2 - 4$ PNGBs receive mass from standard model and other interactions not included here, even as the technifermions become massless, $m \to 0$. These PNGB masses determine the value of $M_P^2/M_{V0}^2 > 0$ at which the S parameter for $N_f > 2$ should be compared to the $M_P^2 \to 0$ limit of the $N_f = 2$ theory, which possesses no additional PNGBs. Our result for $N_f = 2$ is $S = 0.311(21)$, in close agreement with the initial estimate $S = 0.32(3)$ made by scaling up experimental QCD spectrum data to the electroweak scale [18]. Two recent lattice studies performed similar QCD calculations, determining the chiral perturbation theory low energy constant $L_{10}^r(\mu)$ at a renormalization

Table 4.6: $4\pi\Pi'_{V-A}(0)$, ΔS_{SM} and S for $N_f = 2$, $N_f = 6$ and (preliminary) $N_f = 10$. The linear $M_P^2 \to 0$ extrapolation for $N_f = 2$ uses the three lightest points with $M_P L > 4$, which are $0.01 \leq m_f \leq 0.02$. All errors included here are statistical; systematic errors are discussed in the text.

N_f	m_f	M_P^2/M_{V0}^2	$4\pi\Pi'_{V-A}(0)$	ΔS_{SM}	S
2	0.005	0.2615	0.349(18)	0.047	0.302(16)
2	0.010	0.4053	0.323(11)	0.036	0.287(11)
2	0.015	0.5950	0.306(11)	0.027	0.279(11)
2	0.020	0.8771	0.280(11)	0.020	0.260(12)
2	0.025	1.0427	0.252(9)	0.017	0.235(10)
2	0.030	1.2877	0.250(9)	0.014	0.236(10)
2	–	$\to 0$	–	–	0.311(21)
6	0.005	0.4729	0.149(10)	0.032	0.415(30)
6	0.010	0.6546	0.218(9)	0.025	0.628(26)
6	0.015	0.9729	0.252(11)	0.018	0.738(35)
6	0.020	1.3487	0.251(9)	0.013	0.740(32)
6	0.025	1.7190	0.236(9)	0.011	0.699(34)
6	0.030	2.1191	0.253(12)	0.009	0.750(46)
10	0.005	0.570	0.138(12)	0.028	0.664(60)
10	0.010	0.783	0.136(12)	0.022	0.658(60)
10	0.015	1.107	0.203(13)	0.016	0.999(70)
10	0.020	1.473	0.223(9)	0.012	1.100(52)
10	0.025	1.856	0.235(7)	0.010	1.170(54)

scale of $\mu = m_\rho = 770$ MeV. They report

$$L_{10}^r(m_\rho) = -0.0052(2)(^{+0}_{-3})(^{+5}_{-0}) \qquad \text{(Ref. [141])}$$
$$L_{10}^r(m_\rho) = -0.0057(11)(7) \qquad \text{(Ref. [142])},$$

where in both cases the first error is statistical and the others systematic. Both results are consistent with the experimental QCD value of $L_{10}^r(m_\rho) = -0.00509(57)$ [330]. Ref. [142] then scales m_ρ by a factor of v/f_π to find $S = 0.42(7)$ at $M_H^{(ref)} = 120$ GeV from Eqn. 3.40. Shifting the reference mass to 1 TeV via $\Delta S = \log\left(M_H^{(1)}/M_H^{(2)}\right)/(6\pi)$ in order to compare with our result, we find agreement,

$$\text{Ref. [141]} \rightarrow S = 0.27(3) \qquad \text{Ref. [142]} \rightarrow S = 0.31(7).$$

Formally, as discussed in Section 3.2.3, two of the N_f flavors of strongly-interacting fermions must be extrapolated to the chiral limit in order to obtain the three exactly massless NGBs that are eaten by the $W^\pm$ and Z. Such a procedure is too elaborate to carry out consistently in our simulations, which take all of the N_f fermions to be degenerate. However, we expect that the systematic errors introduced by our approach are minor, and are accounted for by the M_P-dependence that we introduce to the standard model subtraction $\Delta S_{SM}(M_P)$. The main point of this subtraction is to remove from the spectrum the three NGBs that are eaten in the course of electroweak symmetry breaking. As $M_P^2 \rightarrow 0$ for the three NGBs, this cancellation continues to function, as illustrated by the smooth extrapolation we observe for $N_f = 2$.

Although our $N_f = 6$ (10) results for S with $N_D = N_f/2$ are always larger than the $N_f = 2$ value $S = 0.311(21)$, these results are well below the $S \approx 0.9$ (1.6) that would be obtained from naïve N_f-scaling. In a model where only a single pair of the strongly-interacting fermions transformed as an electroweak doublet, $N_D = 1$, the resulting values of S would be well below that of the $N_f = 2$ theory. However, even these results would still be positive, $S > 0$, and in 2–3σ disagreement with the experimental $S \approx -0.15(10)$ [13].

Systematics

As discussed above, our calculations are exploratory, not aimed at achieving very high precision. Rather, our goal is to search for significant deviations from conventional wisdom based on QCD, and for this purpose it is sufficient to achieve combined statistical and systematic errors of roughly 10%–20% in our results for the S parameter. From Table 4.6, we see that statistical uncertainties in S are typically around 5%, leaving enough room in our error budget for the systematic effects we now summarize. The list below closely follows the more general discussions in Section 3.2.3.

Discretization errors: Although we use only a single lattice spacing, it is small ($a \approx (5M_{V0})^{-1}$), and our Iwasaki+DWF lattice action suffers only from $\mathcal{O}(a^2)$ artifacts. More concretely, we argued in Section 4.1.2 above that by comparing chiral extrapolations of the different renormalization factors Z_A, Z_V and $Z_A^{(i)}$, we could estimate discretization errors to be below the percent level. While different observables may be affected differently by discretization, we use the same conserved–local current correlators to calculate Z_V and $Z_A^{(i)}$ that we use to determine S. Finally, our procedure of matching scales across all simulations also ensures that results for different N_f can be compared directly with little systematic error.

Finite volume effects: On the other hand, small lattice spacings lead to small physical volumes. By a combination of large ($32^3 \times 64$) lattices and fairly large pseudoscalar masses M_P^2, we are able to satisfy the conventional lattice QCD condition $M_P L > 4$ for all ensembles included in our analyses. However, we mentioned above that finite volume effects tend to become more severe as N_f increases [265, 292]. We are therefore in the process of carrying out direct numerical studies of finite volume effects, to ensure that they are under control.

Chiral extrapolation: The downside of working at large pseudoscalar masses M_P^2 is that long extrapolations are required to reach the chiral limit, with the related problem that chiral perturbation theory cannot yet be applied to our simulations with $N_f > 2$. There are also systematic effects from our procedure of taking all N_f fermions to be degenerate,

rather than extrapolating two of them to the chiral limit to more closely reproduce EWSB phenomenology. We argued in the previous section that these effects should be minor as a result of our standard model subtraction procedure.

Finally, we expect issues due to **autocorrelations, frozen topology and limited statistics** to be most significant. As discussed in Section 4.1.2 above, our use of a small lattice spacing leads to slow topological evolution, with insufficient topological sampling for most $N_f = 10$ simulations, and all simulations with $m_f = 0.005$. The short, exploratory runs summarized in Table 4.2 suggest that the effects of these and other autocorrelations may be significant. These systematic effects related to these issues are being actively studied, but at present remain poorly known.

Comparison to vector and axial spectra

In Secs. 2.2.4 and 2.3 we suggested that parity doubling associated with the proximity of the conformal window might reduce the S parameter in walking theories. We have now seen direct evidence of such a reduction in S for $N_f = 6$ and $N_f = 10$ compared to QCD-based expectations. Earlier, in Section 4.1.2, we observed from the masses and decay constants of the $N_f = 6$ theory that it is more parity doubled than $N_f = 2$. In this section, we explore the potential relation between these two results, considering only the $N_f = 2$ and $N_f = 6$ theories where analyses of the masses and decay constants have been completed.

Of necessity, we adopt the single-pole approximation of the vector and axial spectral functions, Eqn. 4.22. Although this approximation transforms the $M_P^2 = 0$ dispersion relation Eqn. 4.14 into an expression (Eqn. 4.23) with the same Q^2 dependence as the Padé form of Eqn. 4.21, our Padé fits account for a complicated time-like structure with cuts and multiple poles. We must therefore be wary of associating Padé fit parameters with the values we would obtain from inserting the independently measured $M_{V,A}$ and $F_{P,V,A}$ into Eqn. 4.23. Figs. 4·21 and 4·22 compare direct Padé fit results for $\sqrt{-\Pi_{V-A}(0)}$ and

$4\pi\Pi'_{V-A}(0)$ (respectively) against the corresponding single-pole dominance predictions

$$\sqrt{-\Pi^{(pole)}_{V-A}(0)} = F_P \tag{4.28}$$

$$4\pi \left.\frac{d}{dQ^2}\Pi_{V-A}(Q^2)\right|_{Q^2=0} = 4\pi\left[\frac{F_V^2}{M_V^2} - \frac{F_A^2}{M_A^2}\right]. \tag{4.29}$$

These data are also tabulated in Table 4.7 (even though $4\pi\Pi'_{V-A}(0)$ and F_P data appeared above in Tables 4.6 and 4.5, respectively, we reproduce them here for more convenient comparison).

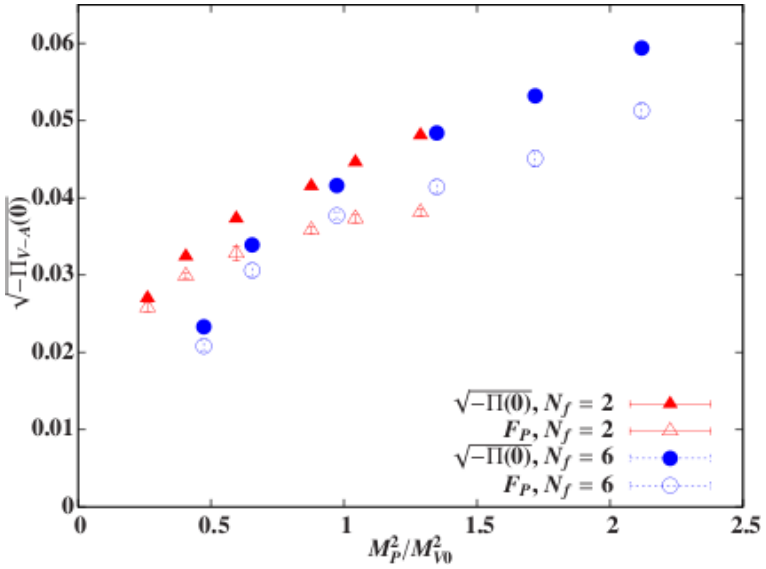

Figure 4·21: $\sqrt{-\Pi_{V-A}(0)}$ from Padé fits (filled) compared to independently measured F_P (empty), for $N_f = 2$ and $N_f = 6$.

While $\sqrt{-\Pi_{V-A}(0)} = F_P$ in the chiral limit $M_P^2 \to 0$, away from the chiral limit there is a statistically significant difference between $\sqrt{-\Pi_{V-A}(0)}$ and F_P, which increases with M_P^2. The single-pole dominance results for $4\pi\Pi'_{V-A}(0)$ are in less disagreement with our direct determination; although systematically lower, they show a similar decrease for $N_f = 6$ compared to $N_f = 2$. We expect that excited states in the vector and axial channels are likely to provide additional positive contributions to $\Pi'_{V-A}(0)$, which will help reconcile these approximate results with the direct fits.

We thus identify two likely sources of discrepancies between our direct results and

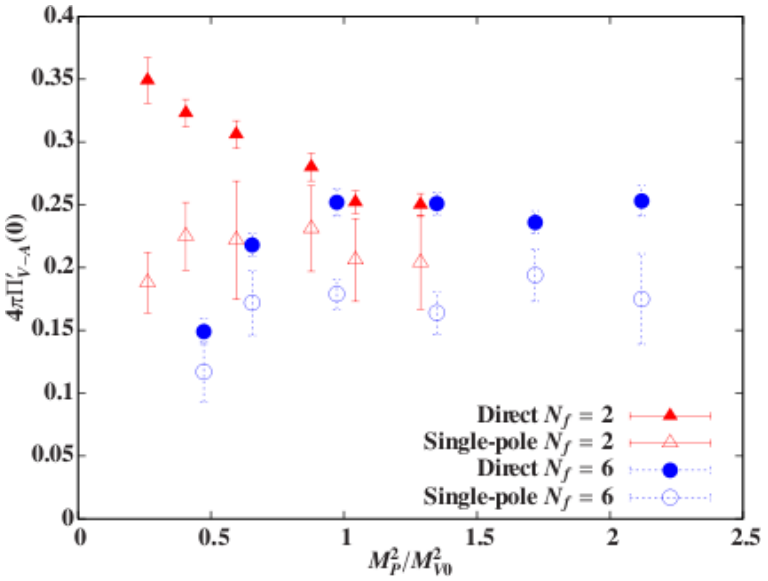

Figure 4·22: $4\pi\Pi'_{V-A}(0)$ from Padé fits (filled) compared to Eqn. 4.29 (empty), for $N_f = 2$ and $N_f = 6$.

Table 4.7: Comparing $4\pi\Pi'(0)$ with Eqn. 4.29, and $\sqrt{-\Pi_{V-A}(0)}$ with F_P, for $N_f = 2$ and $N_f = 6$.

N_f	m_f	M_P^2/M_{V0}^2	$4\pi\Pi'_{V-A}(0)$	Eqn. 4.29	$\sqrt{-\Pi_{V-A}(0)}$	F_P
2	0.005	0.2615	0.349(18)	0.188(24)	0.0270(4)	0.0258(5)
2	0.010	0.4053	0.323(11)	0.225(27)	0.0324(3)	0.0299(4)
2	0.015	0.5950	0.306(11)	0.222(47)	0.0373(3)	0.0328(9)
2	0.020	0.8771	0.280(11)	0.231(34)	0.0415(3)	0.0358(5)
2	0.025	1.0427	0.252(9)	0.206(33)	0.0446(3)	0.0373(5)
2	0.030	1.2877	0.250(9)	0.204(37)	0.0481(4)	0.0381(5)
6	0.005	0.4729	0.149(10)	0.117(24)	0.0233(5)	0.0208(7)
6	0.010	0.6546	0.218(9)	0.172(26)	0.0339(3)	0.0306(8)
6	0.015	0.9729	0.252(11)	0.179(12)	0.0416(4)	0.0377(5)
6	0.020	1.3487	0.251(9)	0.164(17)	0.0484(5)	0.0414(8)
6	0.025	1.7190	0.236(9)	0.194(21)	0.0532(6)	0.0451(11)
6	0.030	2.1191	0.253(12)	0.175(36)	0.0594(6)	0.0513(9)

Eqns. 4.28, 4.29: the effects of working at $M_P^2 > 0$, and the effects of approximating the vector and axial spectral functions by single poles. To further explore the interplay of these two effects, we can consider the single-pole dominance relations resulting from the first and second Weinberg sum rules, Eqns. 4.15 and 4.16,

$$F_P^2 - F_V^2 + F_A^2 = 0 \tag{4.30}$$

$$M_V^2 F_V^2 - M_A^2 F_A^2 = 0. \tag{4.31}$$

We plot data for these expressions in Figs. 4·23 and 4·24, and tabulate it in Table 4.8. Although these relations are not well satisfied at any non-zero $M_P^2 > 0$, we see signs that they may describe our data well in the chiral limit. These single-pole dominance relations may even work better in the chiral limit for $N_f = 6$ than for $N_f = 2$.

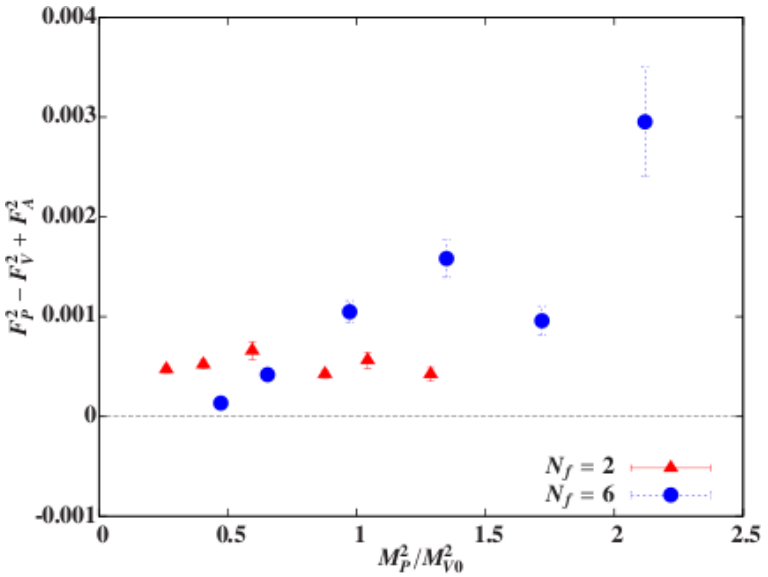

Figure 4·23: Deviations from the single-pole relation $F_P^2 - F_V^2 + F_A^2 = 0$ following from the first Weinberg sum rule, plotted versus M_P^2/M_{V0}^2 for $N_f = 2$ and $N_f = 6$.

4.2.3 Future directions

We have already mentioned ongoing work to improve and extend our investigations of the S parameter on the lattice. These include both finalizing calculations for $N_f = 10$ as well

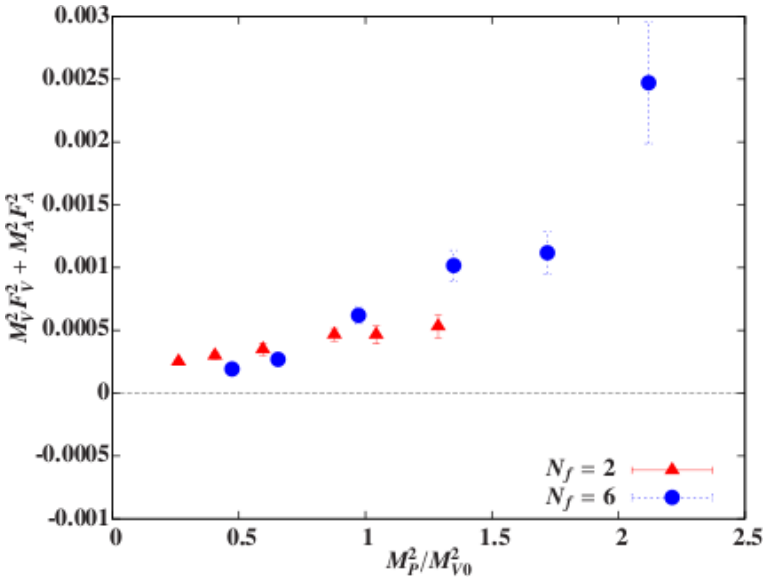

Figure 4·24: Deviations from the single-pole relation $M_V^2F_V^2 - M_A^2F_A^2 = 0$ following from the second Weinberg sum rule, plotted versus M_P^2/M_{V0}^2 for $N_f = 2$ and $N_f = 6$.

Table 4.8: Deviations from the single-pole relations following from the first and second Weinberg sum rules, for $N_f = 2$ and $N_f = 6$.

N_f	m_f	M_P^2/M_{V0}^2	$\left(F_P^2 - F_V^2 + F_A^2\right) \cdot 10^3$	$\left(M_V^2F_V^2 - M_A^2F_A^2\right) \cdot 10^3$
2	0.005	0.2615	0.471(35)	0.250(19)
2	0.010	0.4053	0.520(42)	0.299(26)
2	0.015	0.5950	0.658(88)	0.349(48)
2	0.020	0.8771	0.562(41)	0.466(50)
2	0.025	1.0427	0.562(79)	0.465(69)
2	0.030	1.2877	0.422(68)	0.531(92)
6	0.005	0.4729	0.133(15)	0.193(22)
6	0.010	0.6546	0.418(46)	0.269(30)
6	0.015	0.9729	1.048(112)	0.620(66)
6	0.020	1.3487	1.582(189)	1.017(121)
6	0.025	1.7190	0.958(148)	1.118(169)
6	0.030	2.1191	2.953(550)	2.472(485)

as continuing to explore and constrain systematic effects. In particular, we are analyzing $16^3 \times 32$ and $24^3 \times 32$ lattices (with both fixed β and with a coarser lattice spacing tuned to produce the same physical volume) in order to numerically assess finite volume effects for various N_f. The $16^3 \times 32$ lattices may be too small to obtain much reliable information, but we are taking advantage of their small size to use them as testbeds for the development of GPU code for domain wall fermions. Determining the effects of fixed topology is of similar concern, though here the best course of action is not as clear.

Even from the calculations we have already performed, there may be further physics that we can investigate with our data on the vacuum polarization function $\Pi_{V-A}(Q^2)$. Ref. [331], for example, extracts the strong coupling constant and estimates some four-quark condensates by applying of the operator product expansion [328, 329] for lattice QCD with $N_f = 2$ overlap quarks. We are also working on extending our current results by using partially twisted boundary conditions [332, 333]. This technique would allow $\Pi_{V-A}(Q^2)$ to be measured at smaller Q^2 values, potentially allowing us to supplement Padé fits with analyses based on chiral perturbation theory.

Farther in the future, we will measure the S parameter as part of the LSD Collaboration's studies of $SU(2)$ gauge theories. In addition, the USQCD Collaboration has initiated an investigation of $SU(3)$ gauge theory with $N_f = 8$ fermions in the fundamental representation, generating $63^3 \times 128$ gauge configurations with highly-improved staggered fermions [334]. We plan to measure the S parameter on these lattices, through a mixed-action calculation that uses domain wall fermions for these measurements even though staggered fermions are used by the HMC evolution.

The high level of activity by the many groups applying lattice techniques to study dynamical electroweak symmetry breaking promise an interesting future for this field. Possibilities for future studies are endless, but new results on physics beyond the standard model coming from experiments at the LHC will soon guide the course of these investigations.

Chapter 5

Conclusion

In this dissertation we discussed the application of lattice gauge theory to models of electroweak symmetry breaking that involve new strong dynamics. Such technicolor theories are natural and viable scenarios, in which strong interactions at the TeV scale lead to chiral symmetry breaking that drives EWSB. While the most direct means of extending technicolor to communicate EWSB to fermions produces tension between fermion masses and flavor-changing neutral currents, the most stringent constraints on technicolor itself come from precision electroweak observables, in particular the S parameter. These difficulties may be addressed if the theory possesses approximately conformal (walking) dynamics, as opposed to QCD-like behavior. Walking is characterized by a large mass anomalous dimension $\gamma_m(\mu) \simeq 1$ over a large range of scales μ, and is most likely to occur near the lower (strongly-coupled) end of the conformal window.

To test such proposals, we turn to lattice gauge theory, the premier method for obtaining quantitatively-reliable, non-perturbative predictions from strongly-interacting theories. We formulate theories on the lattice by discretizing euclidean spacetime, in such a way that the original theory is recovered in the infinite-volume, continuum limit. We carry out numerical lattice simulations through Monte Carlo importance sampling, using the hybrid Monte Carlo algorithm to generate ensembles of gauge configurations. Both configuration generation and measurement of observables involving valence fermions requires inverting the lattice Dirac operator, which is the main computational cost of the simulations.

Systematic effects due to autocorrelations and due to working in a finite, discrete spacetime are understood and under control in the case of lattice QCD, but are less certain in other theories beyond QCD. In addition, lattice discretization of fermionic fields introduces

spurious doubler modes, and the most straightforward ways of removing doublers explicitly break chiral symmetry. Although chiral lattice fermion formulations have been developed, these are much more computationally expensive than other lattice actions. The domain wall fermions we use introduce a fifth dimension of length L_s, and possess exact chiral symmetry in the limit $L_s \to \infty$. At finite L_s, we absorb the effects of residual chiral symmetry breaking into a small additive renormalization of the input fermion mass.

In order to gain the greatest possible control over systematic effects, we ground our investigations on lattice QCD ($N_f = 2$), proceeding systematically from this case toward the conformal window ($N_f^c > 8$). Our initial investigations find an enhanced chiral condensate $\langle\overline{\psi}\psi\rangle$ in the $N_f = 6$ theory relative to lattice QCD, and the final focus of this dissertation is our calculation of the S parameter in both of these theories, along with some preliminary results for $N_f = 10$.

On the lattice, we extract S from $\Pi_{V-A}(Q^2)$, the difference of vector and axial current correlators (Eqn. 4.6). It is important to use at least one conserved current in these correlators, to ensure that lattice artifacts cancel in the V–A difference. S is defined to vanish in the standard model, so we use a dispersive integral to calculate and remove the standard model contribution at non-zero PNGB mass $M_P^2 > 0$. Although we work only with all N_f fermions degenerate, we argue that this subtraction adequately approximates the phenomenologically relevant limit where two flavors are exactly massless while the rest remain massive.

For $N_f = 2$ we can perform the $M_P^2 \to 0$ extrapolation to obtain $S = 0.311(21)$, in agreement with both QCD-based estimates as well as recent lattice QCD calculations. For $N_f = 6$ and $N_f = 10$, we observe the expected naïve scaling $S \propto N_D$ in the heavy-fermion limit $M_P^2 \gg M_{V0}^2$, but we discover a substantial suppression for $M_P^2 \lesssim M_{V0}^2$. We also find signs of parity-doubling in the masses and decay constants of the lightest vector and axial mesons, which may be related to a smaller S parameter. Fig. 4·20 presents our results the most pessimistic scenarios with $N_D = N_f/2$. With $N_D = 1$, the $N_f = 6$ and $N_f = 10$ models would possess $S \gtrsim 0.1$, much closer to (although still in tension with) the

experimental $S \approx -0.15(10)$. We repeat that $N_f = 10$ analyses are preliminary, and in particular include only disordered-start simulations.

These results are encouraging for the very active field that has begun applying lattice techniques to strongly-interacting gauge theories beyond QCD. Even though such explorations are broadly valuable to improving our understanding of quantum field theory itself, they are currently motivated in large part by the possibility that new strong dynamics may explain EWSB. This hypothesis is being tested by the LHC, and is likely to be either confirmed or ruled out within the next few years. Although most lattice studies are focusing on the question of whether or not theories lie within the conformal window, phenomenological results like the calculation of the S parameter are of particular importance in this context. Our finding that S can be significantly reduced compared to the conventional wisdom reinforces the continued viability of these theories.

Our calculation of the S parameter is exploratory, and I am working on improving our understanding of and control over the relevant systematic effects. Additional $N_f = 2$ and $N_f = 6$ simulations with $m_f = 0.0075$ are underway, as are ordered-start runs for all $N_f = 10$ mass points. Calculations on smaller $16^3 \times 32$ and $24^3 \times 32$ lattices will allow direct estimation of finite-volume effects, and are being used as testbeds to develop efficient GPU code for domain wall fermions. Partially twisted boundary conditions may allow us to measure $\Pi_{V-A}(Q^2)$ at smaller Q^2 values, and we are exploring prospects for extracting additional physics from this polarization function.

I am also working on studies of other theories, where our investigations are still in their early stages. Measuring the S parameter on $N_f = 8$ lattices generated with staggered fermions will require testing mixed-action methods, while determining vector and axial current correlators in $SU(2)$ gauge theories may require even more significant modifications. The S parameter is only one observable among many being considered in these investigations, but may be one of the most interesting pieces of information we can obtain from applying lattice gauge theory to models of electroweak symmetry breaking through new strong dynamics.

List of Abbreviated Journal Titles

Adv. Theor. Math. Phys.	Advances in Theoretical and Mathematical Physics
Commun. Math. Phys. ...	Communications in Mathematical Physics
Eur. Phys. J.	European Physical Journal
J. Phys.	Journal of Physics
JHEP	Journal of High Energy Physics
Nucl. Phys.	Nuclear Physics
Nucl. Phys. Proc. Suppl. .	Nuclear Physics B Proceedings Supplements
Nuovo Cim.	Nuovo Cimento
Phys. Lett.	Physics Letters
Phys. Rept.	Physics Reports
Phys. Rev.	Physical Review
Phys. Rev. Lett.	Physical Review Letters
PoS	Proceedings of Science
Proc. Nat. Acad. Sci.	Proceedings of the National Academy of Sciences
Prog. Theor. Phys.	Progress of Theoretical Physics
Rept. Prog. Phys.	Reports on Progress in Phyics
Rev. Mod. Phys.	Reviews of Modern Physics
SIAM	Society for Industrial and Applied Mathematics
Zh. Eksp. Teor. Fiz.	Zhurnal Eksperimental'noi i Teoreticheskoi Fiziki

Bibliography

[1] LSD Collaboration, T. Appelquist *et al.*, "Toward TeV Conformality", *Phys. Rev. Lett.* **104** (2010) 071601, arXiv:0910.2224 [hep-ph].

[2] LSD Collaboration, E. T. Neil *et al.*, "Lattice study of ChPT beyond QCD", *PoS* **CD09** (2009) 088, arXiv:1002.3777 [hep-lat].

[3] LSD Collaboration, T. Appelquist *et al.*, "Parity Doubling and the S Parameter Below the Conformal Window", arXiv:1009.5967 [hep-ph]. To appear in *Phys. Rev. Lett* (2011).

[4] LSD Collaboration, T. Appelquist *et al.* In preparation.

[5] S. L. Glashow, "Partial Symmetries of Weak Interactions", *Nucl. Phys.* **22** (1961) 579–588.

[6] F. Englert and R. Brout, "Broken Symmetry and the Mass of Gauge Vector Mesons", *Phys. Rev. Lett.* **13** (1964) 321–322.

[7] P. W. Higgs, "Broken symmetries, massless particles and gauge fields", *Phys. Lett.* **12** (1964) 132–133.

[8] P. W. Higgs, "Broken Symmetries and the Masses of Gauge Bosons", *Phys. Rev. Lett.* **13** (1964) 508–509.

[9] G. S. Guralnik, C. R. Hagen, and T. W. B. Kibble, "Global Conservation Laws and Massless Particles", *Phys. Rev. Lett.* **13** (1964) 585–587.

[10] S. Weinberg, "A Model of Leptons", *Phys. Rev. Lett.* **19** (1967) 1264–1266.

[11] A. Salam, "Weak and electromagnetic interactions", in *Elementary Particle Physics: Relativistic Groups and Analyticity, Proceedings of the Nobel Symposium held in 1968 at Lerum, Sweden*, pp. 367–377. Almquvist and Wiksell, Stockholm, 1968.

[12] P. Langacker, "Physics implications of precision electroweak experiments", *J. Phys.* **G29** (2003) 35–48, arXiv:hep-ph/0102085.

[13] Particle Data Group Collaboration, K. Nakamura *et al.*, "Review of particle physics", *J. Phys.* **G37** (2010) 075021. See in particular J. Erler and P. Langacker, "Electroweak Model and Constraints on New Physics", pages 126–145; R. S. Chivukula, M. Narain and J. Womersley, "Searches for Technicolor", pages 1340–1347.

[14] S. Weinberg, "Implications of Dynamical Symmetry Breaking", *Phys. Rev.* **D13** (1976) 974–996.

[15] S. Weinberg, "Implications of Dynamical Symmetry Breaking: An Addendum", *Phys. Rev.* **D19** (1979) 1277–1280.

[16] L. Susskind, "Dynamics of Spontaneous Symmetry Breaking in the Weinberg-Salam Theory", *Phys. Rev.* **D20** (1979) 2619–2625.

[17] M. E. Peskin and T. Takeuchi, "New Constraint on a Strongly Interacting Higgs Sector", *Phys. Rev. Lett.* **65** (1990) 964–967.

[18] M. E. Peskin and T. Takeuchi, "Estimation of oblique electroweak corrections", *Phys. Rev.* **D46** (1992) 381–409.

[19] W. E. Caswell, "Asymptotic Behavior of Nonabelian Gauge Theories to Two Loop Order", *Phys. Rev. Lett.* **33** (1974) 244.

[20] T. Banks and A. Zaks, "On the Phase Structure of Vector-Like Gauge Theories with Massless Fermions", *Nucl. Phys.* **B196** (1982) 189.

[21] H. J. Rothe, *Lattice gauge theories: An Introduction*, vol. 74 of *World Scientific Lecture Notes in Physics*. World Scientific, Singapore, 2005.

[22] T. DeGrand and C. E. Detar, *Lattice methods for quantum chromodynamics*. World Scientific, Singapore, 2006.

[23] P. Hagler, "Hadron structure from lattice quantum chromodynamics", *Phys.Rept.* **490** (2010) 49–175, arXiv:0912.5483 [hep-lat].

[24] C. Alexandrou, "Hadron Structure and Form Factors", *PoS* **LATTICE2010** (2010) 001, arXiv:1011.3660 [hep-lat].

[25] C. Hoelbling, "Light hadron spectroscopy and pseudoscalar decay constants", *PoS* **LATTICE2010** (2010) 011, arXiv:1102.0410 [hep-lat].

[26] C. Sachrajda, "Phenomenology from the Lattice", *PoS* **Lattice 2010** (2010) 018, arXiv:1103.5959 [hep-lat].

[27] G. Colangelo *et al.*, "Review of lattice results concerning low energy particle physics", arXiv:1011.4408 [hep-lat].

[28] HPQCD Collaboration, E. Follana *et al.*, "High Precision determination of the π, K, D and D_s decay constants from lattice QCD", *Phys. Rev. Lett.* **100** (2008) 062002, arXiv:0706.1726 [hep-lat].

[29] S. Durr *et al.*, "Ab-Initio Determination of Light Hadron Masses", *Science* **322** (2008) 1224–1227, arXiv:0906.3599 [hep-lat].

[30] HPQCD Collaboration, C. T. H. Davies *et al.*, "Precise determination of the lattice spacing in full lattice QCD", *Phys. Rev.* **D81** (2010) 034506, arXiv:0910.1229 [hep-lat].

[31] C. McNeile *et al.*, "High-Precision c and b Masses, and QCD Coupling from Current-Current Correlators in Lattice and Continuum QCD", *Phys. Rev.* **D82** (2010) 034512, arXiv:1004.4285 [hep-lat].

[32] C. T. H. Davies *et al.*, "Update: Precision D_s decay constant from full lattice QCD using very fine lattices", *Phys. Rev.* **D82** (2010) 114504, arXiv:1008.4018 [hep-lat].

[33] S. Durr *et al.*, "Lattice QCD at the physical point: light quark masses", arXiv:1011.2403 [hep-lat].

[34] S. Durr *et al.*, "Lattice QCD at the physical point: Simulation and analysis details", arXiv:1011.2711 [hep-lat].

[35] G. T. Fleming, "Strong Interactions for the LHC", *PoS* **LATTICE2008** (2008) 021, arXiv:0812.2035 [hep-lat].

[36] E. Pallante, "Strongly and slightly flavored gauge theories", *PoS* **LAT2009** (2009) 015, arXiv:0912.5188 [hep-lat].

[37] T. DeGrand, "Lattice studies of QCD-like theories with many fermionic degrees of freedom", arXiv:1010.4741 [hep-lat].

[38] L. Del Debbio, "The conformal window on the lattice", *PoS* **Lattice 2010** (2011) 004, arXiv:1102.4066 [hep-lat].

[39] K. Rummukainen, "QCD-like technicolor on the lattice", arXiv:1101.5875 [hep-lat].

[40] H. B. Nielsen and M. Ninomiya, "Absence of Neutrinos on a Lattice. 1. Proof by Homotopy Theory", *Nucl. Phys.* **B185** (1981) 20. Erratum–*ibid.* **B195** (1982) 541.

[41] H. B. Nielsen and M. Ninomiya, "Absence of Neutrinos on a Lattice. 2. Intuitive Topological Proof", *Nucl. Phys.* **B193** (1981) 173.

[42] H. B. Nielsen and M. Ninomiya, "No Go Theorem for Regularizing Chiral Fermions", *Phys. Lett.* **B105** (1981) 219.

[43] P. H. Ginsparg and K. G. Wilson, "A Remnant of Chiral Symmetry on the Lattice", *Phys. Rev.* **D25** (1982) 2649–2657.

[44] D. B. Kaplan, "Chiral Symmetry and Lattice Fermions", arXiv:0912.2560 [hep-lat].

[45] D. B. Kaplan, "A Method for simulating chiral fermions on the lattice", *Phys. Lett.* **B288** (1992) 342–347, arXiv:hep-lat/9206013.

[46] Y. Shamir, "Chiral fermions from lattice boundaries", *Nucl. Phys.* **B406** (1993) 90–106, arXiv:hep-lat/9303005.

[47] V. Furman and Y. Shamir, "Axial symmetries in lattice QCD with Kaplan fermions", *Nucl. Phys.* **B439** (1995) 54–78, arXiv:hep-lat/9405004.

[48] T. Blum *et al.*, "Quenched lattice QCD with domain wall fermions and the chiral limit", *Phys. Rev.* **D69** (2004) 074502, arXiv:hep-lat/0007038.

[49] H. Fritzsch, M. Gell-Mann, and H. Leutwyler, "Advantages of the Color Octet Gluon Picture", *Phys. Lett.* **B47** (1973) 365–368.

[50] D. J. Gross and F. Wilczek, "Ultraviolet Behavior of Non-Abelian Gauge Theories", *Phys. Rev. Lett.* **30** (1973) 1343–1346.

[51] H. Politzer, "Reliable Perturbative Results for Strong Interactions?", *Phys. Rev. Lett.* **30** (1973) 1346–1349.

[52] C. Quigg, "Spontaneous Symmetry Breaking as a Basis of Particle Mass", *Rept. Prog. Phys.* **70** (2007) 1019–1054, arXiv:0704.2232 [hep-ph].

[53] C. Quigg, "Unanswered Questions in the Electroweak Theory", *Annual Review of Nuclear and Particle Science* **59** (2009) 505–555, arXiv:0905.3187 [hep-ph].

[54] M. E. Peskin and D. V. Schroeder, *An Introduction to Quantum Field Theory*. Westview Press, Boulder, Colorado, 1995.

[55] S. Weinberg, *The Quantum Theory of Fields. Vol. 2: Modern Applications*. Cambridge University Press, Cambridge, UK, 1996.

[56] M. Srednicki, *Quantum field theory*. Cambridge University Press, Cambridge, UK, 2007.

[57] P. Langacker, "Introduction to the Standard Model and Electroweak Physics", arXiv:0901.0241 [hep-ph].

[58] N. Cabibbo, "Unitary Symmetry and Leptonic Decays", *Phys. Rev. Lett.* **10** (1963) 531–533.

[59] M. Kobayashi and T. Maskawa, "CP Violation in the Renormalizable Theory of Weak Interaction", *Prog. Theor. Phys.* **49** (1973) 652–657.

[60] V. L. Ginzburg and L. D. Landau, "On the Theory of Superconductivity", *Zh. Eksp. Teor. Fiz.* **20** (1950) 1064–1082. English translation: L. D. Landau, *Collected Papers* (Oxford: Pergamon Press, 1965), 546.

[61] Y. Nambu, "Axial vector current conservation in weak interactions", *Phys. Rev. Lett.* **4** (1960) 380–382.

[62] J. Goldstone, "Field Theories with Superconductor Solutions", *Nuovo Cim.* **19** (1961) 154–164.

[63] J. Goldstone, A. Salam, and S. Weinberg, "Broken Symmetries", *Phys. Rev.* **127** (1962) 965–970.

[64] P. W. Anderson, "Coherent Excited States in the Theory of Superconductivity: Gauge Invariance and the Meissner Effect", *Phys. Rev.* **110** (1958) 827–835.

[65] Y. Nambu, "Quasi-particles and gauge invariance in the theory of superconductivity", *Phys. Rev.* **117** (1960) 648–663.

[66] J. S. Schwinger, "Gauge Invariance and Mass", *Phys. Rev.* **125** (1962) 397–398.

[67] P. W. Anderson, "Plasmons, Gauge Invariance, and Mass", *Phys. Rev.* **130** (1963) 439–442.

[68] Gargamelle Neutrino Collaboration, F. J. Hasert *et al.*, "Observation of neutrino-like interactions without muon or electron in the Gargamelle neutrino experiment", *Phys. Lett.* **B46** (1973) 138–140.

[69] D. Haidt, "The discovery of neutral currents", *Eur. Phys. J.* **C34** (2004) 25–31.

[70] UA1 Collaboration, G. Arnison *et al.*, "Experimental observation of isolated large transverse energy electrons with associated missing energy at s**(1/2) = 540-GeV", *Phys. Lett.* **B122** (1983) 103–116.

[71] UA2 Collaboration, M. Banner *et al.*, "Observation of single isolated electrons of high transverse momentum in events with missing transverse energy at the CERN anti-p p collider", *Phys. Lett.* **B122** (1983) 476–485.

[72] UA1 Collaboration, G. Arnison *et al.*, "Experimental observation of lepton pairs of invariant mass around 95-GeV/c**2 at the CERN SPS collider", *Phys. Lett.* **B126** (1983) 398–410.

[73] UA2 Collaboration, P. Bagnaia *et al.*, "Evidence for Z0 –¿ e+ e- at the CERN anti-p p collider", *Phys. Lett.* **B129** (1983) 130–140.

[74] C. Rubbia, "Experimental Observation of the Intermediate Vector Bosons W^+, W^-, and Z^0", *Rev. Mod. Phys.* **57** (1985) 699–722.

[75] G. 't Hooft, "Renormalizable Lagrangians for Massive Yang-Mills Fields", *Nucl. Phys.* **B35** (1971) 167–188.

[76] Gfitter Collaboration, H. Flacher *et al.*, "Revisiting the global electroweak fit of the Standard Model and beyond with Gfitter", *Eur. Phys. J.* **C60** (2009) 543–583, arXiv:0811.0009 [hep-ph]. Updated results available at http://www.cern.ch/gfitter.

[77] Gfitter Collaboration, M. Goebel, "Status of the global fit to electroweak precisions data", *PoS* **ICHEP2010** (2010) 570, arXiv:1012.1331 [hep-ph]. Updated results available at http://www.cern.ch/gfitter.

[78] G. Bertone, D. Hooper, and J. Silk, "Particle dark matter: Evidence, candidates and constraints", *Phys. Rept.* **405** (2005) 279–390, arXiv:hep-ph/0404175.

[79] K. G. Wilson, "Renormalization group and critical phenomena. 2. Phase space cell analysis of critical behavior", *Phys. Rev.* **B4** (1971) 3184–3205.

[80] K. G. Wilson and J. B. Kogut, "The Renormalization group and the epsilon expansion", *Phys. Rept.* **12** (1974) 75–200.

[81] M. Aizenman, "Proof of the Triviality of phi**4 in D-Dimensions Field Theory and Some Mean Field Features of Ising Models for D¿4", *Phys. Rev. Lett.* **47** (1981) 1–4. Erratum–*ibid.* **47** (1981) 886.

[82] J. Frohlich, "On the Triviality of Lambda (phi**4) in D-Dimensions Theories and the Approach to the Critical Point in D ¿= Four-Dimensions", *Nucl. Phys.* **B200** (1982) 281–296.

[83] R. F. Dashen and H. Neuberger, "How to Get an Upper Bound on the Higgs Mass", *Phys. Rev. Lett.* **50** (1983) 1897.

[84] A. Hasenfratz *et al.*, "The Triviality Bound of the Four Component phi**4 Model", *Phys. Lett.* **B199** (1987) 531.

[85] J. Kuti, L. Lin, and Y. Shen, "Upper Bound on the Higgs Mass in the Standard Model", *Phys. Rev. Lett.* **61** (1988) 678.

[86] M. Luscher and P. Weisz, "Scaling Laws and Triviality Bounds in the Lattice phi**4 Theory. 3. N Component Model", *Nucl. Phys.* **B318** (1989) 705.

[87] A. Hasenfratz *et al.*, "Study of the Four Component phi**4 Model", *Nucl. Phys.* **B317** (1989) 81.

[88] M. Gockeler *et al.*, "Scaling analysis of the 0(4) symmetric Phi**4 theory in the broken phase", *Nucl. Phys.* **B404** (1993) 517–555, arXiv:hep-lat/9206025.

[89] P. Gerhold and K. Jansen, "Upper Higgs boson mass bounds from a chirally invariant lattice Higgs-Yukawa model", *JHEP* **04** (2010) 094, arXiv:1002.4336 [hep-lat].

[90] S. Dimopoulos and D. W. Sutter, "The Supersymmetric flavor problem", *Nucl. Phys.* **B452** (1995) 496–512, arXiv:hep-ph/9504415.

[91] J. Bardeen, L. N. Cooper, and J. R. Schrieffer, "Microscopic theory of superconductivity", *Phys. Rev.* **106** (1957) 162.

[92] J. Bardeen, L. N. Cooper, and J. R. Schrieffer, "Theory of superconductivity", *Phys. Rev.* **108** (1957) 1175–1204.

[93] C. T. Hill and E. H. Simmons, "Strong Dynamics and Electroweak Symmetry Breaking", *Phys. Rept.* **381** (2003) 235–402, arXiv:hep-ph/0203079. Erratum–*ibid.* **390** (2004) 553-554.

[94] K. Lane, "Two Lectures on Technicolor", arXiv:hep-ph/0202255. Lectures presented at l'Ecole de GIF at LAPP, Annecy-le-Vieux, France, September 2001.

[95] R. Shrock, "Some Recent Results on Models of Dynamical Electroweak Symmetry Breaking", in *The Origin of Mass and Strong Coupling Gauge Theories*, M. Harada, M. Tanabashi, and K. Yamawaki, eds., pp. 227–241. World Scientific, Singapore, 2008. arXiv:hep-ph/0703050.

[96] A. Martin, "Technicolor Signals at the LHC", arXiv:0812.1841 [hep-ph]. Lectures presented at the 46th Course at the International School of Subnuclear Physics, Erice, Sicily, 29 August–7 September 2008.

[97] F. Sannino, "Conformal Dynamics for TeV Physics and Cosmology", *Acta Physica Polonica* **B40** (2009) 3533–3743, arXiv:0911.0931 [hep-ph].

[98] J. R. Andersen *et al.*, "Discovering Technicolor", arXiv:1104.1255 [hep-ph].

[99] C. Quigg and R. Shrock, "Gedanken Worlds without Higgs: QCD-Induced Electroweak Symmetry Breaking", *Phys. Rev.* **D79** (2009) 096002, arXiv:0901.3958 [hep-ph].

[100] M. Gell-Mann and M. Levy, "The axial vector current in beta decay", *Nuovo Cim.* **16** (1960) 705.

[101] J. Gasser and H. Leutwyler, "Chiral Perturbation Theory to One Loop", *Annals of Physics* **158** (1984) 142.

[102] M. Golterman, "Applications of chiral perturbation theory to lattice QCD", arXiv:0912.4042 [hep-lat].

[103] T. Appelquist and G.-H. Wu, "The Electroweak chiral Lagrangian and new precision measurements", *Phys. Rev.* **D48** (1993) 3235–3241, arXiv:hep-ph/9304240.

[104] R. Jackiw and K. Johnson, "Dynamical Model of Spontaneously Broken Gauge Symmetries", *Phys. Rev.* **D8** (1973) 2386–2398.

[105] J. Cornwall and R. Norton, "Spontaneous Symmetry Breaking Without Scalar Mesons", *Phys. Rev.* **D8** (1973) 3338–3346.

[106] M. Weinstein, "Conserved Currents, their Commutators and the Symmetry Structure of Renormalizable Theories of Electromagnetic, Weak and Strong Interactions", *Phys. Rev.* **D8** (1973) 2511.

[107] S. Dimopoulos and L. Susskind, "Mass Without Scalars", *Nucl. Phys.* **B155** (1979) 237–252.

[108] E. Eichten and K. Lane, "Dynamical Breaking of Weak Interaction Symmetries", *Phys. Lett.* **B90** (1980) 125–130.

[109] T. Appelquist, M. Piai, and R. Shrock, "Fermion masses and mixing in extended technicolor models", *Phys. Rev.* **D69** (2004) 015002, arXiv:hep-ph/0308061 [hep-ph].

[110] K. D. Lane, "Asymptotic Freedom and Goldstone Realization of Chiral Symmetry", *Phys. Rev.* **D10** (1974) 2605.

[111] H. Politzer, "Effective Quark Masses in the Chiral Limit", *Nucl. Phys.* **B117** (1976) 397.

[112] A. G. Cohen and H. Georgi, "Walking Beyond the Rainbow", *Nucl. Phys.* **B314** (1989) 7.

[113] A. Manohar and H. Georgi, "Chiral Quarks and the Nonrelativistic Quark Model", *Nucl. Phys.* **B234** (1984) 189.

[114] H. Georgi, "Generalized dimensional analysis", *Phys. Lett.* **B298** (1993) 187–189, arXiv:hep-ph/9207278.

[115] K. D. Lane and E. Eichten, "Two Scale Technicolor", *Phys. Lett.* **B222** (1989) 274.

[116] K. Lane and A. Martin, "An Effective Lagrangian for Low-Scale Technicolor", *Phys. Rev.* **D80** (2009) 115001, arXiv:0907.3737 [hep-ph].

[117] A. Delgado, K. Lane, and A. Martin, "A Light Scalar in Low-Scale Technicolor", *Phys. Lett.* **B696** (2011) 482–486, arXiv:1011.0745 [hep-ph].

[118] D0 Collaboration, V. Abazov *et al.*, "Search for techniparticles in e+jets events at D0", *Phys. Rev. Lett.* **98** (2007) 221801, arXiv:hep-ex/0612013 [hep-ex].

[119] D0 Collaboration, V. M. Abazov *et al.*, "Search for a resonance decaying into WZ boson pairs in $p\bar{p}$ collisions", *Phys. Rev. Lett.* **104** (2010) 061801, arXiv:0912.0715 [hep-ex].

[120] CDF Collaboration, T. Aaltonen *et al.*, "Search for Technicolor Particles Produced in Association with a W Boson at CDF", *Phys. Rev. Lett.* **104** (2010) 111802, arXiv:0912.2059 [hep-ex].

[121] UTfit Collaboration, M. Bona *et al.*, "Model-independent constraints on Delta F=2 operators and the scale of new physics", *JHEP* **0803** (2008) 049, arXiv:0707.0636 [hep-ph].

[122] R. Chivukula and E. H. Simmons, "Condensate Enhancement and D-Meson Mixing in Technicolor Theories", *Phys. Rev.* **D82** (2010) 033014, arXiv:1005.5727 [hep-lat].

[123] S. Glashow, J. Iliopoulos, and L. Maiani, "Weak Interactions with Lepton-Hadron Symmetry", *Phys. Rev.* **D2** (1970) 1285–1292.

[124] R. Chivukula and H. Georgi, "Composite Technicolor Standard Model", *Phys. Lett.* **B188** (1987) 99.

[125] W. Skiba, "Signatures of technicolor models with the GIM mechanism", *Nucl. Phys.* **B470** (1996) 84–112, arXiv:hep-ph/9601217 [hep-ph].

[126] L. Randall, "ETC with a GIM mechanism", *Nucl. Phys.* **B403** (1993) 122–140, arXiv:hep-ph/9210231 [hep-ph].

[127] T. Appelquist *et al.*, "Flavor-changing processes in extended technicolor", *Phys. Rev.* **D70** (2004) 093010, arXiv:hep-ph/0409035 [hep-ph].

[128] G. H. Brooijmans *et al.*, "New Physics at the LHC: A Les Houches Report. Physics at Tev Colliders 2007 – New Physics Working Group", arXiv:0802.3715 [hep-ph].

[129] CMS Collaboration, "Search for technicolor with the cms experiment",.

[130] G. Brooijmans *et al.*, "New Physics at the LHC. A Les Houches Report: Physics at TeV Colliders 2009 - New Physics Working Group", arXiv:1005.1229 [hep-ph].

[131] T. Takeuchi, "Constraints Placed on the Higgs Sector from Precision Electroweak Measurements", *Proceedings of the Nagoya Spring School* **1991, Dynamical Symmetry Breaking** (1991) 299–335.

[132] B. W. Lynn, M. E. Peskin, and R. G. Stuart, "Radiative Corrections in SU(2) x U(1): LEP / SLC", in *Tests of electroweak theories: polarized processes and other phenomena*, B. W. Lynn and C. Verzegnassi, eds., pp. 213–298. World Scientific, Singapore, 1986. Proceedings of the Second Conference on Tests of Electroweak Theories (Trieste Electroweak 1985).

[133] D. C. Kennedy and B. W. Lynn, "Electroweak Radiative Corrections with an Effective Lagrangian: Four Fermion Processes", *Nucl. Phys.* **B322** (1989) 1.

[134] M. Golden and L. Randall, "Radiative Corrections to Electroweak Parameters in Technicolor Theories", *Nucl. Phys.* **B361** (1991) 3–23.

[135] B. Holdom and J. Terning, "Large corrections to electroweak parameters in technicolor theories", *Phys. Lett.* **B247** (1990) 88–92.

[136] G. Altarelli and R. Barbieri, "Vacuum polarization effects of new physics on electroweak processes", *Phys. Lett.* **B253** (1991) 161–167.

[137] G. Altarelli, R. Barbieri, and S. Jadach, "Toward a model independent analysis of electroweak data", *Nucl. Phys.* **B369** (1992) 3–32.

[138] T. Appelquist and C. W. Bernard, "Strongly Interacting Higgs Bosons", *Phys. Rev.* **D22** (1980) 200.

[139] A. C. Longhitano, "Heavy Higgs Bosons in the Weinberg-Salam Model", *Phys. Rev.* **D22** (1980) 1166.

[140] A. C. Longhitano, "Low-Energy Impact of a Heavy Higgs Boson Sector", *Nucl. Phys.* **B188** (1981) 118.

[141] JLQCD Collaboration, E. Shintani *et al.*, "S Parameter and Pseudo Nambu-Goldstone Boson Mass from Lattice QCD", *Phys. Rev. Lett.* **101** (2008) 242001, arXiv:0806.4222 [hep-lat].

[142] RBC and UKQCD Collaboration, P. A. Boyle *et al.*, "The S Parameter in QCD from Domain Wall Fermions", *Phys. Rev.* **D81** (2010) 014504, arXiv:0909.4931 [hep-lat].

[143] R. Contino, "The Higgs as a Composite Nambu-Goldstone Boson", arXiv:1005.4269 [hep-ph]. Lectures given at the Theoretical Advanced Study Institute in Elementary Particle Physics (TASI 2009): Physics of the Large and the Small, Boulder, Colorado, 1-29 Jun 2009.

[144] W. Skiba, "TASI Lectures on Effective Field Theory and Precision Electroweak Measurements", arXiv:1006.2142 [hep-ph]. Lectures given at the Theoretical Advanced Study Institute in Elementary Particle Physics (TASI 2009): Physics of the Large and the Small, Boulder, Colorado, 1-29 Jun 2009.

[145] R. Barbieri *et al.*, "Electroweak symmetry breaking after LEP-1 and LEP-2", *Nucl. Phys.* **B703** (2004) 127–146, arXiv:hep-ph/0405040.

[146] J. M. Maldacena, "The large N limit of superconformal field theories and supergravity", *Adv. Theor. Math. Phys.* **2** (1998) 231–252, arXiv:hep-th/9711200.

[147] S. S. Gubser, I. R. Klebanov, and A. M. Polyakov, "Gauge theory correlators from non-critical string theory", *Phys. Lett.* **B428** (1998) 105–114, arXiv:hep-th/9802109.

[148] E. Witten, "Anti-de Sitter space and holography", *Adv. Theor. Math. Phys.* **2** (1998) 253–291, arXiv:hep-th/9802150.

[149] M. Piai, "Lectures on walking technicolor, holography and gauge/gravity dualities", *Advances in High Energy Physics* **2010** (2010) 464302, arXiv:1004.0176 [hep-ph].

[150] N. Seiberg, "Electric-magnetic duality in supersymmetric non-Abelian gauge theories", *Nucl. Phys.* **B435** (1995) 129–146, arXiv:hep-th/9411149 [hep-th].

[151] K. A. Intriligator and N. Seiberg, "Lectures on supersymmetric gauge theories and electric–magnetic duality", *Nucl. Phys. Proc. Suppl.* **45BC** (1996) 1–28, arXiv:hep-th/9509066.

[152] C. Csaki *et al.*, "Towards a realistic model of Higgsless electroweak symmetry breaking", *Phys. Rev. Lett.* **92** (2004) 101802, arXiv:hep-ph/0308038 [hep-ph].

[153] J. Hirn and V. Sanz, "A Negative S parameter from holographic technicolor", *Phys. Rev. Lett.* **97** (2006) 121803, arXiv:hep-ph/0606086 [hep-ph].

[154] K. Agashe *et al.*, "The S-parameter in holographic technicolor models", *JHEP* **0712** (2007) 003, arXiv:0704.1821 [hep-ph].

[155] F. Sannino, "Magnetic S-parameter", *Phys. Rev. Lett.* **105** (2010) 232002, arXiv:1007.0254 [hep-ph].

[156] H. Fukushima, R. Kitano, and M. Yamaguchi, "SuperTopcolor", *JHEP* **1101** (2011) 111, arXiv:1012.5394 [hep-ph].

[157] M. A. Luty, "Strong Conformal Dynamics at the LHC and on the Lattice", *JHEP* **0904** (2009) 050, arXiv:0806.1235 [hep-ph].

[158] T. Appelquist *et al.*, "The Breaking of Isospin Symmetry in Theories with a Dynamical Higgs Mechanism", *Phys. Rev.* **D31** (1985) 1676.

[159] R. Chivukula, B. A. Dobrescu, and J. Terning, "Isospin breaking and fine tuning in topcolor assisted technicolor", *Phys. Lett.* **B353** (1995) 289–294, arXiv:hep-ph/9503203 [hep-ph].

[160] B. Holdom, "Raising the Sideways Scale", *Phys. Rev.* **D24** (1981) 1441.

[161] B. Holdom, "Techniodor", *Phys. Lett.* **B150** (1985) 301.

[162] T. Akiba and T. Yanagida, "Hierarchic Chiral Condensate", *Phys. Lett.* **B169** (1986) 432.

[163] K. Yamawaki, M. Bando, and K.-i. Matumoto, "Scale Invariant Technicolor Model and a Technidilaton", *Phys. Rev. Lett.* **56** (1986) 1335.

[164] T. W. Appelquist, D. Karabali, and L. Wijewardhana, "Chiral Hierarchies and the Flavor Changing Neutral Current Problem in Technicolor", *Phys. Rev. Lett.* **57** (1986) 957.

[165] T. Appelquist and L. Wijewardhana, "Chiral Hierarchies from Slowly Running Couplings in Technicolor Theories", *Phys. Rev.* **D36** (1987) 568.

[166] K. Lane, "The Importance of Walking",. Talk given at the second workshop on Lattice Gauge Theory for LHC Physics, Boston University, 6–7 November 2009.

[167] K. D. Lane, "Technihadron production and decay in low scale technicolor", *Phys. Rev.* **D60** (1999) 075007, arXiv:hep-ph/9903369 [hep-ph].

[168] K. Lane and S. Mrenna, "The Collider phenomenology of technihadrons in the technicolor straw man model", *Phys. Rev.* **D67** (2003) 115011, arXiv:hep-ph/0210299 [hep-ph].

[169] E. Eichten and K. Lane, "Low-scale technicolor at the Tevatron and LHC", *Phys. Lett.* **B669** (2008) 235–238, arXiv:0706.2339 [hep-ph].

[170] T. Appelquist and F. Sannino, "The physical spectrum of conformal SU(N) gauge theories", *Phys.Rev.* **D59** (1999) 067702, arXiv:hep-ph/9806409 [hep-ph].

[171] M. Harada, M. Kurachi, and K. Yamawaki, "The pi+ - pi0 mass difference and the S parameter in large N(f) QCD", *Prog. Theor. Phys.* **115** (2006) 765–795, arXiv:hep-ph/0509193 [hep-ph].

[172] M. Kurachi and R. Shrock, "Behavior of the S Parameter in the Crossover Region Between Walking and QCD-Like Regimes of an SU(N) Gauge Theory", *Phys. Rev.* **D74** (2006) 056003, arXiv:hep-ph/0607231 [hep-ph].

[173] M. Kurachi and R. Shrock, "Study of the Change from Walking to Non-Walking Behavior in a Vectorial Gauge Theory as a Function of N(f)", *JHEP* **0612** (2006) 034, arXiv:hep-ph/0605290 [hep-ph].

[174] S. R. Coleman and E. J. Weinberg, "Radiative Corrections as the Origin of Spontaneous Symmetry Breaking", *Phys. Rev.* **D7** (1973) 1888–1910.

[175] K. D. Lane and M. Ramana, "Walking technicolor signatures at hadron colliders", *Phys. Rev.* **D44** (1991) 2678–2700.

[176] T. Appelquist, J. Terning, and L. C. R. Wijewardhana, "Postmodern technicolor", *Phys. Rev. Lett.* **79** (1997) 2767–2770, arXiv:hep-ph/9706238.

[177] K. Higashijima, "Dynamical Chiral Symmetry Breaking", *Phys. Rev.* **D29** (1984) 1228.

[178] E. T. Neil, "Technicolor for Lattice Gauge Theorists",. Lectures presented at the Les Houches summer school on *Modern Perspectives in Lattice QCD: Quantum Field Theory and High Performance Computing*, to be published in [201].

[179] T. Appelquist, A. G. Cohen, and M. Schmaltz, "A New constraint on strongly coupled gauge theories", *Phys.Rev.* **D60** (1999) 045003, arXiv:hep-th/9901109 [hep-th].

[180] G. Mack, "All Unitary Ray Representations of the Conformal Group SU(2,2) with Positive Energy", *Commun. Math. Phys.* **55** (1977) 1.

[181] T. Appelquist *et al.*, "Higher Mass Scales and Mass Hierarchies", *Phys. Lett.* **B220** (1989) 223.

[182] T. Takeuchi, "Analytical and Numerical Study of the Schwinger-Dyson Equation with Four Fermion Coupling", *Phys. Rev.* **D40** (1989) 2697.

[183] V. Miransky and K. Yamawaki, "On Gauge Theories with Additional Four Fermion Interaction", *Mod. Phys. Lett.* **A4** (1989) 129–135.

[184] Y. Nambu and G. Jona-Lasinio, "Dynamical model of elementary particles based on an analogy with superconductivity. I", *Phys. Rev.* **122** (1961) 345–358.

[185] Y. Nambu and G. Jona-Lasinio, "Dynamical model of elementary particles based on an analogy with superconductivity. II", *Phys. Rev.* **124** (1961) 246–254.

[186] M. A. Luty and T. Okui, "Conformal technicolor", *JHEP* **0609** (2006) 070, arXiv:hep-ph/0409274 [hep-ph].

[187] J. Galloway *et al.*, "Minimal Conformal Technicolor and Precision Electroweak Tests", *JHEP* **1010** (2010) 086, arXiv:1001.1361 [hep-ph].

[188] J. A. Evans *et al.*, "Flavor in Minimal Conformal Technicolor", arXiv:1012.4808 [hep-ph].

[189] R. Rattazzi *et al.*, "Bounding scalar operator dimensions in 4D CFT", *JHEP* **0812** (2008) 031, arXiv:0807.0004 [hep-th].

[190] V. S. Rychkov and A. Vichi, "Universal Constraints on Conformal Operator Dimensions", *Phys. Rev.* **D80** (2009) 045006, arXiv:0905.2211 [hep-th].

[191] D. Poland and D. Simmons-Duffin, "Bounds on 4D Conformal and Superconformal Field Theories", arXiv:1009.2087 [hep-th].

[192] R. Rattazzi, S. Rychkov, and A. Vichi, "Bounds in 4D Conformal Field Theories with Global Symmetry", *J. Phys.* **A44** (2011) 035402, arXiv:1009.5985 [hep-th].

[193] R. Rattazzi, S. Rychkov, and A. Vichi, "Central Charge Bounds in 4D Conformal Field Theory", arXiv:1009.2725 [hep-th].

[194] C. T. Hill, "Topcolor assisted technicolor", *Phys. Lett.* **B345** (1995) 483–489, arXiv:hep-ph/9411426 [hep-ph].

[195] C. Csaki, Y. Shirman, and J. Terning, "Electroweak Symmetry Breaking From Monopole Condensation", *Phys. Rev. Lett.* **106** (2011) 041802, arXiv:1003.1718 [hep-ph].

[196] I. Montvay and G. Munster, *Quantum fields on a Lattice*. Cambridge Monographs on Mathematical Physics. Cambridge University Press, Cambridge, UK, 1994.

[197] R. Gupta, "Introduction to lattice QCD", *Les Houches lecture notes* **68: Probing the Standard Model of Particle Interactions** (1997) 83–219, arXiv:hep-lat/9807028.

[198] M. Luscher, "Advanced lattice QCD", *Les Houches lecture notes* **68: Probing the Standard Model of Particle Interactions** (1997) 229–280, arXiv:hep-lat/9802029.

[199] J. Smit, *Introduction to quantum fields on a lattice: A robust mate*, vol. 15 of *Cambridge Lecture Notes in Physics*. Cambridge University Press, Cambridge, UK, 2002.

[200] C. Gattringer and C. B. Lang, *Quantum Chromodynamics on the Lattice*, vol. 788. Springer, Berlin Heidelberg, 2010.

[201] L. Lellouch *et al.*, eds., *Modern perspectives in lattice QCD: Quantum field theory and high performance computing*, vol. 93 of *Les Houches lecture notes*. North-Holland, Amsterdam, 2011. Forthcoming.

[202] S. Aoki, "Lattice QCD and Nuclear Physics", arXiv:1008.4427 [hep-lat].

[203] M. Luscher, "Computational Strategies in Lattice QCD", arXiv:1002.4232 [hep-lat].

[204] O. Philipsen, "Lattice QCD at non-zero temperature and baryon density", arXiv:1009.4089 [hep-lat].

[205] R. Sommer, "Introduction to Non-perturbative Heavy Quark Effective Theory", arXiv:1008.0710 [hep-lat].

[206] P. Weisz, "Renormalization and lattice artifacts", arXiv:1004.3462 [hep-lat].

[207] A. Vladikas, "Three Topics in Renormalization and Improvement", arXiv:1103.1323 [hep-lat].

[208] M. Luscher, "Construction of a Selfadjoint, Strictly Positive Transfer Matrix for Euclidean Lattice Gauge Theories", *Commun. Math. Phys.* **54** (1977) 283.

[209] K. G. Wilson, "Confinement of Quarks", *Phys. Rev.* **D10** (1974) 2445–2459.

[210] M. Luscher and P. Weisz, "On-Shell Improved Lattice Gauge Theories", *Commun. Math. Phys.* **97** (1985) 59.

[211] Y. Iwasaki and T. Yoshie, "Renormalization Group Improved Action for SU(3) Lattice Gauge Theory and the String Tension", *Phys. Lett.* **B143** (1984) 449.

[212] Y. Iwasaki, "Renormalization Group Analysis of Lattice Theories and Improved Lattice Action: Two-Dimensional Nonlinear O(N) Sigma Model", *Nucl. Phys.* **B258** (1985) 141–156.

[213] T. Takaishi, "Heavy quark potential and effective actions on blocked configurations", *Phys. Rev.* **D54** (1996) 1050–1053.

[214] QCD-TARO Collaboration, P. de Forcrand *et al.*, "Renormalization group flow of SU(3) lattice gauge theory: Numerical studies in a two coupling space", *Nucl. Phys.* **B577** (2000) 263–278, arXiv:hep-lat/9911033 [hep-lat].

[215] K. Symanzik, "Continuum Limit and Improved Action in Lattice Theories. 1. Principles and phi**4 Theory", *Nucl. Phys.* **B226** (1983) 187.

[216] K. Symanzik, "Continuum Limit and Improved Action in Lattice Theories. 2. O(N) Nonlinear Sigma Model in Perturbation Theory", *Nucl. Phys.* **B226** (1983) 205.

[217] S. D. Drell, M. Weinstein, and S. Yankielowicz, "Variational Approach to Strong Coupling Field Theory. 1. Phi**4 Theory", *Phys. Rev.* **D14** (1976) 487.

[218] S. D. Drell, M. Weinstein, and S. Yankielowicz, "Strong Coupling Field Theories. 2. Fermions and Gauge Fields on a Lattice", *Phys. Rev.* **D14** (1976) 1627.

[219] L. H. Karsten and J. Smit, "Lattice Fermions: Species Doubling, Chiral Invariance, and the Triangle Anomaly", *Nucl. Phys.* **B183** (1981) 103.

[220] J. B. Kogut and L. Susskind, "Hamiltonian Formulation of Wilson's Lattice Gauge Theories", *Phys. Rev.* **D11** (1975) 395.

[221] L. Susskind, "Lattice Fermions", *Phys. Rev.* **D16** (1977) 3031–3039.

[222] H. Sharatchandra, H. Thun, and P. Weisz, "Susskind Fermions on a Euclidean Lattice", *Nucl. Phys.* **B192** (1981) 205.

[223] M. Luscher, "Exact chiral symmetry on the lattice and the Ginsparg–Wilson relation", *Phys. Lett.* **B428** (1998) 342–345, arXiv:hep-lat/9802011 [hep-lat].

[224] R. Narayanan and H. Neuberger, "Chiral determinant as an overlap of two vacua", *Nucl. Phys.* **B412** (1994) 574–606, arXiv:hep-lat/9307006.

[225] R. Narayanan and H. Neuberger, "A Construction of lattice chiral gauge theories", *Nucl. Phys.* **B443** (1995) 305–385, arXiv:hep-th/9411108 [hep-th].

[226] H. Neuberger, "Vector - like gauge theories with almost massless fermions on the lattice", *Phys. Rev.* **D57** (1998) 5417–5433, arXiv:hep-lat/9710089 [hep-lat].

[227] H. Neuberger, "Exactly massless quarks on the lattice", *Phys. Lett.* **B417** (1998) 141–144, arXiv:hep-lat/9707022.

[228] H. Neuberger, "More about exactly massless quarks on the lattice", *Phys. Lett.* **B427** (1998) 353–355, arXiv:hep-lat/9801031.

[229] M. Clark and A. Kennedy, "The RHMC algorithm for two flavors of dynamical staggered fermions", *Nucl. Phys. Proc. Suppl.* **129** (2004) 850–852, arXiv:hep-lat/0309084 [hep-lat].

[230] M. Clark and A. Kennedy, "Accelerating dynamical fermion computations using the rational hybrid Monte Carlo (RHMC) algorithm with multiple pseudofermion fields", *Phys. Rev. Lett.* **98** (2007) 051601, arXiv:hep-lat/0608015 [hep-lat].

[231] M. R. Hestenes and E. Stiefel, "Methods of conjugate gradients for solving linear systems", *Journal of Research of the National Bureau of Standards* **49** (1952) 409–436.

[232] S. A. Gottlieb *et al.*, "Hybrid Molecular Dynamics Algorithms for the Numerical Simulation of Quantum Chromodynamics", *Phys. Rev.* **D35** (1987) 2531–2542.

[233] S. Duane *et al.*, "Hybrid Monte Carlo", *Phys. Lett.* **B195** (1987) 216–222.

[234] A. D. Kennedy, "Algorithms for dynamical fermions", arXiv:hep-lat/0607038.

[235] I. P. Omelyan, I. M. Mryglod, and R. Folk, "Symplectic analytically integrable decomposition algorithms: classification, derivation, and application to molecular dynamics, quantum and celestial mechanics simulations", *Computer Physics Communications* **151** (2003) 272–314.

[236] T. Takaishi and P. de Forcrand, "Testing and tuning new symplectic integrators for hybrid Monte Carlo algorithm in lattice QCD", *Phys. Rev.* **E73** (2006) 036706, arXiv:hep-lat/0505020 [hep-lat].

[237] N. Metropolis *et al.*, "Equation of state calculations by fast computing machines", *Journal of Chemical Physics* **21** (1953) 1087–1092.

[238] J. E. Gubernatis, "Marshall Rosenbluth and the Metropolis algorithm", *Physics of Plasmas* **12** (2005) 057303.

[239] S.-J. Dong and K.-F. Liu, "Stochastic estimation with Z(2) noise", *Phys. Lett.* **B328** (1994) 130–136, arXiv:hep-lat/9308015 [hep-lat].

[240] B. Efron, *The Jackknife, the Bootstrap and Other Resampling Plans*. Conference Board of the Mathematical Sciences and National Science Foundation Regional Conference Series in Applied Mathematics. SIAM, Philadelphia, Pennsylvania, 1982. Lectures given at Bowling Green State University, June 1980.

[241] ALPHA Collaboration Collaboration, S. Schaefer, R. Sommer, and F. Virotta, "Critical slowing down and error analysis in lattice QCD simulations", *Nucl. Phys.* **B845** (2011) 93–119, arXiv:1009.5228 [hep-lat].

[242] R. Brower *et al.*, "QCD at fixed topology", *Phys. Lett.* **B560** (2003) 64–74, arXiv:hep-lat/0302005 [hep-lat].

[243] RBC and UKQCD Collaboration, N. Christ and C. Jung, "Computational requirements of the rational hybrid Monte Carlo algorithm", *PoS* **LAT2007** (2007) 028.

[244] S. Schaefer, "Algorithms for lattice QCD: progress and challenges", arXiv:1011.5641 [hep-ph].

[245] M. Luscher, "Volume Dependence of the Energy Spectrum in Massive Quantum Field Theories. 1. Stable Particle States", *Commun. Math. Phys.* **104** (1986) 177.

[246] J. Gasser and H. Leutwyler, "Chiral Perturbation Theory: Expansions in the Mass of the Strange Quark", *Nucl. Phys.* **B250** (1985) 465.

[247] RBC and UKQCD Collaboration, C. Allton *et al.*, "Physical Results from 2+1 Flavor Domain Wall QCD and SU(2) Chiral Perturbation Theory", *Phys. Rev.* **D78** (2008) 114509, arXiv:0804.0473 [hep-lat].

[248] Y. Kikukawa and T. Noguchi, "Low-energy effective action of domain wall fermion and the Ginsparg-Wilson relation", arXiv:hep-lat/9902022 [hep-lat].

[249] R. G. Edwards and U. M. Heller, "Domain wall fermions with exact chiral symmetry", *Phys. Rev.* **D63** (2001) 094505, arXiv:hep-lat/0005002 [hep-lat].

[250] Y. Aoki *et al.*, "Domain wall fermions with improved gauge actions", *Phys. Rev.* **D69** (2004) 074504, arXiv:hep-lat/0211023 [hep-lat].

[251] Y. Aoki *et al.*, "Lattice QCD with two dynamical flavors of domain wall fermions", *Phys. Rev.* **D72** (2005) 114505, arXiv:hep-lat/0411006.

[252] RBC and UKQCD Collaboration, D. J. Antonio *et al.*, "First results from 2+1-flavor domain wall QCD: Mass spectrum, topology change and chiral symmetry with L(s) = 8", *Phys. Rev.* **D75** (2007) 114501, arXiv:hep-lat/0612005.

[253] RBC and UKQCD Collaboration, C. Allton *et al.*, "2+1 flavor domain wall QCD on a $(2\ \mathrm{fm})^3$ lattice: light meson spectroscopy with Ls = 16", *Phys. Rev.* **D76** (2007) 014504, arXiv:hep-lat/0701013.

[254] RBC and UKQCD Collaboration, D. J. Antonio *et al.*, "Localization and chiral symmetry in 3 flavor domain wall QCD", *Phys. Rev.* **D77** (2008) 014509, arXiv:0705.2340 [hep-lat].

[255] M. Golterman and Y. Shamir, "Localization in lattice QCD", *Phys. Rev.* **D68** (2003) 074501, arXiv:hep-lat/0306002 [hep-lat].

[256] J. C. Ward, "An Identity in Quantum Electrodynamics", *Phys. Rev.* **78** (1950) 182.

[257] Y. Takahashi, "On the generalized Ward identity", *Nuovo Cim.* **6** (1957) 371.

[258] S. R. Sharpe, "Future of Chiral Extrapolations with Domain Wall Fermions", arXiv:0706.0218 [hep-lat].

[259] J. B. Kogut *et al.*, "Simulations and Speculations on Gauge Theories with Many Fermions", *Phys. Rev. Lett.* **54** (1985) 1475.

[260] R. Gavai, "Simulations of Gauge Theories with Many Fermions Using the Pseudofermion Method", *Nucl. Phys.* **B269** (1986) 530.

[261] N. Attig, B. Petersson, and M. Wolff, "The Nature of the Phase Transition in Lattice QCD with Many Flavors", *Phys. Lett.* **B190** (1987) 143.

[262] J. Kogut and D. Sinclair, "SU(2) and SU(3) Lattice Gauge Theories with Many Fermions", *Nucl. Phys.* **B295** (1988) 465.

[263] S. Meyer and B. Pendleton, "First order phase transitions in SU(2) gauge theories with many flavors of staggered fermions", *Phys. Lett.* **B241** (1990) 397–402.

[264] S.-y. Kim and S. Ohta, "QCD thermodynamics with eight staggered quark flavors on a $16^3 \times 6$ lattice", *Phys. Rev.* **D46** (1992) 3607–3617.

[265] F. R. Brown *et al.*, "Lattice QCD with eight light quark flavors", *Phys. Rev.* **D46** (1992) 5655–5670, arXiv:hep-lat/9206001 [hep-lat].

[266] P. H. Damgaard *et al.*, "On lattice QCD with many flavors", *Phys. Lett.* **B400** (1997) 169–175, arXiv:hep-lat/9701008.

[267] U. M. Heller, "The Schroedinger functional running coupling with staggered fermions and its application to many flavor QCD", *Nucl. Phys. Proc. Suppl.* **63** (1998) 248–250, arXiv:hep-lat/9709159.

[268] Y. Iwasaki *et al.*, "Phase structure of lattice QCD for general number of flavors", *Phys. Rev.* **D69** (2004) 014507, arXiv:hep-lat/0309159 [hep-lat].

[269] S. Catterall and F. Sannino, "Minimal walking on the lattice", *Phys. Rev.* **D76** (2007) 034504, arXiv:0705.1664 [hep-lat].

[270] T. Appelquist, G. T. Fleming, and E. T. Neil, "Lattice Study of the Conformal Window in QCD-like Theories", *Phys. Rev. Lett.* **100** (2008) 171607, arXiv:0712.0609 [hep-ph].

[271] F. Sannino, "Mass Deformed Exact S-parameter in Conformal Theories", *Phys. Rev.* **D82** (2010) 081701, arXiv:1006.0207 [hep-lat].

[272] S. Di Chiara, C. Pica, and F. Sannino, "Exact Flavor Dependence of the S-parameter", arXiv:1008.1267 [hep-ph].

[273] L. Del Debbio and R. Zwicky, "Scaling relations for the entire spectrum in mass-deformed conformal gauge theories", arXiv:1009.2894 [hep-ph].

[274] R. S. Chivukula and E. H. Simmons, "Technicolor and Lattice Gauge Theory", *PoS* **LATTICE2010** (2010) 003, arXiv:1011.2535 [hep-lat].

[275] S. Catterall *et al.*, "Probes of nearly conformal behavior in lattice simulations of minimal walking technicolor", arXiv:0910.4387 [hep-lat].

[276] A. J. Hietanen, K. Rummukainen, and K. Tuominen, "Evolution of the coupling constant in SU(2) lattice gauge theory with two adjoint fermions", *Phys. Rev.* **D80** (2009) 094504, arXiv:0904.0864 [hep-lat].

[277] F. Bursa *et al.*, "Mass anomalous dimension in SU(2) with two adjoint fermions", arXiv:0910.4535 [hep-ph].

[278] L. Del Debbio *et al.*, "Mesonic spectroscopy of Minimal Walking Technicolor", *Phys. Rev.* **D82** (2010) 014509, arXiv:1004.3197 [hep-lat].

[279] L. Del Debbio *et al.*, "The infrared dynamics of Minimal Walking Technicolor", *Phys. Rev.* **D82** (2010) 014510, arXiv:1004.3206 [hep-lat].

[280] S. Catterall *et al.*, "MCRG Minimal Walking Technicolor", *PoS* **LATTICE2010** (2010) 057, arXiv:1010.5909 [hep-ph].

[281] T. DeGrand, Y. Shamir, and B. Svetitsky, "Infrared fixed point in SU(2) gauge theory with adjoint fermions", arXiv:1102.2843 [hep-lat].

[282] S. Catterall *et al.*, "Phase diagram of SU(2) with 2 flavors of dynamical adjoint quarks", *JHEP* **0811** (2008) 009, arXiv:0807.0792 [hep-lat].

[283] L. Del Debbio, A. Patella, and C. Pica, "Fermions in higher representations. Some results about SU(2) with adjoint fermions", *PoS* **LATTICE2008** (2008) 064, arXiv:0812.0570 [hep-lat].

[284] A. J. Hietanen *et al.*, "Spectrum of SU(2) lattice gauge theory with two adjoint Dirac flavours", *JHEP* **0905** (2009) 025, arXiv:0812.1467 [hep-lat].

[285] L. Del Debbio *et al.*, "Conformal versus confining scenario in SU(2) with adjoint fermions", *Phys. Rev.* **D80** (2009) 074507, arXiv:0907.3896 [hep-lat].

[286] F. Bursa *et al.*, "Improved Lattice Spectroscopy of Minimal Walking Technicolor", arXiv:1104.4301 [hep-lat].

[287] S. Muroya, A. Nakamura, and C. Nonaka, "Behavior of hadrons at finite density: Lattice study of color SU(2) QCD", *Phys. Lett.* **B551** (2003) 305–310, arXiv:hep-lat/0211010 [hep-lat].

[288] S. Hands, S. Kim, and J.-I. Skullerud, "Quarkyonic phase in dense two color matter", *Phys. Rev.* **D81** (2010) 091502, arXiv:1001.1682 [hep-lat].

[289] S. Hands *et al.*, "Lattice Study of Dense Matter with Two Colors and Four Flavors", arXiv:1101.4961 [hep-lat].

[290] F. Bursa *et al.*, "Mass anomalous dimension in SU(2) with six fundamental fermions", *Phys. Lett.* **B696** (2011) 374–379, arXiv:1007.3067 [hep-ph].

[291] H. Ohki *et al.*, "Study of the scaling properties in SU(2) gauge theory with eight flavors", *PoS* **LATTICE2010** (2010) 066, arXiv:1011.0373 [hep-lat].

[292] C.-Z. Sui, "Flavor dependence of quantum chromodynamics",. PhD thesis, UMI-99-98219.

[293] A. Hasenfratz, "Investigating the critical properties of beyond-QCD theories using Monte Carlo Renormalization Group matching", *Phys. Rev.* **D80** (2009) 034505, arXiv:0907.0919 [hep-lat].

[294] Z. Fodor *et al.*, "Chiral symmetry breaking in nearly conformal gauge theories", *PoS* **LAT2009** (2009) 055, arXiv:0911.2463 [hep-lat].

[295] T. Appelquist, G. T. Fleming, and E. T. Neil, "Lattice Study of Conformal Behavior in SU(3) Yang-Mills Theories", *Phys. Rev.* **D79** (2009) 076010, arXiv:0901.3766 [hep-ph].

[296] A. Deuzeman, M. P. Lombardo, and E. Pallante, "The Physics of eight flavours", *Phys. Lett.* **B670** (2008) 41–48, arXiv:0804.2905 [hep-lat].

[297] X.-Y. Jin and R. D. Mawhinney, "Evidence for a First Order, Finite Temperature Phase Transition in 8 Flavor QCD", *PoS* **LATTICE2010** (2010) 055, arXiv:1011.1511 [hep-lat].

[298] A. Hasenfratz, "Conformal or Walking? Monte Carlo renormalization group studies of SU(3) gauge models with fundamental fermions", *Phys. Rev.* **D82** (2010) 014506, arXiv:1004.1004 [hep-lat].

[299] M. Hayakawa *et al.*, "Running coupling constant of ten-flavor QCD with the Schrödinger functional method", arXiv:1011.2577 [hep-lat].

[300] Z. Fodor *et al.*, "Chiral symmetry breaking in fundamental and sextet fermion representations of SU(3) color", *PoS* **Lattice 2010** (2010) 060, arXiv:1103.5998 [hep-lat].

[301] Z. Fodor *et al.*, "Twelve massless flavors and three colors below the conformal window", arXiv:1104.3124 [hep-lat].

[302] A. Deuzeman, M. P. Lombardo, and E. Pallante, "Evidence for a conformal phase in SU(N) gauge theories", *Phys. Rev.* **D82** (2010) 074503, arXiv:0904.4662 [hep-ph].

[303] E. Itou *et al.*, "Search for the IR fixed point in the Twisted Polyakov Loop scheme (II)", *PoS* **LATTICE2010** (2010) 054, arXiv:1011.0516 [hep-lat].

[304] Z. Fodor *et al.*, "Calculating the running coupling in strong electroweak models", *PoS* **LAT2009** (2009) 058, arXiv:0911.2934 [hep-lat].

[305] J. Kogut and D. Sinclair, "Thermodynamics of lattice QCD with 2 flavours of colour-sextet quarks: A model of walking/conformal Technicolor", *Phys. Rev.* **D81** (2010) 114507, arXiv:1002.2988 [hep-lat].

[306] D. Sinclair and J. Kogut, "New results with colour-sextet quarks", *PoS* **LATTICE2010** (2010) 071, arXiv:1008.2468 [hep-lat].

[307] Y. Shamir, B. Svetitsky, and T. DeGrand, "Zero of the discrete beta function in SU(3) lattice gauge theory with color sextet fermions", *Phys. Rev.* **D78** (2008) 031502, arXiv:0803.1707 [hep-lat].

[308] T. DeGrand, Y. Shamir, and B. Svetitsky, "Phase structure of SU(3) gauge theory with two flavors of symmetric-representation fermions", *Phys. Rev.* **D79** (2009) 034501, arXiv:0812.1427 [hep-lat].

[309] T. DeGrand, Y. Shamir, and B. Svetitsky, "Running coupling and mass anomalous dimension of SU(3) gauge theory with two flavors of symmetric-representation fermions", *Phys. Rev.* **D82** (2010) 054503, arXiv:1006.0707 [hep-lat].

[310] M. Luscher *et al.*, "The Schrödinger functional – a renormalizable probe for non-abelian gauge theories", *Nucl. Phys.* **B384** (1992) 168–228, arXiv:hep-lat/9207009 [hep-lat].

[311] S. Sint, "On the Schrödinger functional in QCD", *Nucl. Phys.* **B421** (1994) 135–158, arXiv:hep-lat/9312079 [hep-lat].

[312] ALPHA Collaboration, A. Bode *et al.*, "First results on the running coupling in QCD with two massless flavors", *Phys. Lett.* **B515** (2001) 49–56, arXiv:hep-lat/0105003 [hep-lat].

[313] M. Creutz, "Asymptotic Freedom Scales", *Phys. Rev. Lett.* **45** (1980) 313.

[314] E. Bilgici *et al.*, "A New scheme for the running coupling constant in gauge theories using Wilson loops", *Phys. Rev.* **D80** (2009) 034507, arXiv:0902.3768 [hep-lat].

[315] A. Hasenfratz *et al.*, "Improved Monte Carlo Renormalization Group Methods", *Phys. Lett.* **B140** (1984) 76.

[316] A. Hasenfratz *et al.*, "The Beta Function of the SU(3) Wilson Action", *Phys. Lett.* **B143** (1984) 193.

[317] K. C. Bowler *et al.*, "Monte Carlo Renormalization Group Studies of SU(3) Lattice Gauge Theory", *Nucl. Phys.* **B257** (1985) 155–172.

[318] T. DeGrand and A. Hasenfratz, "Remarks on lattice gauge theories with infrared-attractive fixed points", *Phys. Rev.* **D80** (2009) 034506, arXiv:0906.1976 [hep-lat].

[319] T. DeGrand, "Finite-size scaling tests for SU(3) lattice gauge theory with color sextet fermions", *Phys. Rev.* **D80** (2009) 114507, arXiv:0910.3072 [hep-lat].

[320] L. Del Debbio and R. Zwicky, "Hyperscaling relations in mass-deformed conformal gauge theories", *Phys. Rev.* **D82** (2010) 014502, arXiv:1005.2371 [hep-ph].

[321] J. Sexton and D. Weingarten, "Hamiltonian evolution for the hybrid Monte Carlo algorithm", *Nucl. Phys.* **B380** (1992) 665–678.

[322] M. Hasenbusch, "Speeding up the hybrid Monte Carlo algorithm for dynamical fermions", *Phys. Lett.* **B519** (2001) 177–182, arXiv:hep-lat/0107019 [hep-lat].

[323] R. Sommer, "A New way to set the energy scale in lattice gauge theories and its applications to the static force and alpha-s in SU(2) Yang-Mills theory", *Nucl. Phys.* **B411** (1994) 839–854, arXiv:hep-lat/9310022 [hep-lat].

[324] M. Gell-Mann, R. J. Oakes, and B. Renner, "Behavior of current divergences under SU(3) x SU(3)", *Phys. Rev.* **175** (1968) 2195–2199.

[325] J. Bijnens and J. Lu, "Technicolor and other QCD-like theories at next-to-next-to-leading order", *JHEP* **0911** (2009) 116, arXiv:0910.5424 [hep-ph].

[326] S. Weinberg, "Precise relations between the spectra of vector and axial vector mesons", *Phys. Rev. Lett.* **18** (1967) 507–509.

[327] T. Das, V. Mathur, and S. Okubo, "Low-energy theorem in the radiative decays of charged pions", *Phys. Rev. Lett.* **19** (1967) 859–861.

[328] M. A. Shifman, A. Vainshtein, and V. I. Zakharov, "QCD and Resonance Physics. Sum Rules", *Nucl. Phys.* **B147** (1979) 385–447.

[329] M. A. Shifman, A. Vainshtein, and V. I. Zakharov, "QCD and Resonance Physics: Applications", *Nucl. Phys.* **B147** (1979) 448–518.

[330] G. Ecker, "Chiral low-energy constants", *Acta Physica Polonica* **B38** (2007) 2753–2762, arXiv:hep-ph/0702263 [hep-ph].

[331] JLQCD Collaboration, TWQCD Collaboration Collaboration, E. Shintani *et al.*, "Lattice study of the vacuum polarization function and determination of the strong coupling constant", *Phys. Rev.* **D79** (2009) 074510, arXiv:0807.0556 [hep-lat].

[332] C. T. Sachrajda and G. Villadoro, "Twisted boundary conditions in lattice simulations", *Phys. Lett.* **B609** (2005) 73–85, arXiv:hep-lat/0411033.

[333] J. M. Flynn, A. Juttner, and C. T. Sachrajda, "A numerical study of partially twisted boundary conditions", *Phys. Lett.* **B632** (2006) 313–318, arXiv:hep-lat/0506016.

[334] MILC collaboration Collaboration, A. Bazavov *et al.*, "Scaling studies of QCD with the dynamical HISQ action", *Phys. Rev.* **D82** (2010) 074501, arXiv:1004.0342 [hep-lat].

Curriculum Vitae

David Schaich

CONTACT INFORMATION

Physics Department and Center for Computational Science
Boston University
590 Commonwealth Ave.
Boston, MA 02215

617/353-6034 (office, preferred)
617/694-6276 (cell)
schaich@physics.bu.edu

EDUCATION

Boston University, Boston, MA
Ph.D., Physics, to be completed May 2011
Thesis: *Strong Dynamics and Lattice Gauge Theory*
Advisors: Claudio Rebbi and Rich Brower
Certificate in Computational Science, to be completed May 2011
M.A., Physics, May 2008

Amherst College, Amherst MA
B.A. *summa cum laude*, Physics, History, and Mathematics, May 2006
Thesis: *Lattice Simulations of Nonperturbative Quantum Field Theories*
Advisor: Will Loinaz

RESEARCH BACKGROUND

Lattice gauge theory and lattice QCD
Dynamical electroweak symmetry breaking and new strong dynamics
Quantum field theory and physics beyond the Standard Model
High-performance computing and computational physics

PROFESSIONAL EXPERIENCE

Boston University, Boston MA
Member of Center for Computational Science **since Sept. 2006**
Member of Particle Theory Group **since Sept. 2007**
NSF IGERT Fellow **May 2007–April 2009**
Dean's Fellow **September 2006–April 2007**
Researched lattice field theory and physics beyond the standard model
Member of the Lattice Strong Dynamics Collaboration
Helped organize two international workshops:
Lattice Gauge Theory for LHC Physics, 6–7 November 2009
Numerical Analysis for Lattice Gauge Theory, 8–10 September 2010
Graded Quantum Field Theory I–II under E. Katz (2008–09) and M. Schmaltz (2010–11)

Lawrence Livermore National Lab, Livermore CA
Visiting Researcher **January–February 2010**
Worked with members of the Lattice Strong Dynamics Collaboration on numerical studies of new strong dynamics, through Livermore's Academic Cooperation program.

CERN, Geneva, Switzerland
Summer Research Assistant **June–August 2005**
Developed and tested software to reconstruct the mass of the top quark from dilepton decay events at the Large Hadron Collider. Member of the ATLAS experiment.

Amherst College, Amherst MA
Physics Teaching Assistant **January 2003–May 2006**
Mathematics Teaching Assistant **September 2004–May 2006**
Assisted introductory and intermediate courses in physics, mathematics and statistics. Duties included grading homework or lab reports, and running review sessions.
Summer Astronomy Intern **May–July 2004**
Produced educational simulations of tidal interactions.

Hope College, Holland MI
Summer Research Assistant **May–July 2003**
Used cubic equations of state to calculate series solutions for fluid properties as direct functions of temperature.

Honors and Awards

National Science Foundation (NSF) EAPSI Fellowship, 2011
NSF IGERT Fellowship, 2007–2009
Boston University Physics Department Chair's Book Prize, 2008
("In recognition of excellence in achievement by a first year graduate student")
Boston University Dean's Fellowship, 2006–2007
Forris Jewett Moore Fellowship (Amherst College), 2006–2007
Sigma Xi (national scientific honor society), 2006
Phi Beta Kappa (national honor society), 2005
John Petropulos Prize in Historical Scholarship (Amherst College), 2005

Technical Skills

Programming: C/C++; Fortran; Java; Perl; Python; Bash/csh scripting
High-performance computing: IBM Blue Gene/L; Cray XT5; Sun Constellation; clusters
Visualization: VTK; ParaView
System administration: UNIX/Linux
Markup: TEX; LATEX; BIBTEX; HTML; PHP; SQL
Applications: Mathematica; Maple; Matlab; ROOT

PUBLICATIONS

Exploring strange nucleon form factors on the lattice
Ronald Babich *et al.*
Submitted to *Physical Review D* (2010) [arXiv:1012.0562]

Parity Doubling and the S Parameter Below the Conformal Window
Thomas Appelquist *et al.* (LSD Collaboration)
To appear in *Physical Review Letters* (2011) [arXiv:1009.5967]

Hybrid Monte Carlo Simulation of Graphene on the Hexagonal Lattice
R. C. Brower, C. Rebbi and D. Schaich
arXiv:1101.5131 (2011)

Toward TeV Conformality
Thomas Appelquist *et al.* (LSD Collaboration)
Physical Review Letters **104**:071601 (2010) [arXiv:0910.2224]

Improved lattice measurement of the critical coupling in ϕ_2^4 theory
David Schaich and Will Loinaz
Physical Review **D79**:056008 (2009), [arXiv:0902.0045].

PROCEEDINGS

Lattice study of ChPT beyond QCD
Ethan T. Neil *et al.* (LSD Collaboration)
Proceedings of Science **CD09**:088 (2009) [arXiv:1002.3777]

Möbius Algorithm for Domain Wall and GapDW Fermions
Richard Brower, Ron Babich, Kostas Orginos, Claudio Rebbi, David Schaich and Pavlos Vranas
Proceedings of Science **LATTICE 2008**:034 (2008) [arXiv:0906.2813]

TALKS PRESENTED

Measuring the S Parameter on the Lattice
Boston University, 12 May 2011

Lattice QCD – and Beyond
Boston University Center for Computational Science Seminar, 29 April 2011

Monte Carlo Renormalization Group
MIT Lattice Club, 30 March 2011

Exploring the Origin of Mass with High-Performance Computing
Boston University, 10 December 2010

Lattice Strong Dynamics for Electroweak Symmetry Breaking
MIT Lattice Club, 20 October 2010

Flavor dependence of the S parameter in SU(3) gauge theory (for the LSD Collaboration)
XXVIII International Symposium on Lattice Field Theory, Villasimius, Italy, 17 June 2010

Exploring Electroweak Symmetry Breaking on the Lattice
Boston University, 13 October 2009

Electroweak Symmetry Breaking: An enduring mystery of the standard model of particle physics, and how we hope to solve it
Amherst College Colloquium, 1 October 2009

Technicolor at the LHC
Boston University LHC Physics Symposium, 30 April 2009

Lattice Simulations of Nonperturbative Quantum Field Theories
Amherst College, 2 May 2006

Life on the Lattice: Markov Chain Monte Carlo and all that
Amherst College, 29 November 2005

Top Quark Physics at the LHC
Five-College Physics Symposium, University of Massachusetts, 1 October 2005

Posters Presented

Lattice Strong Dynamics: Using high-performance computing to explore the mystery of mass
National Science Foundation IGERT Project Meeting, Washington DC, 24-25 May 2010

Lattice Strong Dynamics: Using high-performance computing to explore electroweak symmetry breaking
Boston University Science and Engineering Research Symposium, 30 March 2010

Interdisciplinary Cluster Computing at a Liberal Arts College
AAPT Topical Conference on Computational Physics for Upper Level Courses, Davidson College, 27-28 July 2007

Physical Property Modeling from Equations of State
NSF REU Symposium, Hope College, 25 July 2003

Summer Schools Attended

Les Houches Summer School in Lattice Gauge Theory, Les Houches, France, 3–28 August 2009

CTEQ Summer School on QCD Analysis and Phenomenology, Madison WI, 30 May–7 June 2007

CERN Summer Students Lecture Programme, Geneva, Switzerland, 6 July–12 August 2005